An Evaluation of The Performance and Comparative Cost of Ground-mounted and Rooftop Mounted Solar Photovoltaic Systems

Prepared by:

Michael Leighton

LGHMIC001

Energy Research Centre
University of Cape Town

Prepared for:

Alison Hughes

Energy Research Centre
University of Cape Town

October 2020

Submitted to the Department of Mechanical Engineering at the University of Cape Town in partial fulfilment of the academic requirements for a Master of Science degree in Sustainable Energy Engineering.

Key Words: Solar photovoltaic, Ground-mounted, rooftop mounted, LCOE, payback, asbestos

Declaration

I, Michael Leighton, know the meaning of plagiarism and declare that all the work in the document, save for that which is properly acknowledged, is my own. This thesis/dissertation has been submitted to the Turnitin module (or equivalent similarity and originality checking software) and I confirm that my supervisor has seen my report and any concerns revealed by such have been resolved with my supervisor.

Name: **Michael Leighton**

Signature: Signed by candidate **Date:** 26 October 2020

Terms of Reference

The objective of this study is to investigate which of the two solar photovoltaic system configurations, being rooftop mounted or ground-mounted, is the better performing configuration from an annual specific yield and a financial feasibility perspective.

A key factor in this study is that there remain several unknown factors concerning how a ground-mounted solar photovoltaic system will perform, in comparison to a rooftop mounted solar photovoltaic system, which will affect the financial payback period. This uncertainty in yield generation prompts financiers to be reluctant to allocate debt.

Since the examined solar photovoltaic systems are all located in the same area (namely, Atlantis in the Western Cape), they are exposed to the same environmental conditions thus, allowing for a perfect opportunity to examine the rooftop and ground-mounted configurations in equal ambient conditions.

Acknowledgements

I would like to thank the following people, without whom the completion of this study would not be possible:

My supervisors, Alison Hughes and Bryce McCall for their continuous support, patience and allowing me to progress through this study at my own pace.

Natheera Ravat and Robert Timmis from Emergent Energy, Helmut Herzog and Ryan Dearlove from The South African Renewable Energy Incubator (SAREBI), Menno Sulsters from Shared Energy Management (SEM) Solutions, Ronnie Shaw from Stripform Packaging, Ryno Jordaan and Albertu Prins from New Southern Energy, Zaheer Khan from Canadian Solar and the Energy Team at GreenCape.

My friends, Allan Palmer, Justin Shanks, Alasdair McCulloch, Simon Ball, Aman Baboolal and Nicholas Fordyce for the support and putting things into perspective.

My parents Gail and Jeremy Leighton for the continuous harassment, asking when I will submit, and for the financial support. Lastly thank you to Natalie Sessions for the consistent support, proof reading and encouragement.

Abstract

In South Africa, there is an increasing interest in installing rooftop mounted solar photovoltaic systems. However, financing the photovoltaic systems causes most interest to be abandoned, largely due to the cost required to replace a building's asbestos roof. An alternative solution to replacing an asbestos roof is to install a ground-mounted photovoltaic system, which is more costly compared to a rooftop mounted system. This study aims to determine if a ground-mounted or a rooftop mounted solar photovoltaic system is the most financially feasible solar photovoltaic configuration.

In this study three photovoltaic systems were analysed, all of which are installed in Atlantis, Western Cape (WC). Since all three systems are in the same area, they are all exposed to the same metrological conditions, allowing for identical energy generation potential. Two of the photovoltaic systems are ground-mounted systems located respectfully at the South African Renewable Energy Incubator (SAREBI) and at Stripform Packaging. The third system is a rooftop mounted system located at SA Tyre Recyclers. The photovoltaic system at SAREBI is a 9.75 kWp system consisting of 30 Canadian Solar CS6U-325P modules, one Schneider Electric 20 kW inverter, a tilt angle of 15° and an azimuth angle of -19°. The photovoltaic system at SA Tyre Recyclers is a 231 kWp system consisting of 700 JA Solar JAP72S-01-330-SC modules, 7 SolarEdge 27.6 kW inverters, a tilt angle of 13° and an azimuth angle of 22°. The photovoltaic system at Stripform Packaging is a 20.1 kWp system consisting of 60 Canadian Solar CS6U-335P modules, one SMA 20 kW inverter, a tilt angle of 15° and an azimuth angle of 46°.

To achieve the aim of this study, the performance of each of the solar photovoltaic systems was examined, by comparing their annual specific yield. After which the technical aspects and differences of each of the photovoltaic systems were explored, to illustrate how each of the systems differ technically and how each system can be improved. Finally, the comparative cost of each of the solar photovoltaic systems was examined by analysing the levelized cost of energy (LCOE) and the payback period for each of the photovoltaic systems.

The results demonstrated that from an annual specific yield perspective, the ground-mounted configuration was the best performing, whilst from a financial perspective, the rooftop mounted configuration had the lowest levelized cost of energy (LCOE) and payback period. However, installing a ground-mounted system is more financially feasible than replacing an asbestos roof and then installing a rooftop mounted system.

In conclusion, by fully understanding the performance, payback period and levelized cost of energy, a clear understanding of potential risk can be determined, thus making the installation of photovoltaic systems more appealing for financiers.

It is recommended that this study be repeated in a manner in which each of the photovoltaic system configurations are constructed consisting of all the same photovoltaic components, measuring equipment,

tilt and azimuth angles. All of which would result in two identical photovoltaic systems where one is installed on a rooftop and the other installed on the ground. Once the two photovoltaic system configurations are equal in all aspects, an accurate comparison to determine which configuration is the most optimal performer and which is the most financially viable will be possible.

Table of Contents

List of Figures

List of Tables

1. Introduction

1.1. Background to the study

1.1.1. Solar photovoltaics in South Africa

South Africa has massive potential for solar photovoltaic generated energy, simply due to its exposure to high levels of solar radiation (Brent, 2020). From Figure 1, the majority of the country has an average annual energy generation potential of greater than 2 000 kWh/m^2 whilst the poorest levels of radiation occur around Durban with an annual energy generation potential of 1 500 kWh/m^2 (Solargis, 2017).

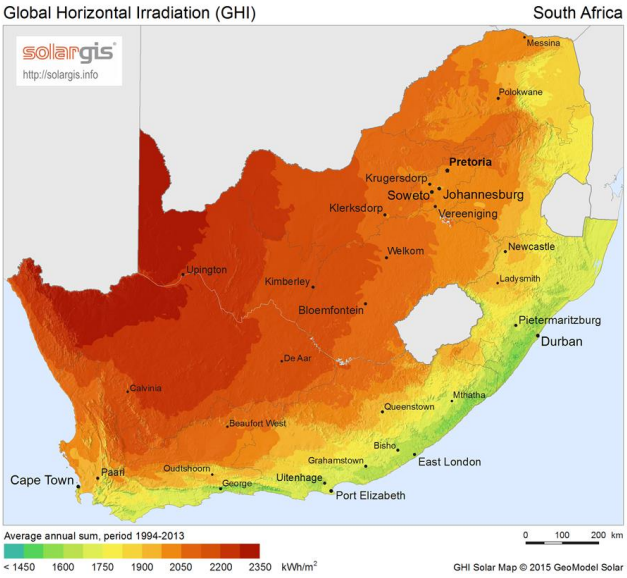

Figure 1: Germany GHI solar resource map (Solargis, 2017)

This seems poor when compared to the Karoo region of the country which is approximately 2 500 kWh/m^2, but compared to the average annual generation of Germany, which has previously had the greatest uptake of photovoltaics, of 1 050 kWh/m^2 (Solargis, 2017), South Africa clearly illustrates great potential for photovoltaics (Solargis, 2017).

Within South Africa the energy sector is seeing an increase in the cost of electricity coupled with the decrease in the cost of renewable and energy efficiency technologies (GreenCape, 2017). The price of electricity in South Africa has significantly increased since 2006, due to Eskom's new build programme and the increased cost of plant maintenance and fuel (GreenCape, 2017). The resulting effect is that for Eskom to recover its operational and new build costs, the electricity costs have been significantly increased compared to Eskom's historical cheap cost of electricity (GreenCape, 2017).

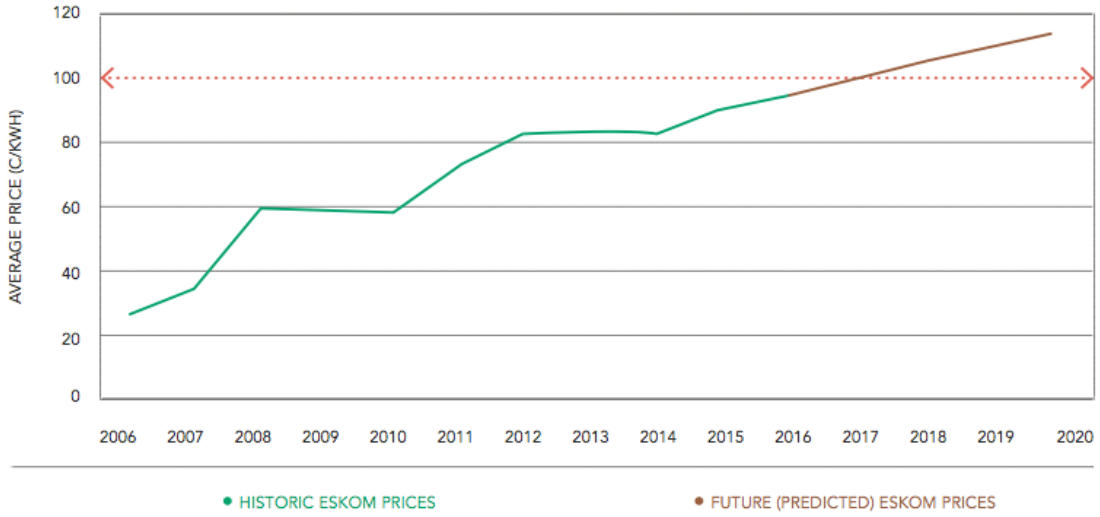

Figure 2: Historic and future Eskom price trajectory (GreenCape, 2017)

In Figure 2, the super-imposed red dotted line illustrates the R1/kWh price point. This is the critical point at which Eskom customers will find the case for own generation considerably attractive. (GreenCape, 2017).

Another key driver for the growth in the energy services market is the decreasing costs of both renewable technologies and technologies that improve energy efficiency (Gielen et al., 2019). However, solar photovoltaic technologies have shown the greatest decrease in cost in comparison to other small-scale renewable technologies (GreenCape, 2017).

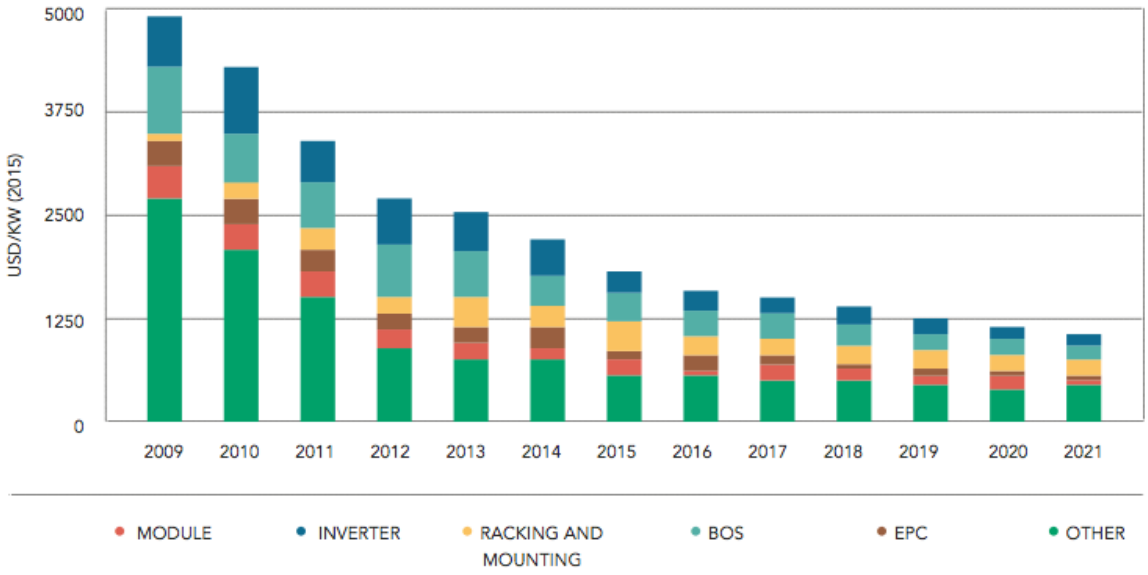

Figure 3: Component costs decrease over time for utility scale solar photovoltaic systems (GreenCape, 2017)

In Figure 3, the annual reduction in the solar photovoltaic component costs between 2009 and 2021 is clearly illustrated. The Engineering, Procurement and Construction (EPC) components are the costs to design, procure, construct, and install the photovoltaic system. The Balance of System (BOS) components are the

components that are required to transport the generated energy through the system such as wiring and breaker switching.

The effect of these decreases in component costs is the significant reduction in solar photovoltaic system installation costs, which is noted in Figure 4 (GreenCape, 2017).

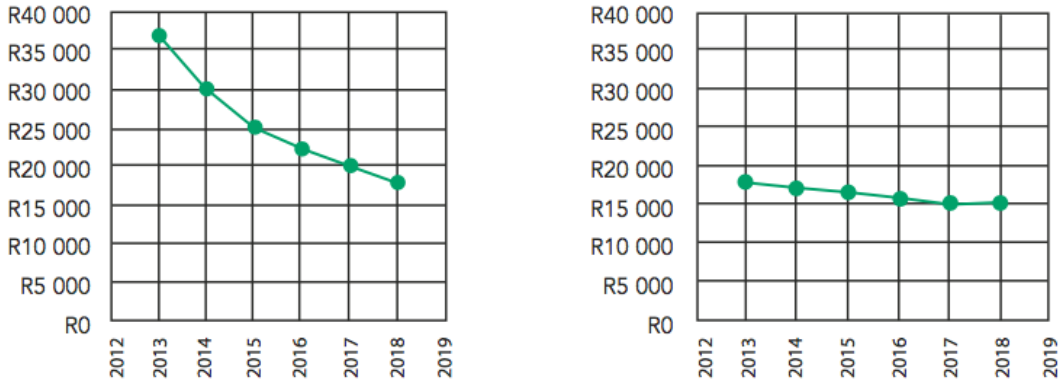

Figure 4: Rooftop solar PV with battery storage R/kWh (Left) and Rooftop solar PV without battery storage R/kWh (Right) (GreenCape, 2017)

The size of the South African solar photovoltaic market is steadily growing as renewable technologies costs decrease (GreenCape, 2017). One of the greatest drivers in the growth of the energy services market is the increased uptake of rooftop solar photovoltaic systems (IRENA, 2019). Not only were the costs of energy services the main driver to increase the uptake of solar photovoltaic systems, but also the incorporation of new financing mechanisms to offer methods to finance the installation and hardware costs. In 2016 the PQRS database estimated that there were over 100 000 systems installed throughout South Africa at a total installed capacity of over 170 MWp (GreenCape, 2017).

According to the PQRS database, Figure 5 illustrates the sector that has demonstrated the greatest level of growth for solar photovoltaic uptake has been the commercial and industrial sector at an approximate installed capacity of just less than 120 MWp.

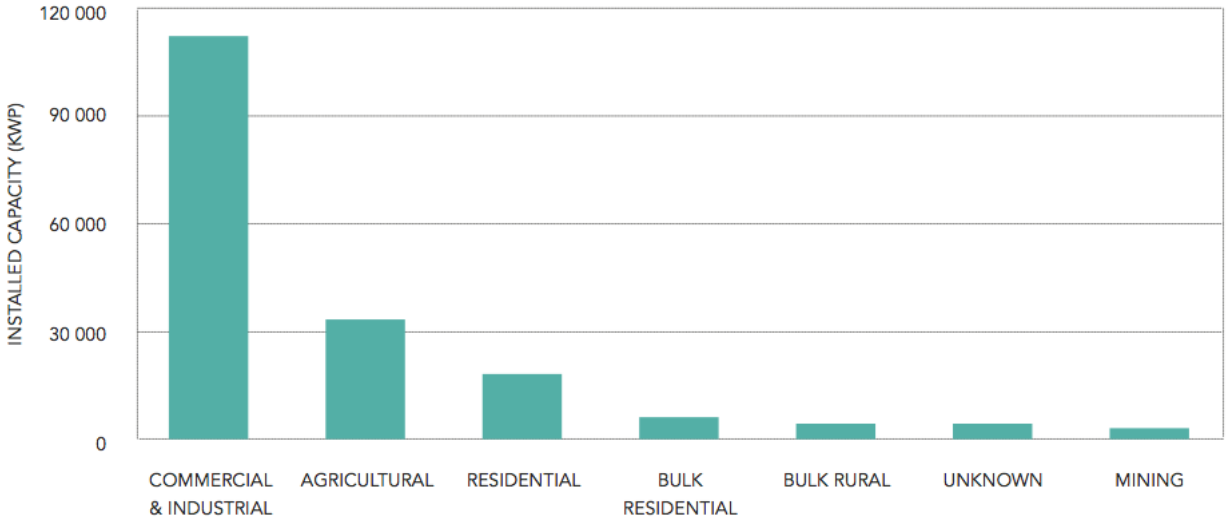

Figure 5: Distribution of installed solar photovoltaics throughout end-user sectors (GreenCape, 2017)

1.1.2. Solar Photovoltaic System Financing

As the costs of electricity rise, so too does the demand for renewable technology due to the steady decrease in the cost of renewables. However, in South Africa obtaining the financing for these systems becomes a massive stumbling block, leaving many small to medium industrial and commercial entities unable to secure substantial investment the renewable technology (Muringathuparambil, 2019). The most important factor to consider when it comes to financing a solar photovoltaic system is the 'payback period', which is the time period it takes to recover the financing debt to fund the system. There are factors to consider when investigating the feasibility of the solar photovoltaic system, one of which is the unit cost of electricity, such as the R/kWh tariff applied by the municipality, another is the daytime consumption baseload of the facility and finally the performance of the solar photovoltaic system. The performance of the system will determine the yield of energy that the system can generate from the solar irradiation.

A facility that is purchasing electricity at a relatively higher cost, has a large daytime baseload and has no constraints affecting the performance of a solar photovoltaic system, is a perfect case to invest in a solar photovoltaic system. These facilities are usually large utility customers such as shopping centres, large commercial offices, and large industrial facilities. Smaller utility customers are generally restricted due to a relatively lower cost of electricity and reduced daily baseloads. The resulting effect is that these smaller industrial and commercial entities are unable to obtain financing for their solar photovoltaic systems, since the 'payback' periods are too long and risky for financial institutions to finance debt. This risky financing profile leaves a significant gap in the solar photovoltaic market since small and medium entities are unable to obtain financing for solar photovoltaic systems (Derrick, 1998).

1.1.3. Solar Photovoltaic System Financial Implications

A further factor that affects the financial viability of a rooftop solar photovoltaic system is the insufficient structural strength of the roof or the use of poor quality of roofing material (Mishra, 2018).

Throughout South Africa's commercial and industrial sector, the most commonly used roofing material is asbestos roofing, due to the fibres having an extra ordinary tensile strength, being poor conductors of heat and having a very low cost (DoEA. n.d). However, in recent years the World Health Organisation as well as several South African Governmental Departments have concluded that the use of asbestos material is highly toxic and thus illegal to be used on buildings. (DoEA, n.d.). Given these findings, it has been noted that all buildings with asbestos roofing must replace the roofing if the asbestos material has been moved, damaged or disturbed.

The resulting effect is that the asbestos material must be removed and replaced with a modern and safe replacement before a solar photovoltaic system can be installed on a roof of a building. The financial implication to change a roof's material significantly affects the payback period of a solar photovoltaic system, often making the project financially unfeasible.

To combat the asbestos drawback in addition to a rooftop that is not structurally sound, a ground-mounted solar photovoltaic system can be installed instead of a rooftop mounted system. However, this too will incur financial implications due to ground-mounted systems being more expensive than rooftop mounted systems.

Exploring the comparative performance between the rooftop mounted and the ground-mounted solar photovoltaic systems is of value due to a lack of currently available research on comparing the performance and the payback periods of the two configurations being exposed to similar locations. However, the general understanding throughout the solar photovoltaic industry is that the ground-mounted systems have a greater performance compared to rooftop systems but come at a greater financial cost. The location of Atlantis in the Western Cape proved to be an opportune location to explore these comparative factors and test this commonly held understanding.

1.2. Atlantis Climate and Location Site Analysis

1.2.1. Background

Atlantis is a small town located approximately 40 km North of Cape Town, along the West Coast of the Western Cape. As of the 2011 Census, Atlantis consists of a population of 67 491 (15 565 households) and has an area of 28.84 m^2 (Census 2011, 2011).

1.2.2. Climate

Atlantis has a Mediterranean climate, resulting in a warm and temperate climate in which most of its rainfall occurs during the winter months, as seen in Figure 6 (Climate Data, 2018).

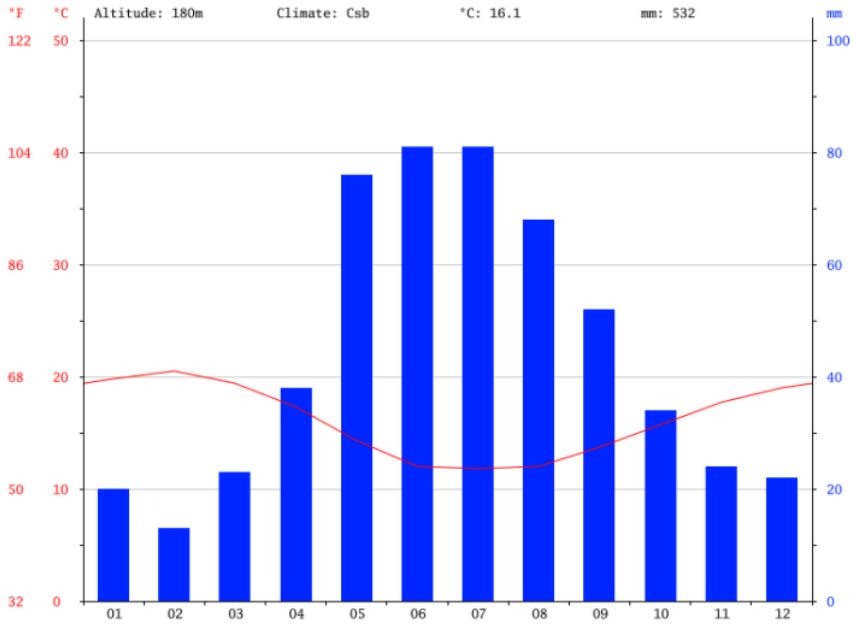

Figure 6: Climograph of Atlantis (Climate Data, 2018)

Throughout a year in Atlantis, there is a difference of 68 mm of precipitation between the driest month, being February with an average rainfall of 13 mm, and the wettest month being June, with a rainfall peak averaging 81 mm (Climate Data, 2018).

February is the hottest month of the year, with an overall average of 20.5 °C and an average max temperature of 26.9 ^{o}C. July is the coldest month of the year with an average overall temperature of 11.8 °C and an average minimum temperature of 6.3 ^{o}C (Climate Data, 2018).

1.2.3. Atlantis Irradiation

Using the PVSyst simulation software, the global horizontal and diffuse horizontal irradiation levels were obtained for Atlantis (GPS Co-ordinates: -33.587973, 18.491704). Table 1 and Figure 7 both illustrate that the irradiation levels for Atlantis follow the season changes, in which there are greater levels of irradiation during the summer months.

Table 1: Atlantis irradiation data (PVSyst, 2018)

Month	Monthly Global Horizontal Irradiation (kWh/m²)	Daily Global Horizontal Irradiation (kWh/m²)	Monthly Diffuse Horizontal Irradiation (kWh/m²)	Daily Diffuse Horizontal Irradiation (kWh/m²)
January	255	8.23	67	2.15
February	205	7.32	53	1.88
March	189	6.10	46	1.50

April	130	4.33	39	1.29
May	94	3.03	33	1.07
June	76	2.53	29	0.98
July	86	2.77	32	1.03
August	112	3.61	39	1.25
September	149	4.97	46	1.53
October	197	6.35	64	2.08
November	232	7.73	68	2.26
December	258	8.32	69	2.21
Total	**1 983**	**65.29**	**585**	**19.23**

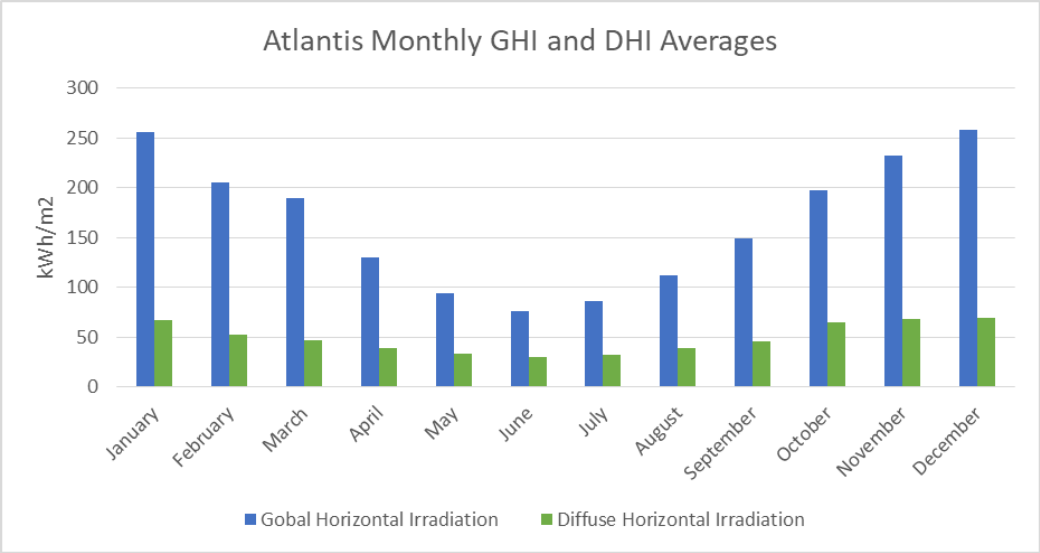

Figure 7: Atlantis irradiation data (PVSYS, 2018)

1.2.4. Atlantis Terrain Horizon and Day Length

In Figure 8 the path of the sun over a year is simulated. The Terrain horizon (grey filling) and module horizon (blue filling) may have a shading effect on solar radiation. The black dots illustrate the True Solar Time, whilst the blue labels illustrate Local Clock Time.

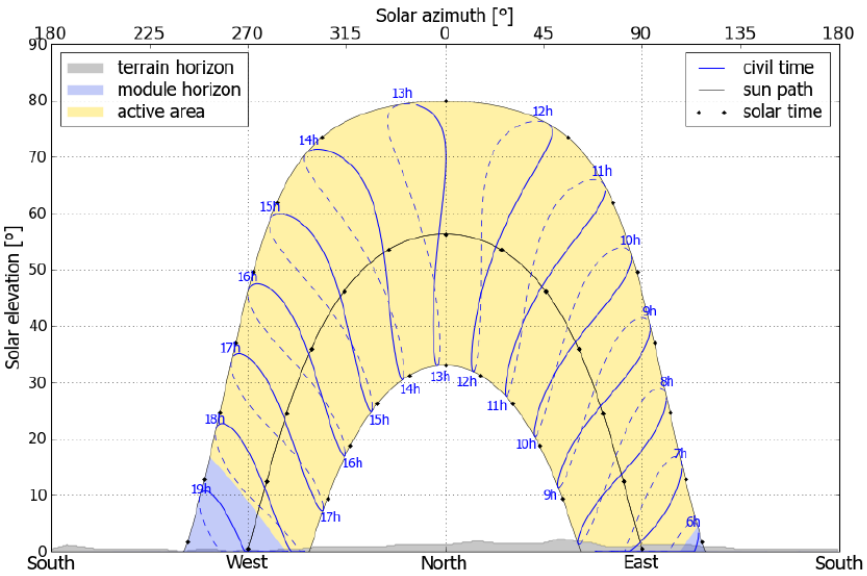

Figure 8: Sun path and terrain horizon (SolarGIS, 2017)

In Figure 9 the change of the day length and solar zenith angle during a year is illustrated. It must be noted that the local day length (time when the sun is above the horizon) is shorter compared to the astronomical day length, if obstructed by higher terrain horizon.

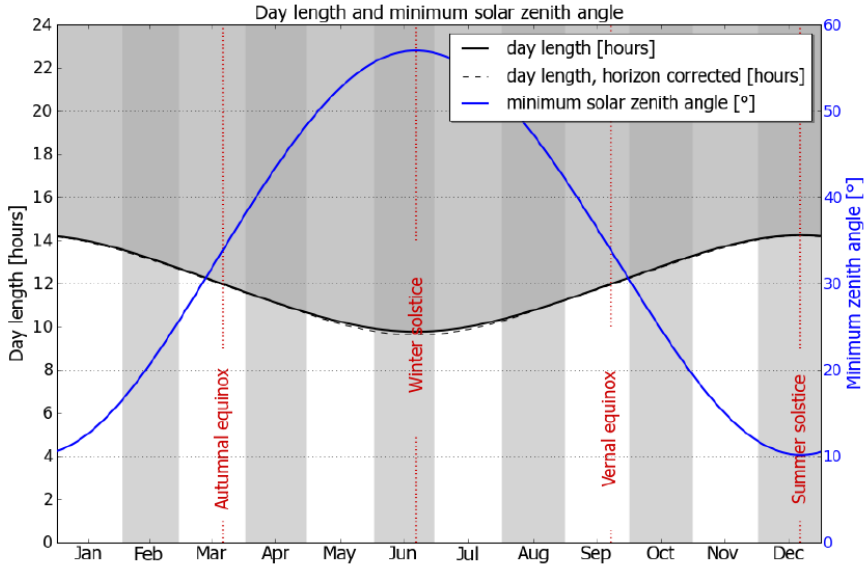

Figure 9: Length of day and zenith angle (SolarGIS, 2017)

Making use of charting software such as Sun Earth Told the solar chart at Atlantis is illustrated below as Figure 10.

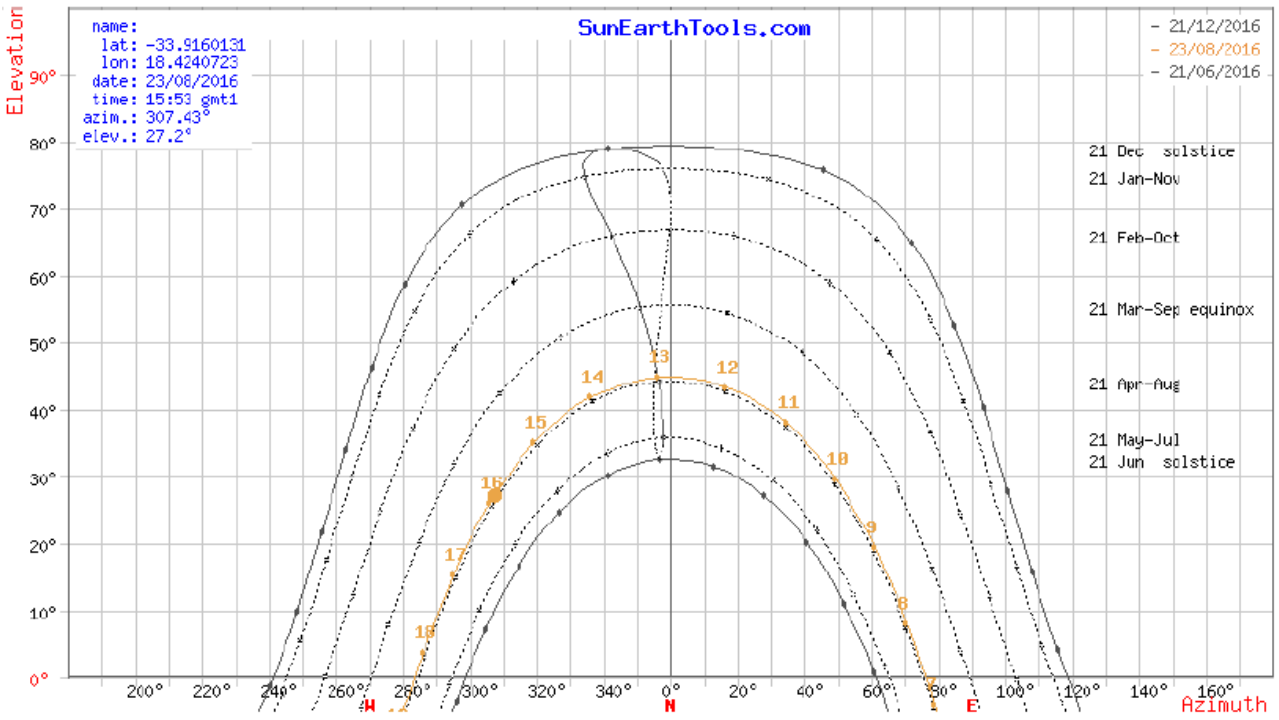

Figure 10: Solar Chart of Atlantis on the 23rd of August 2016 at 15h53 (Sun Earth Tools, 2016).

From Figure 10, it is clear that at 15h53 on the 23rd of August 2016, which is the time and date that the chart was generated, the position of the sun had an Azimuth angle of 307.43° and an elevation angle of 27.2° (Sun Earth Tools, 2016). During the Summer Solstice at 12h00, the sun has an Azimuth angle of 345.14° and an elevation angle of 79.19°. During the Winter Solstice at 12h00, the sun has an Azimuth angle of 355.76° and an elevation angle of 32.55° (NOAA, 2016).

From the simulated solar charts for Atlantis, it must be noted that the daily highest position of the sun occurs at approximately 12h48. Therefore, by harnessing the sun's radiation to generate energy or to make use of thermal heating practices, the Atlantis solar energy system must be designed to maximise the sun's radiation at approximately 12h48 each day. Table 2 illustrates the highest point of elevation for all for Solstices as well as the daily time of each maximum point of elevation (NOAA, 2016).

Table 2: Highest point of elevation and time in Cape Town during the Solstices (NOAA, 2016).

	Summer Solstice	Autumn Solstice	Winter Solstice	Spring Solstice	Average
Max Elevation	80.4273°	56.4991°	33.5645°	56.5537°	56.7611°
Time (24hrs)	12h48	12h54	12h48	12h42	12h48

1.1. Problem Statement

1.1.1. The Primary Problem

Currently, there is an under allocation of debt to finance rooftop solar photovoltaic systems in the commercial and industrial sectors of South Africa. There is a compelling desire to install solar photovoltaic systems; however, the financing hurdle causes most interest to be abandoned.

The driver factors relating to this under allocation of debt are the perception of risk by the financier and the time at which the financed debt can be recovered.

1.1.2. The Secondary Problem

The major factors that prevent the financial feasibility of installing a solar photovoltaic system on a commercial or industrial building's rooftop are the insufficient structural strength of a roof and the use of asbestos roofing material.

Throughout the commercial and industrial sector, buildings are old and have asbestos roofing. The resulting effect is that if a rooftop consists of asbestos then the asbestos must be removed and replaced with a modern and safe replacement before a solar photovoltaic system can be installed. The financial implication to change a roof's material significantly affects the payback period of a solar photovoltaic system, making it unfeasible.

To combat the asbestos drawback in addition to a rooftop that is not structurally sound, a ground-mounted solar photovoltaic system can be installed instead of a rooftop mounted system. However, available ground space is not readily available with properties within the commercial and industrial sectors. Even though open space is an issue, most commercial and industrial buildings have sufficient parking area available for their employees. This allows for the perfect opportunity to install carport solar photovoltaic systems, where rooftop mounted systems are not feasible.

1.1.3. The Tertiary Problem

There remain several unknown factors concerning how a ground-mounted solar photovoltaic system will perform, in comparison to a rooftop mounted solar photovoltaic system, which will affect the financial payback period. This uncertainty in yield generation prompts financiers to be reluctant to allocate debt.

However, since the examined solar photovoltaic systems are all located in the same area, they are exposed to the same environmental conditions thus, allowing for a perfect opportunity to examine the rooftop and ground-mounted configurations in equal ambient conditions.

1.2. Aim and Objectives of this study

1.2.1. Aim

This study aims to determine if a ground-mounted or a rooftop mounted solar photovoltaic system is the most financially feasible solar photovoltaic configuration for the South African Commercial and Industrial sectors. This will be accomplished by examining the solar photovoltaic systems performance of a rooftop and two ground-mounted systems in Atlantis, WC, and their comparative cost, which will demonstrate the period over which the financed debt can be recovered.

1.2.2. Objective

To achieve the aim of this thesis, the performance of each of the solar photovoltaic system configurations will be examined, by recording hourly data of the energy generated by each of the photovoltaic systems and analysing how the local environmental conditions affect energy yields. A key factor in this study is that the solar photovoltaic system configurations are all located in the same Atlantis area, thus exposing both to the same environmental conditions.

Once the performance of each of the solar photovoltaic systems has been examined, the extent to which technical aspects and differences of both photovoltaic system configurations influence performance will be explored. This will illustrate how each of the system configurations differs technically and how each system can be improved.

Finally, the comparative cost of the solar photovoltaic system configurations will be examined by analysing the cost per produced kWh of energy for the two solar photovoltaic system configurations. This will be accomplished by comparing the engineering, procurement and construction (EPC) costs to install the solar photovoltaic systems and the financial savings from the generated energy. This financial analysis will result in two comparative factors to compare the three photovoltaic systems: namely the levelized cost of energy (LCOE) and the payback period.

1.2.3. Research Question and Sub Questions

This dissertation will examine the following research question:

Comparing the performance of a ground-mounted solar photovoltaic system to a rooftop mounted solar photovoltaic system; which of the two has the better performance and comparative cost, and how does this affect the solar photovoltaic system's payback period?

Sub Questions:

- How do the following aspects affect the performance of the solar photovoltaic systems?:
    - Global Horizontal Irradiance (GHI), ambient temperature, module surface temperature, wind speed and direction, rainfall, air pressure, humidity, module tilt angle, mounting structure, shading, azimuth angle, component selection, operation and maintenance (O&M)
- Can the performance of the systems be improved, and if so how?
- How does the following affect the comparative cost of the solar photovoltaic systems?:
    - Engineering procurement and construction (EPC) cost, operation and maintenance (O&M), component selection, energy generation (kWh)
- Can the comparison cost be improved, and if so how?
- How does the comparison cost and the performance affect the photovoltaic system's financial feasibility?

2. Theoretical Background

In this chapter aspects of the theoretical background to solar photovoltaic systems will be discussed. Sections 2.1. and 2.2. discuss the background to solar energy and solar cell technology.

Sections 2.3. to 2.5. discuss the technical aspects of a solar photovoltaic system and Section 2.6. to 2.10 discuss the financial mechanicals and aspects of a solar photovoltaic system.

2.1. Solar Energy

In this section, the background to solar energy, which is essential to understanding the principles relating to solar photovoltaic systems, is discussed.

2.1.1. Solar Geometry

To fully grasp the basics of solar energy, one must first have a sufficient understanding of solar geometry. Solar geometry is key to describing the sun's position relative to an observer on the surface of the earth as well as designing and modelling a solar photovoltaic system.

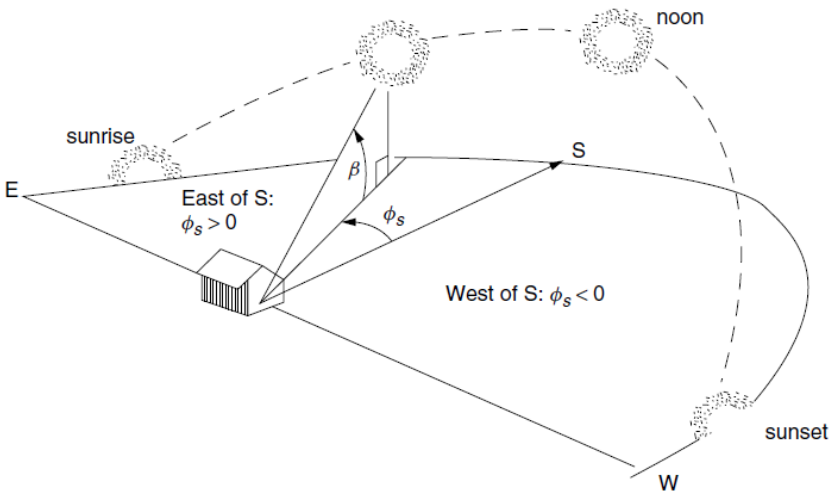

Figure 11: The position of the sun described by solar geometry (Master, 2004: 396).

In Figure 11 the exact position of the sun relative to a point on the surface of the earth can be described by the solar altitude/elevation angle (β) and the solar azimuth angle $(\emptyset_S)$

- **The solar azimuth angle** $(\emptyset_S)$ is the angle of the sun's position relative to the North-South axis. Therefore, in the Southern Hemisphere, the azimuth angle is measure relative to North. The azimuth angle can be represented by the following equation (Master, 2004):

$$\sin \emptyset_S = \frac{\cos \delta \sin H}{\cos \beta}$$

- **The solar elevation angle** (β) is the angle between the horizontal plane (the surface of the earth) and the line of sight position of the sun, along the vertical plane. The elevation angle can be represented by the following equation (Master, 2004):

$$\sin\beta = \cos L \cos\delta \cos H + \sin L \sin\delta$$

- **The hour angle** (H) is the number of degrees that the earth must rotate before the sun will be directly over the local line of longitude. Therefore, the hour angle is the difference between the local line of longitude and the sun's longitude. Since the earth rotates 360° around the sun in 24 hours or 15° per hour, the hour angle can be described as follows:

$$Hour\ angle\ (H) = \left(\frac{15°}{hour}\right)(hours\ before\ noon)$$

Therefore at 11h00, the hour angle will be +15° and at 14h00 the hour angle will be -30°

2.1.2. Solar Radiation

The sun is the main source of life on planet Earth, without the sun, life would cease to exist. The sun's energy reaches the Earth's surface in the form of radiation. The radiation from the sun is absorbed by plants by means of photosynthesis, and the radiation heats the land and the oceans causing convection resulting in the flow of currents and the flow of wind. The sun's radiation can also be harnessed to generate electricity by means of photovoltaic cells (Laughton, 2010).

The quantity of solar radiation reaching the surface of the Earth is quantified as power per unit area (or the energy per unit time per unit area) and is known as irradiance. The average irradiance at the outmost edge of the earth's atmosphere is 1 353 W/m^2 (Goswami, 2015). However, due to the radiation scattering and absorption from the Earth's atmosphere, surroundings, clouds and the angle of the sun's rays, the average irradiance at sea level on a clear day is approximately 1 000 W/m^2 as illustrated in Figure 12.

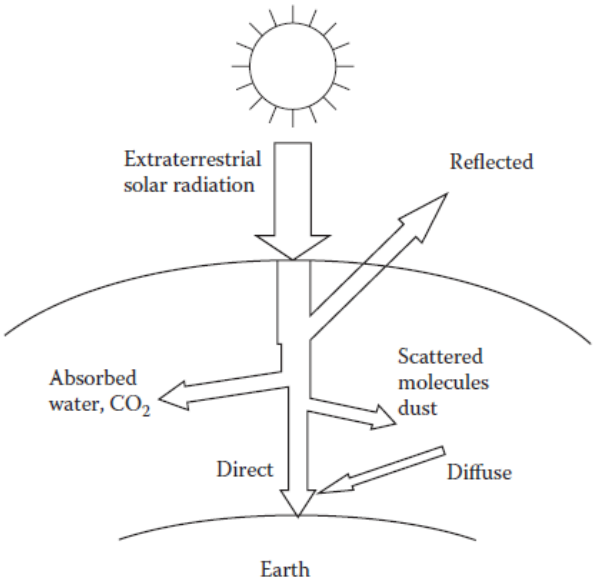

Figure 12: Attenuation of solar radiation as it passes through the Earth's atmosphere (Goswami. 2015: 65).

2.1.3. Solar Season

The orbital path of the Earth around the sun is elliptical. The resulting effect is that the distance from the sun to the Earth varies depending on the time of year. Figure 13 illustrates the change in distance between the Earth and the sun throughout the year, as well as the effects of the seasons for each hemisphere (Foster *et al.*, 2009).

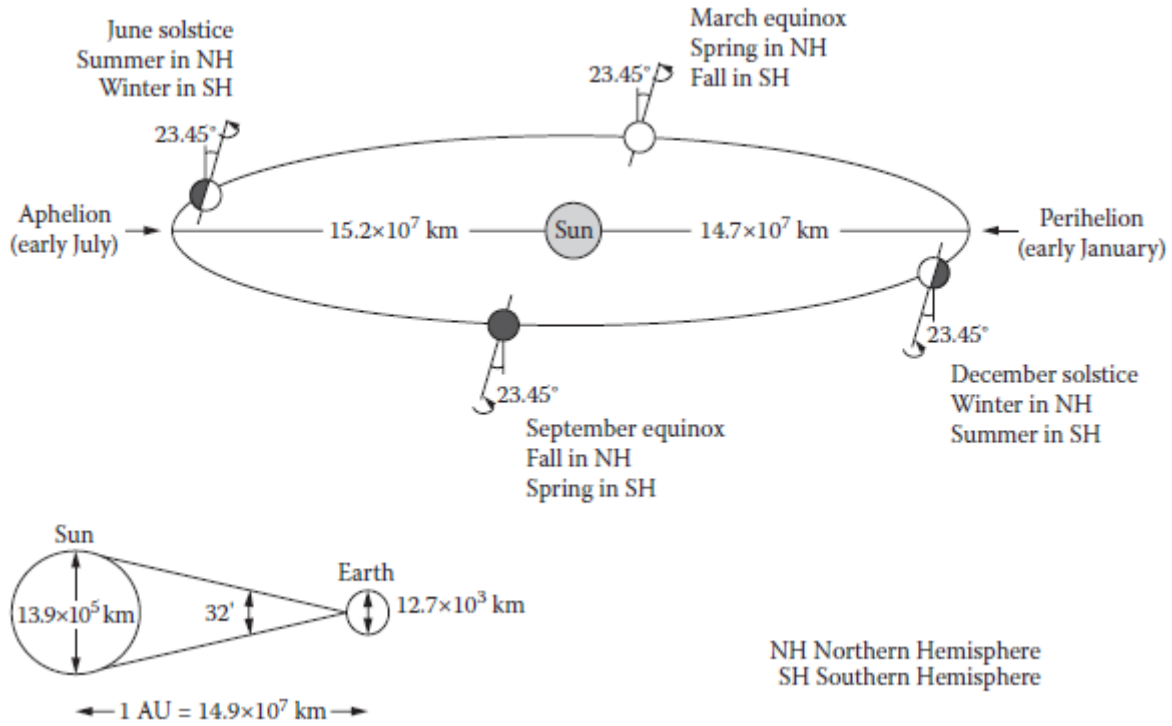

Figure 13: The Earth and sun geographical relationship (Foster et al, 2009: 8).

The Earth also rotates on its axis completing a full rotation every 24 hours which is the sun's path in the sky moving east to west during the day. The angle of rotation on the Earth's axis is a constant 23.45° (Foster *et al.*, 2009: 9). The resulting effect is that the angle between the sun and a point on the surface of the Earth varies throughout the year, thus changing the length of day.

During the Southern Hemisphere winter, the days are shorter because the sun is at the lowest angle in the sky. The sun also does not rise exactly in the East, but instead slightly North of East and sets North of West. The shortest day of the year occurs on the 21st of June, namely the Winter Solstice which is when the sun is at its lowest position in the sky. Every day after the Winter Solstice, the sun rises closer to East and sets closer to West until the 21st of September, which is called the Spring Equinox, where the sun rises and sets exactly in the East and the West (Foster *et al.*, 2009).

After the Spring Equinox, the sun continues to move higher through the sky, until it reaches the highest point in the sky being the Summer Solstice, which occurs on the 21st of June. This day is the longest because the sun is at its highest position the sky and will rise and set South of East and South of West. Every day after the

Summer Solstice, the sun lowers its position in the sky until it reaches the Autumn Equinox, being the 21st of March, where the sun rises and sets at exactly East and West. After the Autumn Equinox, the sun moves lower through the sky until reaching the Winter Solstice (Foster *et al.*, 2009).

In Figure 14 the same cycle occurs for the Northern Hemisphere during the year except the Winter Solstice occurs on the 21st of December, the Summer Solstice on the 21st of June and the spring and Autumn Equinoxes on the 21st of March and the 21st of September (Foster *et al*., 2009).

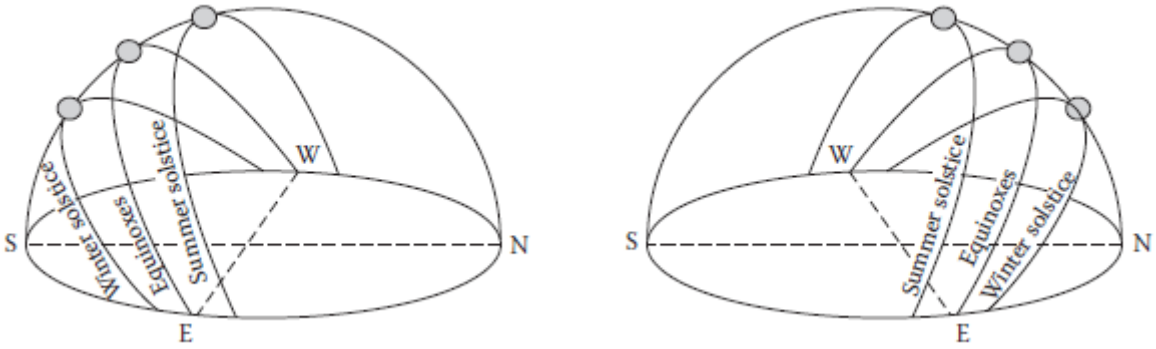

Figure 14: Daily path of the Sun throughout the year in the Northern Hemisphere (Lefts) and Southern Hemisphere (Right) (Foster et al, 2009: 10).

2.1.4. Daily Solar Chart

The angular distance of the solar radiation can be seen in Figure 15. The figure illustrates the incoming solar radiation during the summer and the Winter Solstice. For δ = –23.45°, being the December solstice, the South Pole is more exposed to the sun's radiation. However, when δ = +23.45°, being the June solstice, the South Pole is exposed to less of the sun's Radiation (Foster *et al.*, 2009).

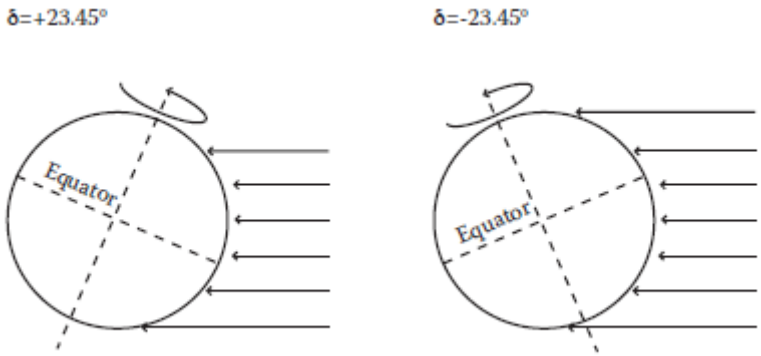

Figure 15: Direction of incoming solar radiation beam into Earth on the June Solstice at δ = +23.45°, and on the December Solstice at δ = –23.45° (Foster et al, 2009: 15).

A solar chart illustrating the solar altitude for a day for several latitudes is shown in Figure 16. Comparing the two zenith angles, where δ = –23.45° and δ = 23.45°, the solar altitudes during the day are not symmetrical. During the December Solstice (δ = –23.45°) locations with ϕ = 70° to 90° in the Northern Hemisphere are not illuminated at all during the day and at the South Pole, the sun does not set at all. During the June Solstice (δ

= +23.45°) locations with ϕ = –70° to –90° in the Southern Hemisphere are not illuminated at all during the day and at the North Pole, the sun does not set at all (Foster et al, 2009).

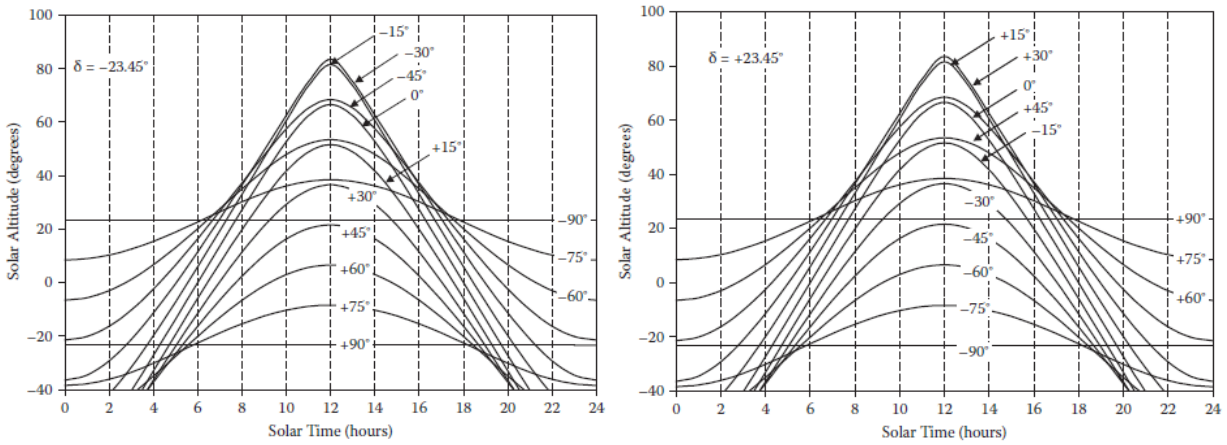

Figure 16: Solar altitude during the day for different latitudes during the December Solstice when δ = –23.45° and the June Solstice when δ = +23.45° (Foster et al, 2009: 15).

2.1.5. Solar Irradiation

Solar irradiation is the instantaneous measurement of solar power over an area represented as watts per square meter (W/m^2) (Stein, 2017). However, for every measurement of irradiance several factors must be defined to ensure that the irradiance measurements are accurate. The factors are as follows (Stein, 2017):

- Irradiance measurements must be a defined collection plane, which can be orientated normal to the sun or horizontal to the surface of the earth,
- Irradiance measurements must be classified by the portion of sunlight that is being measured. This is due to some measurements only being able to measure direct irradiance, diffuse irradiance, or a combination of both known as Global Horizontal Irradiance (GHI),

2.1.5.1. Air mass

The air mass (AM) is a ratio of the solar path length through the atmosphere with the sun directly overhead (h_1) and the path length through the atmosphere to reach a specific point on the surface of the earth (h_2). The air mass ratio can be expressed as follows (Master, 2004):

$$AM = \frac{h_2}{h_1} = \frac{1}{\cos \delta} = \sec \delta$$

At sea level and when the sun is directly overhead the zenith angle (δ) is zero, hence the $AM = 1$. Therefore, an air mass ratio of 1 is known as AM1. Thus, AM0 means no atmosphere. However, an air mass ratio of AM1.5 is assumed to be the average solar spectrum or the standard spectrum of the earth's surface (Master, 2004).

However, seen in Figure 17, two international standards (ASTM G-173-03) were set for AM1.5, one being AM1.5 for global spectrum which was set for all testing or rating of solar cells in a flat plate configuration and

has a power density of 1000 W/m^2 (Honsberg & Bowden, 2017). The second standard is the AM1.5 direct spectrum which was set for testing and rating of concentrator operations and has a power density of 900W/m^2 (Honsberg & Bowden, 2017).

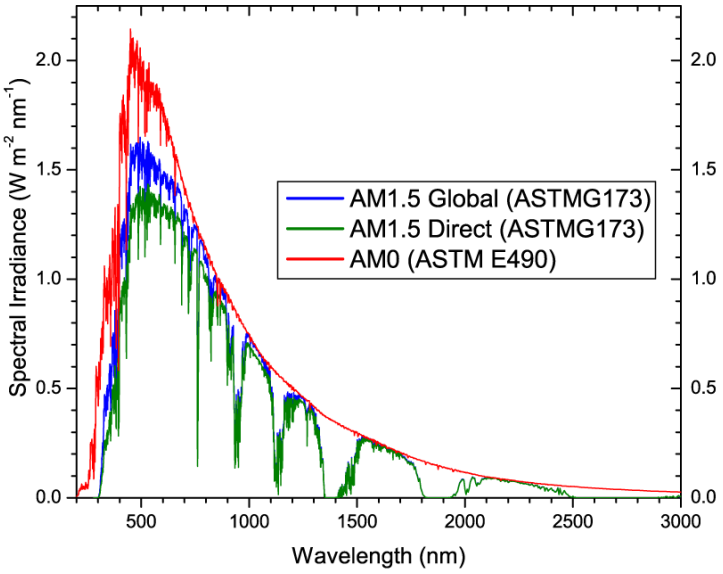

Figure 17: The standard spectrum modelled using SMARTS (Simple Model of the Atmospheric Radiative Transfer of Sunshine) program (Honsberg & Bowden, 2017)

2.1.5.2. Global horizontal irradiation (GHI)

Global horizontal irradiation (GHI) is the amount of irradiance that makes contact with a surface horizontal to the surface of the earth (Stein, 2017).

The GHI can be measured by many different instruments, however, the most common instrument used to measure the GHI is known as a pyrometer. A pyrometer has a hemispherical (180^o) view angle which allows for 180^o of light to be measured. However, if the GHI cannot be measured then it can be calculated by using the diffuse horizontal irradiance (DHI), the direct normal irradiance (DNI) and the zenith angle ($\emptyset_S$) (Stein, 2017), illustrated in Figure 18.

$$GHI = DHI + DNI \cos \emptyset_S$$

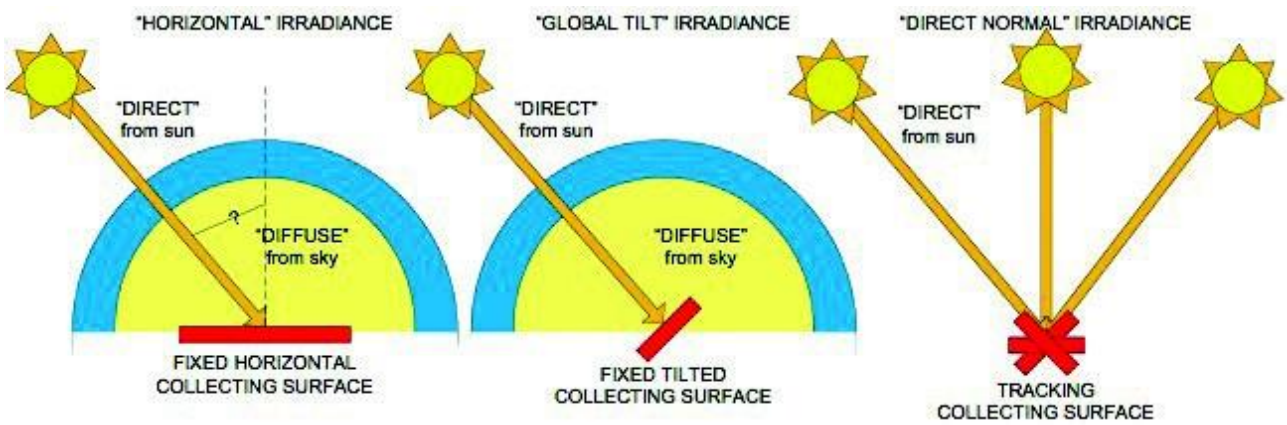

Figure 18: Global horizontal irradiance (GHI) (Vashishtha, 2012)

The diffuse horizontal irradiance is the amount of irradiance that reaches a horizontal surface that has been scattered or diffused by the atmosphere. The direct normal irradiance (DNI) is the amount of direct solar radiation that is always normal (perpendicular) to the solar radiation that reaches the surface of the earth in a straight line (Stein, 2017).

2.1.5.3. Plane of array (POA) radiance

A critical step in calculating a photovoltaic system's performance is determining the irradiance incident on the plane of the array (POA) as a function of time. The plane of array irradiance (G_{POA}) can be determined by the following equation (Stein, 2017):

$$G_{POA} = G_b + G_g + G_d$$

Illustrated in Figure 19, $G_b$is the direct beam irradiance component of the plane array, G_g is the ground reflection irradiance in the plane array and G_d is the sky diffuse irradiance component of the plane array (Stein, 2017).

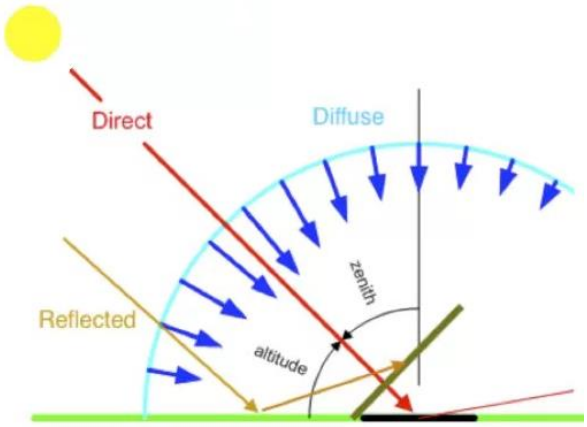

Figure 19: Direct and diffused irradiation on a tilted module (ECOSMART, 2017)

The direct beam irradiance component can be calculated from the DNI values using the following equation (Stein, 2017):

$$G_b = G_n \cos\theta_i$$

Where, G_n is the direct normal irradiance and θ_i is the solar angle of incidence. The ground reflection irradiance in the plane array can be calculated using the following equation (Stein, 2017):

$$G_n = (GHI)(\rho_g)\left(\frac{1-\cos\theta_T}{2}\right)$$

Where, ρ_g is the ground albedo and θ_T is the surface tilt angle. Albedo is the fraction of GHI that is reflected, therefore $albedo = 0$ when the surface is very dark and $albedo \approx 1$ when the surface is bright white or metallic (Stein, 2017).

2.2. The Solar Cell

In this section the background to the solar cell is discussed in addition to the operation of how the photovoltaics convert photons into electrical current.

2.2.1. History of solar cells

The history of photovoltaics began as early as 1839, when a French physicist named Edmund Becquerel, was able to generate a potential difference when he illuminated a metallic electrode in a weak electrolyte solution. The illumination of the solid electrode resulted in a change in the electromotive force (EMF) and was the first demonstration of the 'photovoltaic effect' (Goetzberger et al., 2002).

After Becquerel's discovery in 1839, there was no significant revelation in the photovoltaic effect until 1876, when William Adams and Richard Day were the first to demonstrate that electricity could be produced from light photons by building cells made of selenium. At the time, these selenium cells were quickly adopted by the photography industry as photometric light meters (Goetzberger et al., 2002).

In 1904 Albert Einstein published a theoretical explanation of the photovoltaic effect as part of his quantum theory, which resulted in him being awarded a Nobel Prize in 1923 (Luque, 2011). At the same time, a Polish scientist named Jan Czochralski developed a method, known as the Czochralski process, to grow perfect silicon crystals (Master, 2004). By the 1950s the Czochralski process was used to develop the first generation of single-crystal silicon photovoltaics and is still used today to manufacture photovoltaics (Master, 2004).

The first commercial use of photovoltaics came in 1958 when they were used for the Vanguard I satellite to generate electricity to operate the satellite while in orbit (Luque, 2011). Since the inclusion of photovoltaics on the Vanguard I, photovoltaics have played a significant role in providing satellites and space crafts with on-board electricity (Luque, 2011). However, the biggest push for photovoltaic efficiency improvements came in the 1970s during the Oil embargo and energy crisis. Figure 20 illustrates that by the 1980s lower costs and higher efficiencies drastically changed the photovoltaic industry allowing for many commercial applications, such as small homes, pocket calculators, buoys, isolated water pumps and many other off-grid applications (Master, 2004).

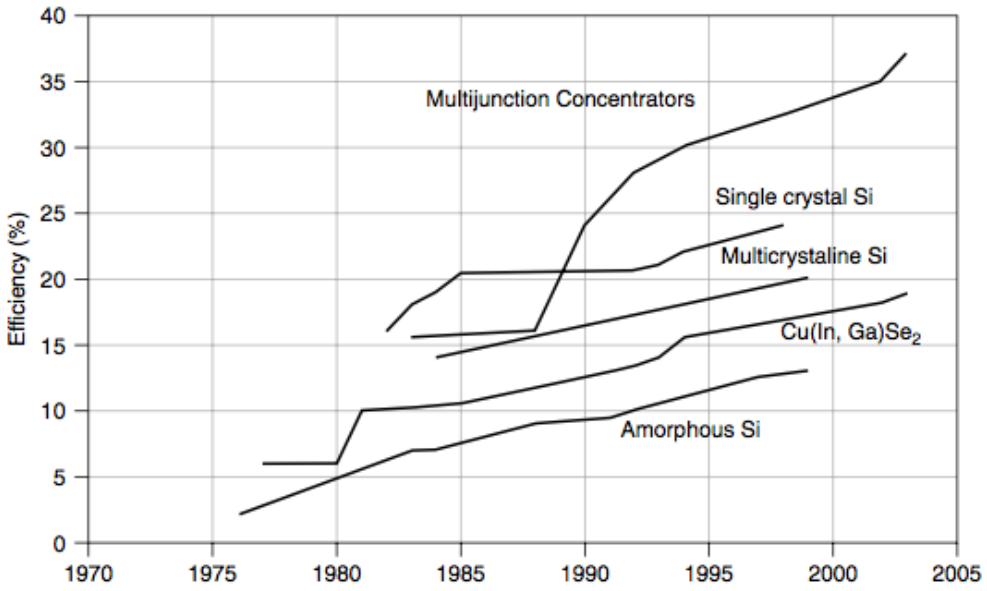

Figure 20: Photovoltaic efficiencies for various technologies (Master, 2004)

Even though the cost of photovoltaics continued to drastically decrease during the 1990s, the commercial installations of photovoltaics still struggled to become a game changer in the energy sector. This was due to the levelised costs of energy for photovoltaics that were still greater than the levelised costs for fossil fuel generation technologies (Masters, 2004).

2.2.2. Solar cell appearance

The solar cell, which is also known as a photovoltaic cell, is a solid-state semiconductor that converts light energy into direct current (DC) electricity by using the photovoltaic effect. The solar cell consists of millions of diodes and is almost identical to a light emitting diode (LED), however, instead of emitting light like an LED, the solar cell absorbs light (Boyle, 2004).

2.2.3. The photovoltaic effect

The photovoltaic effect is the key behind the working principles of solar cells and involves the generation of a potential difference at the junction of two differently bonded materials. This photovoltaic effect is similar to the photoelectric effect in which light photons are absorbed which excites an electron to a higher energy state (Jäger et al., 2014).

The key difference between the photoelectric effect and the photovoltaic effect is that during the photoelectric effect the excited electron is ejected out of the material whilst in the photovoltaic effect the electron is still bound by the material (Jäger et al., 2014). Light emitting diodes make use of the photoelectric effect, whilst solar cells make use of the photovoltaic effect.

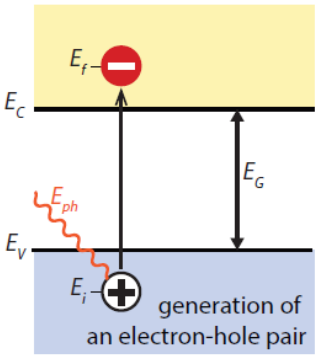

Figure 21: Illustration of the photon being absorbed by the material (Jäger et al., 2014: 24)

Figure 21 illustrates a light photon (E_{ph}) being absorbed by the material (E_V), with a bandgap (E_G), thus exciting an electron $(E_{f\_})$ into a higher energy level and moving the electron over the bandgap and into the adjacent material (E_C). The resulting effect is a generation of a potential difference between the two types of material (Jäger et al., 2014).

2.2.4. The operation of a solar cell

Since solar cells consist of many semiconductor diodes, they follow the same principles as the conventional diode with a p-n junction.

If you apply a voltage across a diode's terminals such as in Figure 22, a forward flowing current will flow easily through the diode from the p-side to the n-side of the diode. However, if you reverse bias the diode by sending the current in the opposite direction then only a very small amount of current will flow, which is approximately 1 x 10^{-12} A/cm^2. The voltage-current characteristics curve for the p-n junction is described by the following Shockley diode equation (Masters, 2004):

$$I_d = I_0\left(e^{\left(\frac{qV_d}{kT}\right)} - 1\right)$$

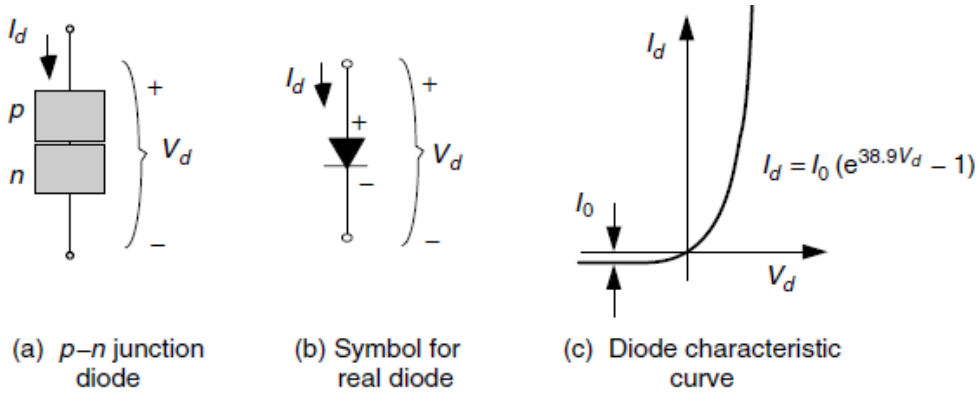

Figure 22: A p–n junction diode characteristics (Masters, 2004: 458)

The key to the operation of a solar cell is the events that occur at the p-n junction, which is where electrons move from one side of the p-n junction to the other. When a p-type material, which has a positive charge, and an n-type material, which has a negative charge, are joined together without an externally applied

voltage, shown in Figure 23, the n-type and p-type material both obtain a neutral charge. This is due to the 'excess' electrons from the n-type side jumping over the p-n junction to fill the 'holes' in the p-type side (Goshwami, 2015).

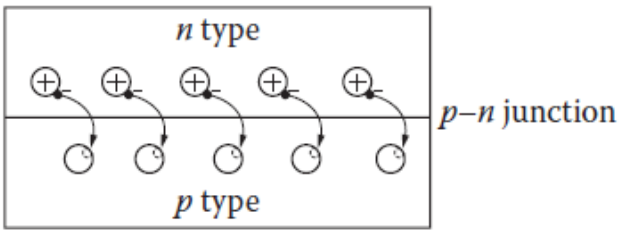

Figure 23: Movement of electrons at the p-n junction (Goshwami, 2015: 519)

2.2.5. The equivalent solar cell circuit

To fully understand the electrical behaviour of a solar cell, an equivalent electrical circuit can be modelled. As seen in Figure 24, an ideal solar cell can be modelled by having a current source and a series resistor. However, in reality, a solar cell will never function in an ideal practice. Therefore, a shunt resistance and a series resistor must be incorporated into the equivalent model.

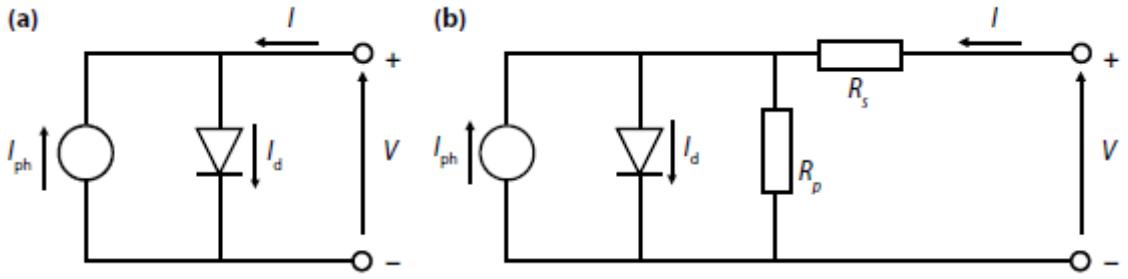

Figure 24: The equivalent circuit of an (a) ideal solar cell and (b) a solar cell with a series resistor R_s and a shunt resistance R_p (Jäger et al., 2014: 109)

The current density (J) and the voltage characteristics of a solar cell in ideal conditions can be given by the equation below:

$$J\,(V_a) = J_0\left(e^{\left(\frac{qV_a}{kT}\right)} - 1\right) - J_{ph}$$

As the resistive components are varied, as in Figure 25, the operation of the solar cell is affected. In the series resistance case, as the resistance of the resistive components are increased, the current density too is increased. In the parallel resistance case, as the resistance is increased the current density is decreased.

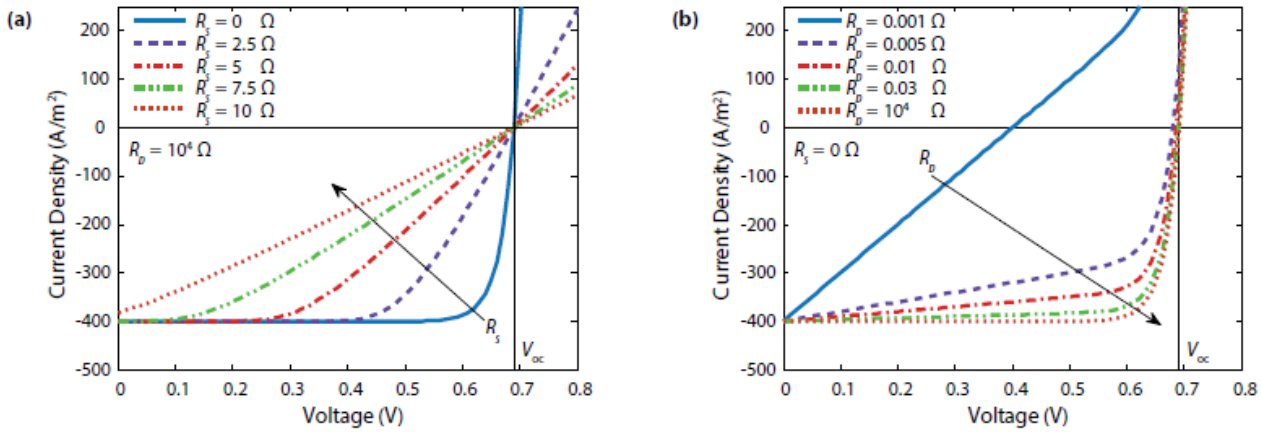

Figure 25: Effect of the (a) series resistance and (b) parallel resistance on the current density (J) and the voltage (V) characteristic of a solar cell (Jäger et al., 2014: 110)

The resistive component of a solar cell has a direct relationship between the current and voltage characteristics, which plays a crucial role in the operation and the performance of a solar cell. Solar modules, panels and arrays.

2.2.5.1. Solar photovoltaic modules

Occasionally, there is confusion between solar cells and solar modules (photovoltaic modules), the difference is that solar modules are a larger device that consists of many solar cells all connected in series, which can typically consist of up to 36 solar cells (Canadian Solar, 2018).

The difference between a solar module and a solar panel is that the solar panel consists of several solar modules that are electrically connected and mounted on a supporting structure, as shown in Figure 26 (Jäger et al., 2014).

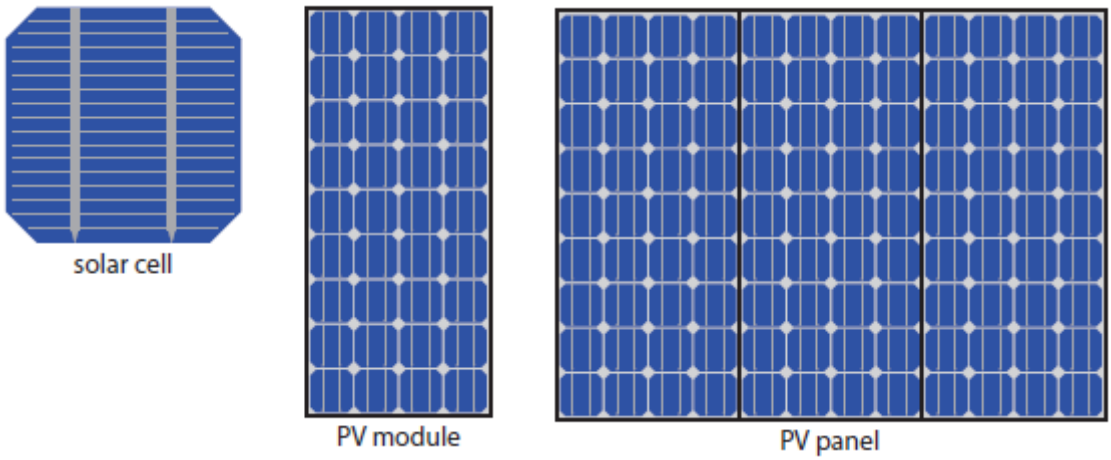

Figure 26: Solar cell (left), a solar module (middle) and a solar panel (right) (Jäger et al., 2014: 252)

A solar photovoltaic array consists of several solar panels connected in either a series or a parallel configuration (Jäger et al., 2014). In Figure 27 an example of a solar array consisting of two strings of two solar panels each connected in series.

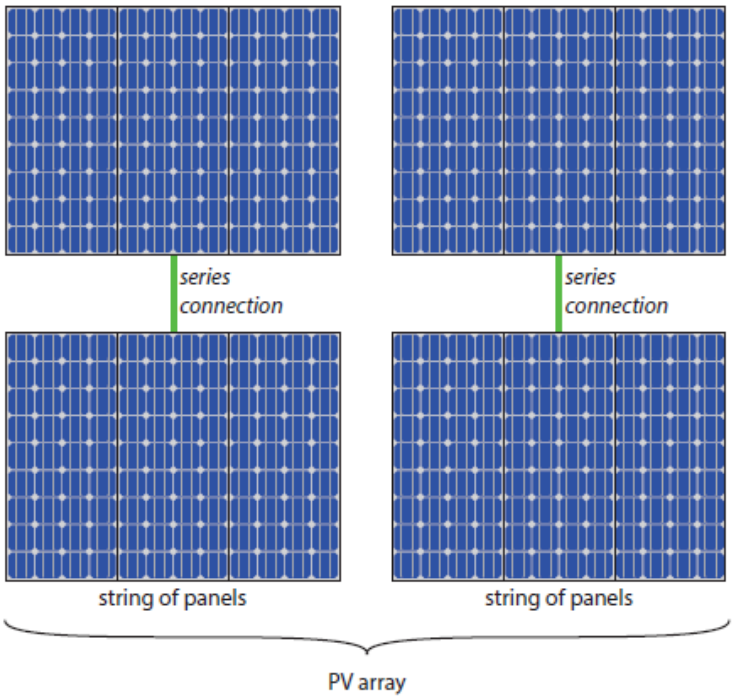

Figure 27: Illustration of a series connected solar photovoltaic array (Jäger et al., 2014: 252)

2.2.5.2. Series and parallel connections of solar modules

In a series connection, the potential difference of each solar cell is summated together giving a total potential difference (voltage rating) (Halliday et al., 2011). In Figure 28, the open circuit voltage of one solar cell is equivalent to 0.6 V. However, a series string of three solar cells in an open circuit configuration will give a potential difference of 1.8 V.

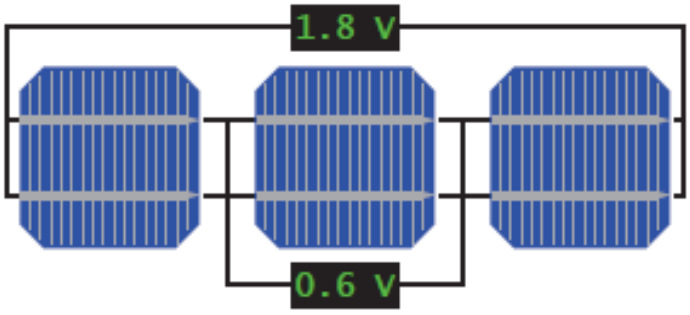

Figure 28: Three solar cells connected in series (Jäger et al., 2014: 253)

In a series connection, the generated current of the solar cells will not be summated together but is equivalent to the current of one single solar cell (Jäger et al., 2014).

For a complete solar module, the voltage and current output can be pre-determined by modifying the connections of the solar cells. Figure 29 illustrates a photovoltaic module containing 36 solar cells all

connected in series. If a single junction solar cell has a short circuit current of 5 Amperes and an open circuit voltage of 0,6 V, then the total solar module would have an open circuit voltage (V_{OC}) of 21.6 V and a short circuit current (I_{SC}) of 5 A. However, if two series strings consisting of 18 solar cells are connected in parallel, then the output of the module will be V_{OC} = 10.8V and I_{SC} = 10 A (Jäger et al., 2014).

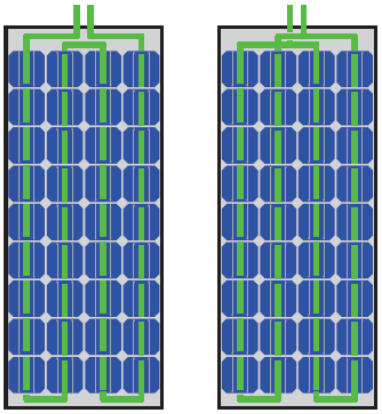

Figure 29: A Solar module consisting of a string of 36 solar cells connected in series (left) and of two strings of 18 solar cells each connected in parallel (right) (Jäger et al., 2014: 255)

If the three solar cells are connected in parallel, as in Figure 30, the potential difference over all the solar cells will be equal. However, the current of each solar cell will be summated, resulting in the total current being three times greater than the current of a single solar cell (Jäger et al., 2014).

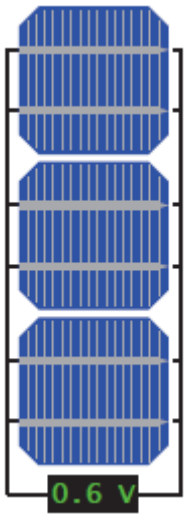

Figure 30: Three solar cells connected in series (Jäger et al., 2014: 253)

2.2.6. Photovoltaic I-V curve

In Figure 31, the current and voltage (I-V) characteristic curves of solar cells connected in series and parallel are illustrated. A (I-V) characteristic curve is used to illustrate the short circuit current and voltage of a solar cell as well as the solar cell's open circuit voltage and current characteristics. These factors are critical in describing an electrical component's operation and performance (Luque, 2011).

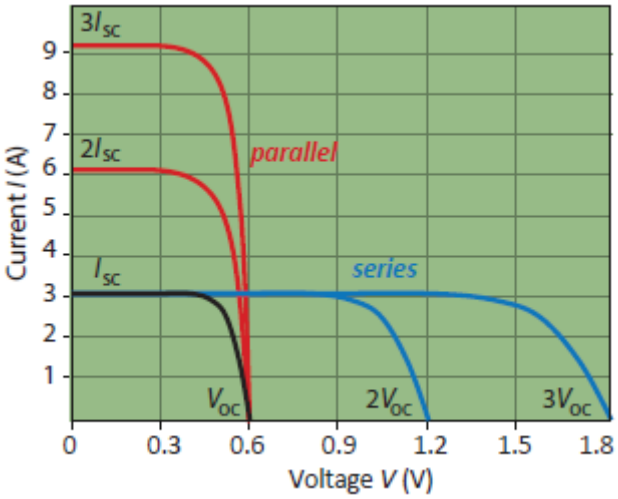

Figure 31: I-V characteristics curve of solar cells connected in series and in parallel (Jäger et al., 2014: 253)

One of the key findings that can be observed from the solar cell's I-V curve, is the solar cell's maximum power point (MPP) (Luque, 2011). The maximum power point is an operating point on the I-V curve that corresponds to the highest power output that the solar cell can generate at a specific current and voltage pair. The MPP is given by the equation $P = IV$. In Figure 32 the MPP is illustrated on the I-V curve and at the peak of the P-V curve.

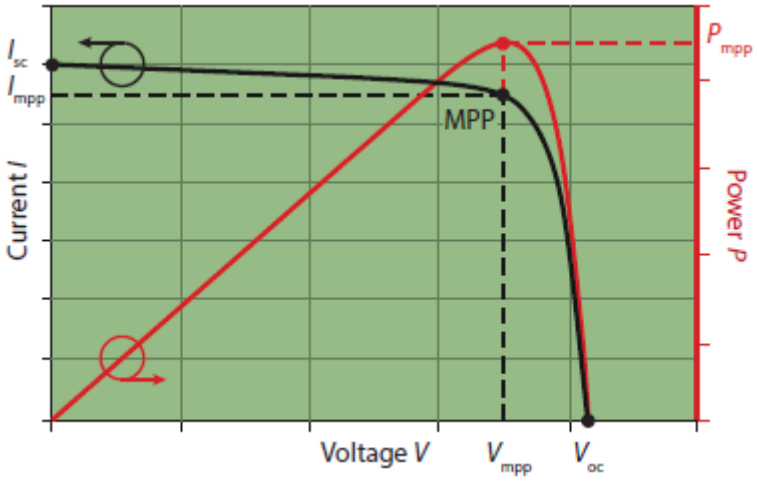

Figure 32: Maximum power point (MPP) of I-V curve and associated P-V curve (Jäger et al., 2014: 266)

If a solar module or array is connected directly to an electrical load, then the operating point is dictated by the load. Therefore, to obtain the maximum power output, the solar module has to be forced to reach the MPP (Luque, 2011). This is accomplished by either forcing the voltage of the solar module to the MPP on the I-V curve (V_{MPP}) or regulating the current to the relative MPP on the I-V curve (I_{MPP}). However, the MPP is dependent on ambient conditions such as irradiance levels and temperature. Therefore, as these ambient temperatures change, then so does the MPP on the I-V curve (Luque, 2011).

To ensure that the solar module continually operates at the MPP, a technique called maximum power point tracking (MPPT) must be implemented (Luque, 2011). MPP tracking can be accomplished in two different

methods, namely, indirect MPP tracking and direct MPP tracking. Indirect MPPT is accomplished by adjusting the operating voltage as the levels of irradiance changes. Direct MPPT is accomplished by Perturb and Observer (P&O), also known as Mountain-Climb algorithms or by Incremental Conductance method (Luque, 2011).

Another key factor to consider when examining the maximum output of a solar cell, is the Fill Factor. The Fill Factor (FF) is the ratio between the maximum power generated by the solar cell and the product of the open circuit voltage (V_{OC}) and the short circuit current (I_{SC}). The FF can be expressed by the following equation (Luque, 2011):

$$FF = \frac{P_{Max}}{V_{OC} I_{SC}}$$

Since the Fill Factor is a function of V_{OC} as seen in Figure 33, the FF does not drastically change as the V_{OC} is varied. However, the variation in maximum FF can be significant for solar cells made from different materials (Luque, 2011).

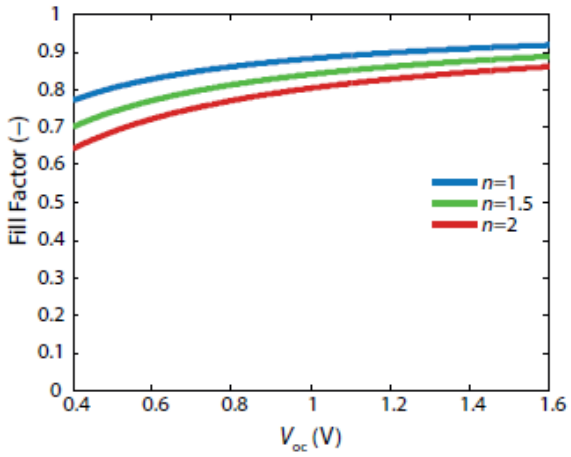

Figure 33: The FF as a function of Voc for a solar cell with ideal diode behaviour with different ideality factors of n (Jäger et al., 2014: 103)

2.3. Solar PV system Components

Even though the solar photovoltaic panel is the heart of a solar photovoltaic system, many other components are required for the system to operate correctly and generate electricity, namely the inverter, batteries and solar tracking (Luque, 2011).

These components defined in this section form part of the core components of a solar photovoltaic system. They offer the ability to convert the generated energy to South African electricity grid standards, improve energy generation performance in addition to energy storage capabilities.

2.3.1. Photovoltaic cell technology

Photovoltaic cell technology can be classified into three different categories, namely, crystalline silicon (c-Si), non-crystalline silicon used in thin-film and other non-silicon materials such as cadmium telluride (CdTe) or copper indium gallium selenide (CIGS) (Bergmann, 2002).

The crystalline silicon technology is manufactured as a wafer, which acts as a very thin 'slice' of semi-conductor material. The crystalline silicon technology can be differentiated into two different types of silicon wafers, namely, monocrystalline silicon and multi-crystalline silicon. Monocrystalline silicon is known as the single or solid crystalline due to it having an unbroken and continuous lattice structure. Whereas the multi-crystalline silicon consists of many small grains of crystalline silicon (Bergmann, 2002).

The second generation of solar cell technology is known as thin-film solar cell technology. This form of solar cells are made from semi-conductor layered films, much thinner than the wafers, and are sandwiched between a transparent conductive oxide (TCO) layer and the electrical back contact. The TCO layer, which usually is glass, stainless steel or polymer foils, is used to offer mechanical stability. The use of these TOC layers allow the thin-film solar cells to be flexible and be much thinner than the crystalline silicon solar cells (Bergmann, 2002).

Thin-film solar cells are not classified as crystalline silicon due to the solar cells consisting of different materials, namely, amorphous silicon (a-Si), cadmium telluride (CdTe), copper indium diselenide (CIS) and copper indium gallium selenide (CIGS). In several instances the efficiency of the thin film solar cells can be improved by layering with different types of materials. This type of thin-film technology is known as multi-junction solar cells (Bergmann, 2002).

If a low bandgap material is used, then a large quantity of photons are not used. However, if the number of bandgaps are increased, then the same quantity of photons can be used with less energy being wasted as heat. Therefore, as demonstrated in Figure 34, if more than one p-n junction is used then, larger portions of the solar spectrum can be used at the same time, thus improving the solar cells efficiency (Bergmann, 2002).

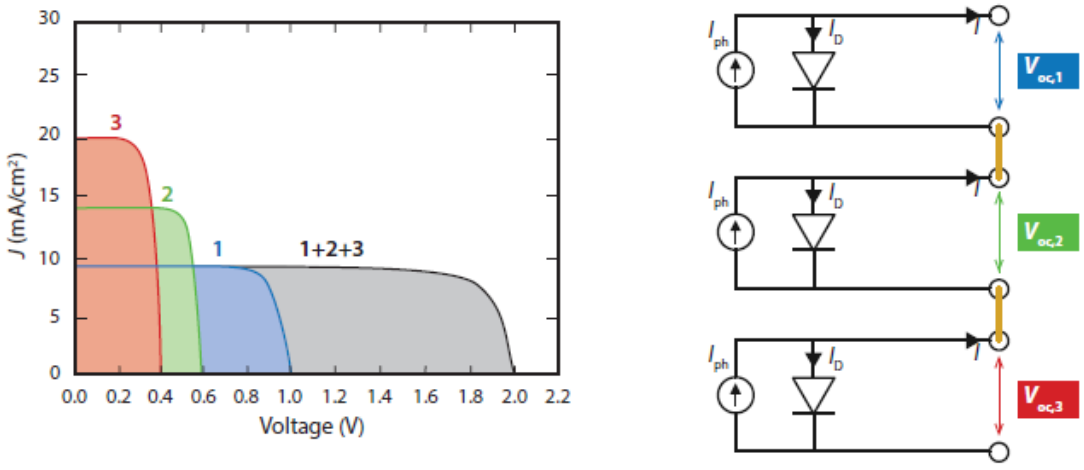

Figure 34: J-V Curve of a three junction solar cell (left) the equivalent circuit of the three junction material connected in series (right) (Jäger et al., 2014: 172)

Comparison of the crystalline silicon and non-crystalline silicon technologies can become very complex, as the crystalline silicon has proven its worth over many decades, whilst the thin-film technology is still relatively new.

From a manufacturing perspective, the thin-film solar cells require less material and less energy to be produced, therefore making them more cost effective in comparison to crystalline silicon technology. However, the reduced cost has a drawback of a lower energy generation efficiency, although the efficiencies of the thin film technology is gradually improving (Rome et. al., 2010).

Thin-film offers several advantages over the crystalline technologies including it's transparent conductive oxide layer which can be cut into any shape and size, allowing for thin film technology to be able to be installed anywhere, and is not limited to the standard sizes of the crystalline silicon wafers (Basha, 2012).

Thin film technology has a better temperature coefficient in comparison to crystalline silicon technology, thus making the thin-film technology less sensitive to high operating temperatures. Thin-film technology is also less sensitive to shading, since the thin film module is one long strip of material, and thin-film technology also operates more efficiently in low light intensity scenarios (Basha, 2012).

2.3.2. Inverters

One of the most essential components of a solar photovoltaic system is the inverter (Luque, 20110). The inverter is a power electronics device used to convert the direct current (DC) generated electricity to alternating current (AC) electricity which will be compatible with South African grid power requirements, such as a voltage of 220 V_{AC} and a frequency of 50 Hz.

In an ideal scenario, an inverter would draw the maximum amount of power generated from a solar photovoltaic panel whilst producing the least number of harmonics and at a power factor of unity. Even though this is not physically possible, the configuration of an inverter can be used to optimise the output of a solar photovoltaic system (Jäger et al., 2014).

Figure 35 illustrates the different inverter configurations that are utilised, each having their own advantages and disadvantages.

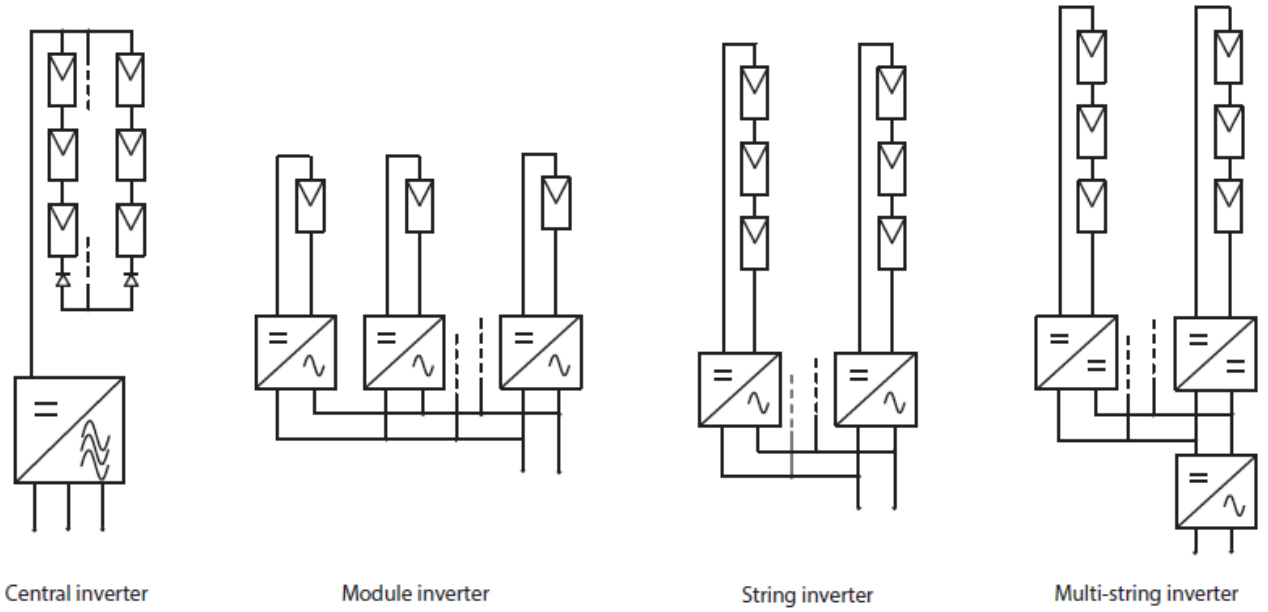

Figure 35: Illustration of the different inverter configurations (Jäger et al., 2014: 273)

A notable point is that the operational life span of a photovoltaic system inverter is approximately 10 years (New Southern Energy, 2020). The inverter will not cease to operate in year 11 but will stop operating at the manufacturers' specified efficiency rate. This will result in less energy being generated by the photovoltaic system and thus reducing the system's overall performance.

2.3.3. Batteries

Battery technology plays a vital role in energy storage, specifically in renewable energy systems (Jäger et al., 2014). Battery technology has the ability to solve the intermittency and unreliability faults that face renewable energy sources. In the case of solar photovoltaic systems, intermittence occurs both daily, with generation on during day light hours, and seasonally, with reduced irradiance levels in winter (Jäger et al., 2014).

There are many different types of energy storage technologies, each with their own advantages and disadvantages (Jäger et al., 2014). The most commonly used energy storage for solar photovoltaic systems are lead acid batteries, lithium ion batteries and redox-flow batteries. Lead acid batteries are the oldest and most mature technology used in the solar photovoltaic industry (Jäger et al., 2014).

Even though battery storage offers solutions to solar photovoltaic system's intermittence faults, batteries are not a core component of the solar photovoltaic system (NREL, 2015). This is due to the high cost of batteries as well as the lack of demand for 'off grid' solar photovoltaic systems (NREL, 2015).

Despite the growth of the solar photovoltaic industry, the current economics do not always justify the high installation costs of incorporating batteries (NREL, 2015). While solar photovoltaic system costs have fallen

rapidly and are expected to continue their downward trajectory, growth in this market is largely dependent on the demand by energy storage customers and as well as the involvement by suppliers (NREL, 2015) illustrated in Figure 36.

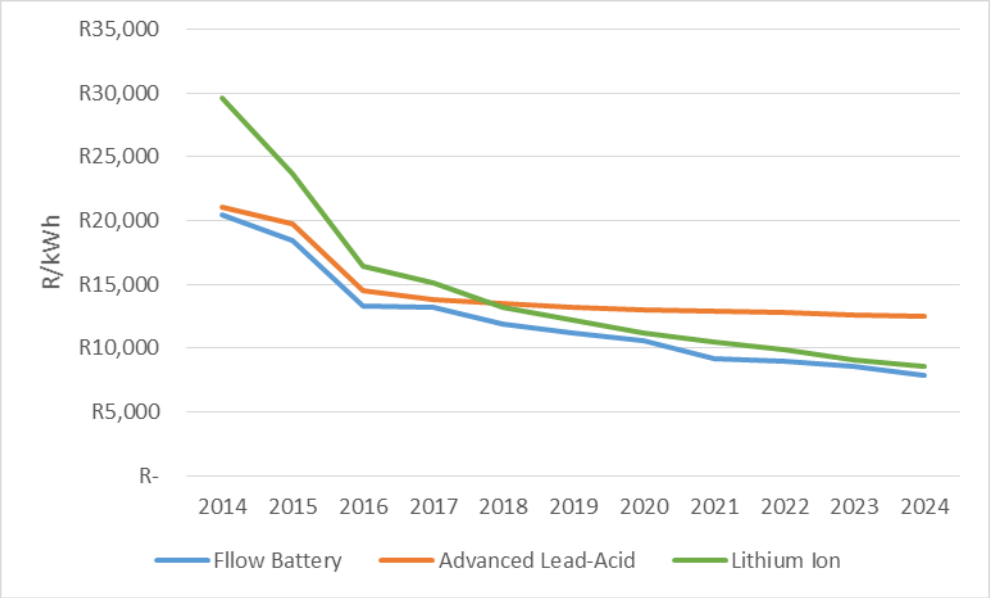

Figure 36: Energy system cost trends by technology, global averages: 2014–2024 (R13.17/US$) (NREL, 2015)

2.3.4. Photovoltaic module tracking systems

To ensure that a solar photovoltaic system generates at its maximum power point (MPP), a solar tracking system can be installed. Tracking the sun's movements can be accomplished by implementing three different tracking techniques, namely fixed-tilt, single-axis and two-axis tracking (Luque, 2011).

With fixed tilt, the solar photovoltaic modules are permanently fixed to a surface such as a roof top or a ground-mounted system that is a non-moving structure. In Cape Town, the optimal tilt angle of the solar modules is 30^{o} and in Johannesburg, it is 29^{o} (Jacobson & Jadhav, 2018). This allows for the solar modules to maximize the annual production of energy. However, this value will vary depending on the physical location of the solar photovoltaic system (Jacobson & Jadhav, 2018). Another factor to consider is that a slightly higher angle of orientation will result in more of an energy yield during the winter months and a lower angle will give a greater energy yield during the summer months (Masters, 2004).

During single-axis tracking, the solar photovoltaic modules are tilted along only one axis, being the north south axis and rotated from east to west (Luque, 2011). Therefore, single axis trackers only allow for the tracking of one angle. When the tilt angle is set equal to the local latitude, the optimum angle for annual yield is obtained. As the earth rotates at 15^{o}/hour, then the solar photovoltaic modules must follow the same trajectory, allowing for the modules to always directly face the sun throughout the day (Masters, 2004) as noted in Figure 37.

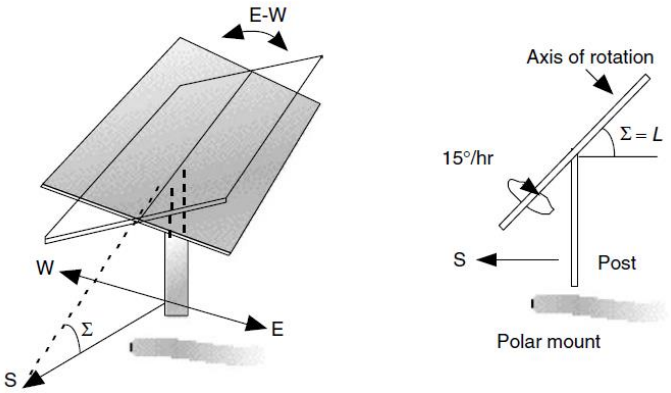

Figure 37: A single-axis tracking mount with east–west tracking (left) a polar mount has the axis of rotation facing south and tilted at an angle equal to the latitude (right)(Masters, 2004)

During two-axis tracking, solar photovoltaic modules are rotated from east to west as well as following the sun's angular height (Luque, 2011). Therefore, two-axis trackers track the sun both in azimuth and altitude angles as illustrated in Figure 38.

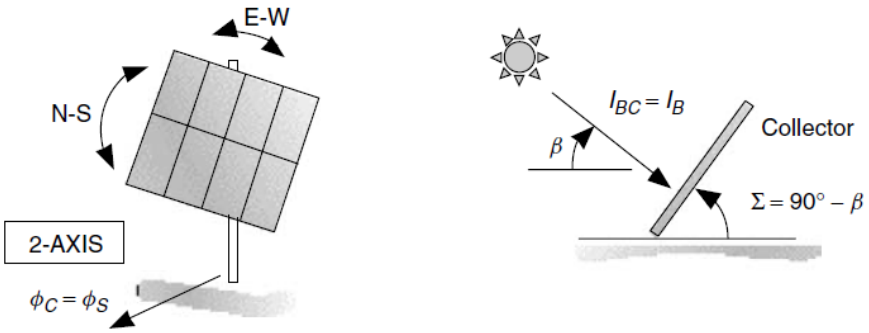

Figure 38: Illustration of two axis tracking angular relationships (Masters, 2004)

Comparing the efficiencies of the different tracking systems, two-axis trackers are known to have the best generation efficiency in cloudy days, whereas the single axis trackers operate as efficiently as a fixed tilt tracking system when exposed to the same cloudy conditions (Masters, 2004). The disadvantage of two axis tracking systems is the higher cost and higher mechanical complexity, which results in increased maintenance intervals and cost (Masters, 2004).

2.4. Solar System Faults

Several factors can impact a solar photovoltaic system's performance in addition to the system's lifespan. The following are the most common solar photovoltaic system faults that can affect a systems performance:

2.4.1. Shading

The output performance of a solar photovoltaic module can dramatically be reduced when even a small portion of the module is partially shaded. The shading can occur from any nearby object, such as a tree, a chimney, a neighbouring building or even a fallen leaf from a tree. By merely shading a single cell in a long string of cells, the output power of the module can easily be reduced by more than half (Masters, 2004).

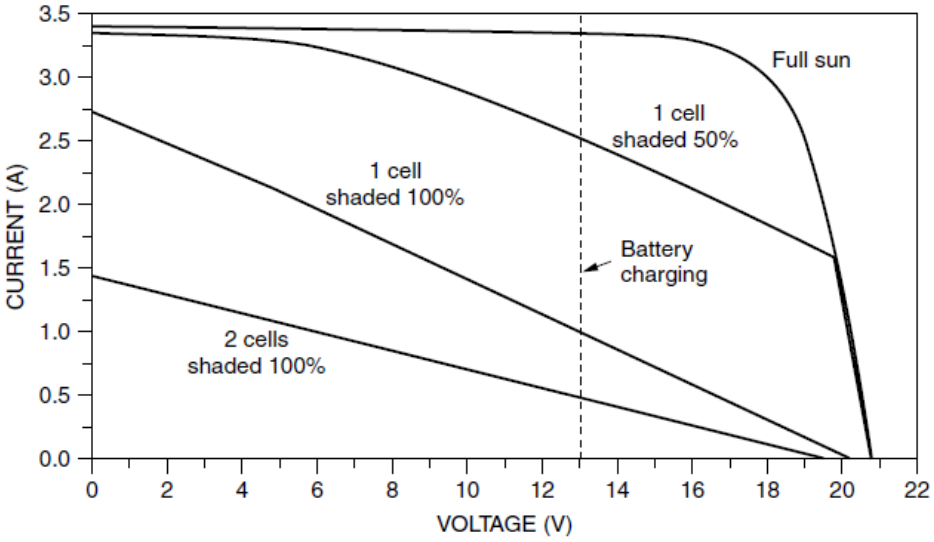

Figure 39: Effects of shading on the I-V Curve for a photovoltaic module (Masters, 2004)

In Figure 39 the effects of shading are clearly illustrated. The greater the shading, the poorer the system's performance. The 'dotted' line illustrates a typical voltage that the module would operate at when charging a 12V battery (Masters, 2004).

To prevent the effects of shading and preserve the performance of the photovoltaic module, bypass diodes connected in parallel to the modules are added to the photovoltaic system, either purposely installed by the module manufacture or by the system designer (Masters, 2004). The bypass diodes ensure that the current flows around the shaded module in the string. This improves the performance of the system as well as preventing hot spots from developing in the individual shaded cells (Masters, 2004).

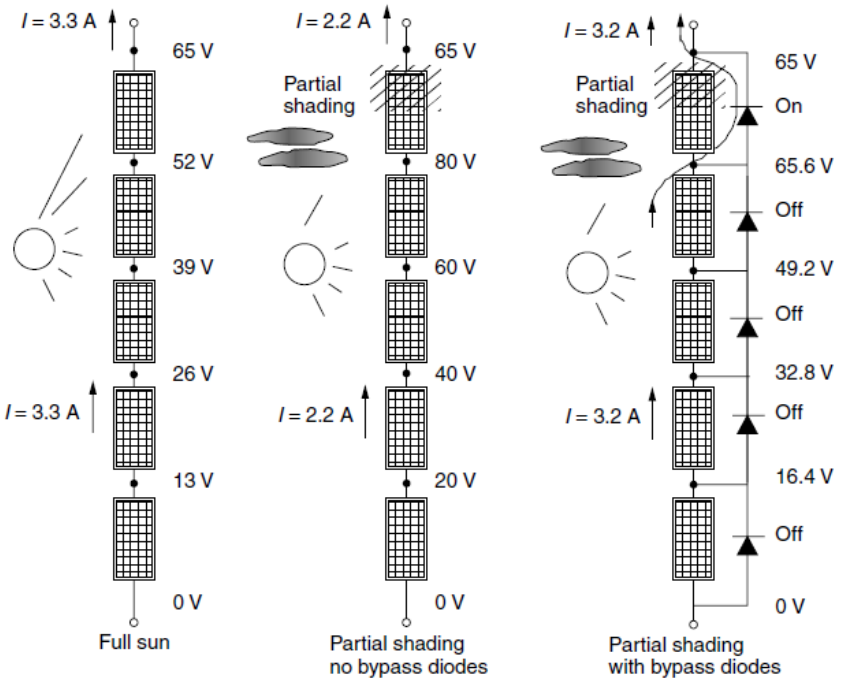

Figure 40: Illustration of bypass diodes preventing shading when modules are charging a 65V battery (Masters, 2004)

Figure 40 shows that a partially shaded module without a bypass diode will have a reduced current flowing to the load. However, with a bypass diode, the current is diverted around the shaded module, thus preventing the effects of shading (Masters, 2004).

However, when strings of modules are in parallel, a similar problem occurs when one of the strings is shaded. Instead of supplying current to the array, the shaded string will draw current from the rest of the array. The current drawn by the shaded string can be prevented by adding blocking diodes (isolation diodes) to the top of each string. This reverse current by the shaded string is prevented (Masters, 2004).

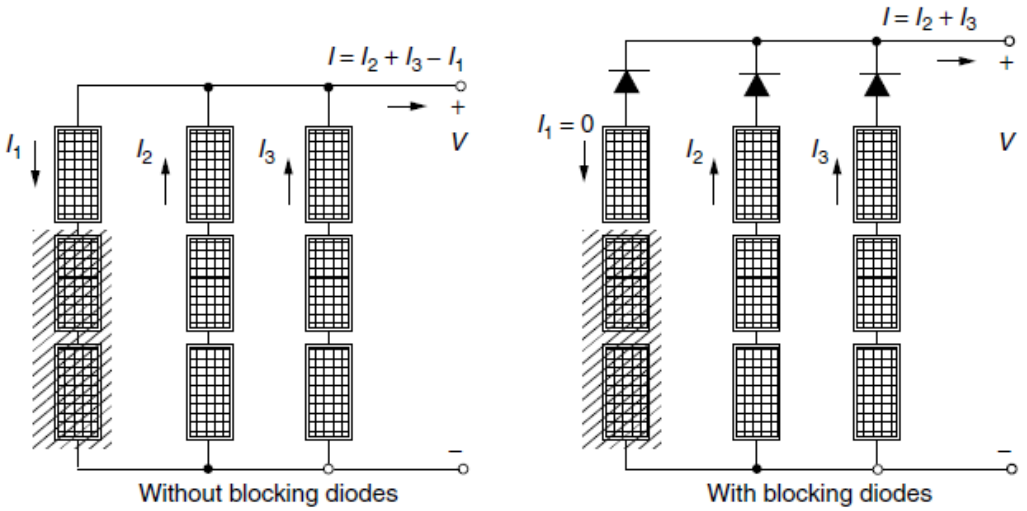

Figure 41: Illustration of blocking diodes used to prevent reverse current (Masters, 2004)

2.4.2. Hot Spots

Hot spots on solar photovoltaic modules are certain areas of the module that are at a much greater temperature (DuPont, 2017). The resulting effect of the elevated temperatures is a decrease in the localised performance of that portion of the solar photovoltaic module, which reduces the overall performance of the system as well as accelerating the degradation and reducing the lifespan of the module (DuPont, 2017).

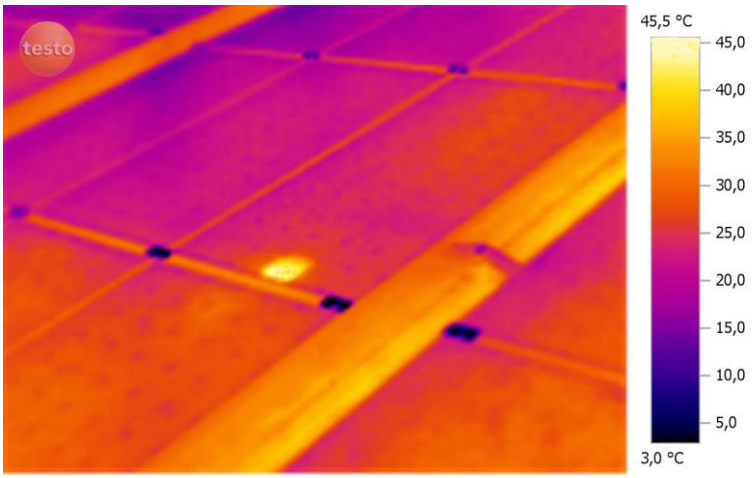

Figure 42: Illustration of hot spots on a solar photovoltaic module (Skelton, 2012)

Hot spots can be caused by many different factors and can be divided into two types of causes: functional and operational causes. The functional causes of hot spots are cell mismatch, in which cells connected in

series produce different quantities of current, and cell damage. Cell damage can occur when the silicon cell is subjected to stresses during lamination, handling or transportation (DuPont, 2017).

The operational causes of hot spots can occur from soiling as well as specific rooftop conditions (DuPont, 2017). Soiling is due to dirt, dust and other forms of contamination that can cover the solar cells and prevent the photons from colliding with the silicon cells as illustrated in Figure 43. Frequent cleaning of the solar module will prevent the effects of soiling on the solar photovoltaic module. The conditions of the rooftop can play a crucial role in causing hot spots, due to possible shading from growing vegetation (DuPont, 2017).

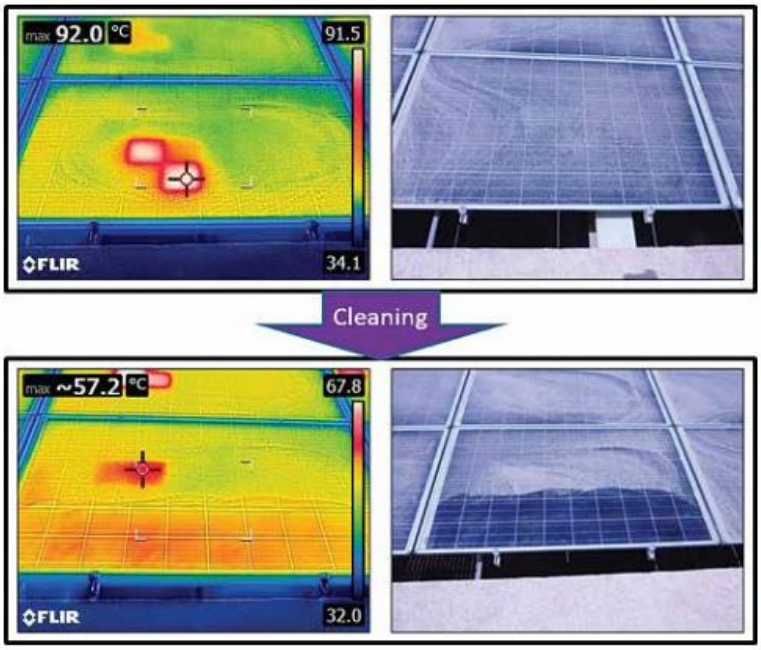

Figure 43: Reduction of hot spots once the solar photovoltaic panel has been cleaned (DuPont, 2017)

The impact of hot spots on a solar photovoltaic module not only reduces their performance, accelerates their ageing, but can also lead to fires, bubbling cracking of the back sheet illustrated in Figure 44.

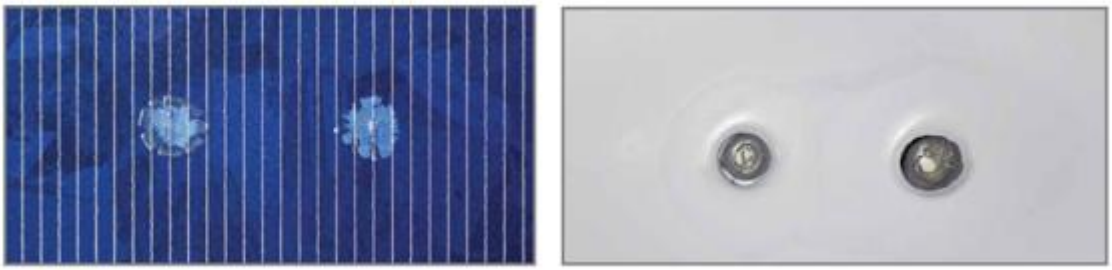

Figure 44: (Left) Bubbling and (Right) back sheet cracking (DuPont, 2017)

To mitigate the effects of hot spots and regulate the performance of the solar photovoltaic system, bypass diodes must be included in the system design.

2.4.3. Microcracks

Microcracks are not a rare occurrence and are inevitable, generally developing over time. This is due to the solar cells being manufactured with silicon sheets that are 700 times wider than they are thick. Additionally,

the solar cells are subsequently exposed to the environment for 20 to 30 years. Therefore, after years of daily thermal cycles and mechanical stresses, micro cracks are bound to develop (Kernahan et al., 2012).

Previously it was believed that microcracks were just a result of the manufacturing process and did not affect the performance of the solar cells. This is somewhat true since the performance of a solar cell in forward biased is not affected by microcracks. In the forward biased configuration, the electrons flow through the cell's junction as they should. All holes and electrons are in contact, there is no depletion zone, and the electric field is relatively small (Kernahan et al., 2012).

However, in the reverse biased configuration micro cracks affect the performance of the solar cell. Since the solar cell's junction is reverse biased the electrons and the holes oppose each other, thus forming a depletion zone. As the reverse potential difference increases, this gap becomes wider and the charge on the electrons on one side increases, the strength of the electric field across the depletion zone also increases. Thus, increasing the chance of hot spots, further micro-cracks and possible failure (Kernahan et al., 2012).

2.4.4. Snail Trails

Snail trails are a discolouration of a solar photovoltaic panel which only appears a few years after the panel has been installed (Dorala et al., 2016). The key cause of snail trails is due to the manufacturing process, from a result of defective front metallisation silver paste which can lead to moisture in the panel, resulting in oxidation between the silver paste and the encapsulation material EVA (Sharma, 2014).

Figure 45: Illustration of snail trails on a solar photovoltaic module (Sharma, 2014)

The formation of the snail trails can also cause microcracks to appear at the back sheet of the panel, thus reducing the solar module's performance (Dolara et al., 2016)

2.4.5. Temperature

Photovoltaics are designed and modelled for Standard Test Conditions (STC) of 25^{o}C and therefore, as mentioned in section 2.2.6 on the IV characteristic curve of photovoltaics, temperature plays a crucial role in a solar photovoltaic systems performance (Dash et al., 2015). A modules performance will be reduced if the module temperature is greater or less than 25^{o}C (Jäger et al., 2014) as illustrated in Figure 46.

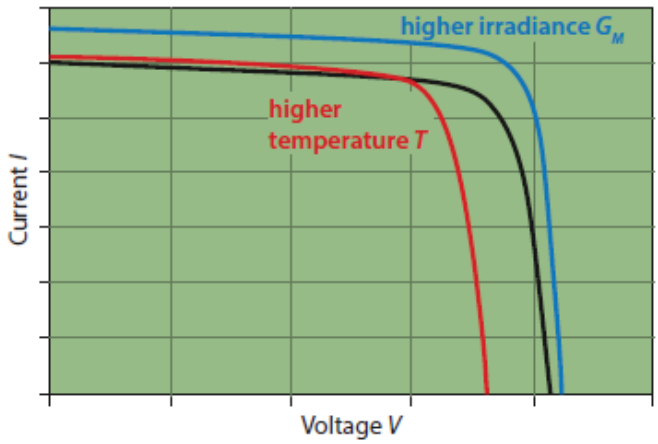

Figure 46: Effect of a change in module temperature (Jäger et al., 2014)

The effects of a solar module's temperature as it changes from the STC of 25°C can be expressed by the following equation (Jäger et al., 2014):

$$\eta(T_M, G_{STC}) = \eta(STC) + \frac{\partial \eta}{\partial T}(STC)(T_M - 25°C)$$

Where η = Efficiency

$\frac{\partial \eta}{\partial T}$ = Efficiency temperature coefficient

T_M = Module Temperature

G_{STC} = Irradiance at STC

2.4.6. Other factors

There are more meteorological factors to consider when evaluating the performance of a solar module. One of these factors is the wind speed, and that too affects the solar module's performance.

Since wind can cool objects, it counteracts the performance issues brought on by increases in a module's surface temperature. Therefore, the greater the wind speed, the greater the cooling ability (Jäger et al., 2014).

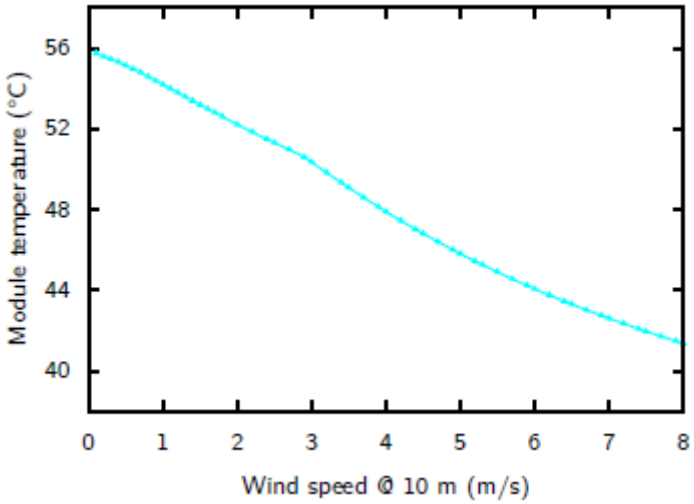

Figure 47: Effects of wind speeds and module temperature reduction (Jäger et al., 2014)

Figure 47 illustrates the effects wind speeds have on influencing the surface temperature of a solar module. As there is an increase in wind speed, there is a correlating overall increase in the heat transfer. For this study it was assumed the ambient temperature was 25^{o}C, a clear sunny day, the module was at a height of 10 m and that there was a fixed radiation of 1 000W/m2 (Jäger et al., 2014).

2.5. Types of Solar Photovoltaic Systems

The complexity of solar photovoltaic systems is relative to the system's application and requirements. The simplest form of a solar photovoltaic system consists of a photovoltaic module and a DC load. However, as the complexity of the systems requirements increase, so does the complexity of the system. There are many different types of solar photovoltaic systems including grid-tied systems, off-grid systems and hybrid systems (Luque, 2011).

2.5.1. Off-grid solar photovoltaic systems

Off-grid systems, also known as stand-alone systems, are solar photovoltaic systems that are solely powered by solar energy and no other form of energy, such as utility grid electricity or diesel-powered electricity from a generator (Jäger et al., 2014). These off-grid systems can consist of solar photovoltaic modules and a load when there is no requirement for energy storage (Jäger et al., 2014).

However, if there is a load during hours in which the solar modules cannot generate electricity, i.e. at night, then energy storage components are required, such as batteries and charge controllers (Jäger et al., 2014). The use of a charge controller ensures that the batteries lifespan is not reduced during the charging process. The charge controllers switch off the photovoltaic modules when the batteries are fully charged and occasionally switched off the load to ensure that the batteries are not discharged below a pre-determined charge limit (Jäger et al., 2014).

2.5.2. Grid-tied solar photovoltaic systems

Grid-tied systems are solar photovoltaic systems that are connected to the utility grid via inverters that convert the generated DC electricity to AC (Luque, 2011). This type of solar photovoltaic system is the most common used throughout the solar photovoltaic market. This is due to the lack of expensive energy storage batteries, thus making this system the cheapest configuration (GreenCape, 2017).

Another incentive to connect to the grid is the offing of a Small Scale Embedded Generation (SSEG) tariff, in which excess energy generated can be fed back into the grid and the owner of the solar photovoltaic system is paid by the local municipality for the excess energy (GreenCape 2017).

The disadvantage of a grid-tied system occurs when the utility grid fails, the inverters implement a safety feature that shutdowns the solar photovoltaic system, thus ceasing all forms of electricity generation (NRS, 2017). This is implemented to prevent the flow of electricity back into the grid whilst technicians are working on the electrical infrastructure.

2.5.3. Hybrid solar photovoltaic systems

Hybrid systems consist of a combination of solar photovoltaic modules and an additional electricity supply that does not include grid electricity, the most common being a diesel generator (Jäger et al., 2014).

The disadvantage of a hybrid system is that it requires a more sophisticated control system in comparison to an off-grid or grid-tied system. As the battery charge levels fall below a pre-determined set point, then an additional power source, such as a generator, must start immediately and supply the system with electricity. Alternatively, when the battery charge level reaches an adequate state of charge, then the generator must shutdown (Jäger et al., 2014).

2.6. Mounting Configurations of Solar Photovoltaic Systems

One of the most influential factors of solar photovoltaic systems is their versatility to be installed anywhere, on condition that the photovoltaic cells can absorb the sun's energy. The result of this versatility is that the two most common mounting configurations of solar photovoltaic systems are rooftop-mounted systems and ground-mounted systems (Luque, 2011).

Each of the two different mounting configurations has its own strengths and weaknesses. However, several factors are key in determining which type of mounting configuration is feasible at a specific location (Dabrowski, 2014). Some of these key factors include the cost of the system, the available space or surface area, the orientation, the operation and maintenance (O&M), the obstacle shading, roofing structure, the physical electrical infrastructure, health and safety risks, access to the location, and the aesthetics of the system (Dabrowski, 2014).

Figure 48: Ground-mount carport system at Old Mutual Park, Cape Town (left) and rooftop mounted system at Cape Quarter, Cape Town (right) (WCG, 2016) (Solar Future Energy, 2017)

These key factors can play a crucial role in whether a rooftop mounted system is feasible or not. An example of such an instance is if a building has an East-West orientation or if the roofing structure is not structurally sound or consists of asbestos material. In an instance such as this, a ground-mounted system can be considered, if there is sufficient unused area available.

The key positive factors of a ground-mounted system are that the orientation of the solar panels can be positioned at the most efficient orientation to meet the best performance of the system. In addition to the orientation, the structure of the ground-mounted system can be constructed to be as strong and stable as the system design engineer sees fit.

Despite all these factors, the most important detail to be considered when comparing the two different configurations of photovoltaic systems is the generation performance of the systems. The performance of the system plays a significant role in the payback period of the solar photovoltaic system. However, two contrasting types of payback periods must be considered, namely the financial payback period and the energy payback period.

2.7. Performance of Rooftop and Ground-mounted Photovoltaic Systems

The comparative performance of the two solar photovoltaic system configurations is an interesting and widely discussed topic. This is because there has been scarce research internationally and locally comparing the performance of the two configurations being exposed to similar locations. By exposing both configurations to the same ambient and irradiate environment, one would be able to compare 'like with like' and thus conclude which configuration will generate the greater yield of energy.

An extensive review of published literature revealed that such a comparison has only been conducted once before in 2015 by Remo Alessio Malagnino from the Department of Agricultural and Food Sciences at the University of Bologna. Malagnino published an article in which three different solar photovoltaic systems, installed at the same dairy cattle farm, were investigated. Two of the three systems were both 99 kW_p rooftop

mounted systems and the third system was a 480 kW_p ground-mounded system. The results of the investigation were that the best performing system was the ground-mounted photovoltaic system, which too corresponded with the PVGIS simulated results (Malagnino, 2015).

2.8. Economics of Solar Energy Systems

The economics of a solar energy system differs largely from that of a fossil fuel energy system. This is due to solar systems having a relatively large initial cost, but much lower operational cost during their lifetime. Therefore, a life cycle cost must be adopted to compare the feasibility of installing a solar energy system (Goswami, 2015).

A life cycle cost takes into account the initial capital costs as well as the year-to-year operational costs during the system's lifetime. However, other financial factors also have to be considered including an interest charge if capital was financed, insurance, tax benefits and net metering (Goswami, 2015).

The financial performance parameters most commonly used for comparing the economic feasibility of solar systems are the payback period and the internal rate of return (IRR) (Goswami, 2015). The payback period, which is the length of time required for the investor to recover the cost of the initial investment, is more commonly used (USDOE, 2014).

Determining the financial payback period of a solar system is not an exact science and has to be accomplished on a case by case basis. This is due to the location's solar irradiation levels, the applied electricity tariff, and the size of the photovoltaic system (USDOE, 2014). The Levelised Cost of Energy (LCOE) of the solar system can be determined by comparing the life cycle cost of the solar system and the total amount of energy generated during the life span of the system. The LCOE can be calculated by the following equations (USDOE, 2014):

$$LCOE\ \ (Rands/kWh) = \frac{Total\ life\ cycle\ cost}{Total\ lifetime\ energy\ production}$$

In 2004, the US Department of Energy completed a study which compared the payback period of two solar photovoltaic system configurations, one being a ground-mounted system and the other, a rooftop mounted system (USDOE, 2004). It was concluded that, the ground-mounted system had a shorter payback period. This was due to the improved system performance, which was linked to the improved airflow and cooling of the solar modules (USDOE, 2004).

2.9. Financing Mechanisms

Financing a solar photovoltaic system is a key and integral part of the implementation process.

Currently, in South Africa's solar photovoltaic market, there are two different types of procurement options: system procurement and service procurement. Each procurement option has its own strengths and

weaknesses and are both proposed to the client by the EPC or ESCO which are evaluated on a separate case by case basis.

The system procurement option involves a client investing their own capital at a once-off lump sum investment to purchase the solar photovoltaic system upfront. The positives of this system are that solar photovoltaic system ownership solely belongs to the client; it is a straightforward asset procurement and financing transaction (a value-added asset acquisition). Another incentive for this option is that the client will be able to apply for SARS 12B tax benefit, which is an accelerated asset depression for the first year of the system's operation.

The negatives of the system procurement option are that it comes with a higher financial risk to the client due to the entire capital expenditure (CAPEX) of the system being invested upfront as a lump sum. Another negative issue is that most solar photovoltaic systems takes six to eight years to be fully paid off. The resulting effect is that the client will sit with a negative balance on their books until the system has been fully paid off (i.e. the client will only start seeing a return after year eight).

The service procurement option is the second procurement option offered by EPCs and ESCOs and requires no upfront capital investment from the client. In theory, the client gets a solar photovoltaic system 'for free' since the photovoltaic system is financed by the EPC or the ESCO. The resulting effect is that the clients save money from day one of the installation. The client will purchase the electricity at a reduced rate, in comparison to the local municipality or Eskom, achieve budgetary goals and achieve sustainability targets with minimal risk.

The negatives associated with the service procurement option is that, since the system is not financed by the client, the client must sign a long-term, typically ten to fifteen-year power purchase agreement (PPA), with the system installer. Additionally, since the ownership of the solar photovoltaic system lies with the installer, the 12B tax benefit is only relevant to the owner of the system, hence the system installer. Several contracting options do exist such as 'lease to own' or 'rent to own' agreements. These agreements offer a timeline in which the client can purchase the solar photovoltaic system from the installer once the installer has recovered their initial investment. The usual practice is after year 10 or 15 of system operation the client it able to purchase the solar photovoltaic system.

Both these two procurement options have great potential to improve the renewable energy market and stimulate solar photovoltaic uptake. However, both these options are still heavily reliant on acquiring large amounts of financing, which inevitably relies on large financial institutions such as banks. South African banks are gatekeepers to the solar photovoltaic industry, and by not offering readily available financing for solar photovoltaic, are crippling the market.

Currently, all the large financial institutions offer financing for solar photovoltaic system. However, the majority do not offer specific financing products for renewable technology. Instead, banks use the same

financing mechanisms and products as those used for home loan and property financing where the loan period is usually for eight years or less. This significantly impacts the renewable market because some photovoltaic systems are only profitable after 10 years and the equipment has a lifespan of 25 to 30 years.

Due to the lack of financing options in South Africa, local insurance companies and international investors are looking overseas at other financing options that can be implemented in the South African market to stimulate the solar photovoltaic industry in the country. Currently, two interesting financial models are being investigated for adoption in South Africa's market, namely the Property Assessed Clean Energy (PACE) financial model (Muringathuparambil, 2019), the Pay As You Save (PAYS) financial model (The GreenAge, 2017) and a third financing model that has recently been adopted by a company named The Sun Exchange.

The Sun Exchange financing model has a similar funding mechanism as a crowdfunding model in the way that projects only go ahead once all the investment has been raised. The model works through an individual being able to purchase the solar cells of a solar photovoltaic system which is used to power business and communities. Once the individual has purchased the solar cells and the system has been installed, the individual can lease his/her solar cells to the building, which generates electricity for the building, and the building purchases the generated electricity from the individual's solar cells. Thus, creating a passive stream of income for the individual powered by the sun (The Sun Exchange, 2017).

The Property Assessed Clean Energy (PACE) financial model was originally developed in the United States and is currently active in 33 states within the US (PACENation, 2017). PACE is a mechanism that offers long-term funding for up to 20 years and 100% funding of the project's installation costs, with monthly repayments less than the energy savings. The key difference with the PACE model compared to other models is that it is linked to the property and not to an individual. The monthly repayments are then added to the property tax, thus the monthly property rates, from a South African point of view. Therefore, the financing is linked to the building and not the owner of the building. Once the building is sold, the solar photovoltaic system remains on the building as well as the PACE financed debt. After the 20-year period the ownership of the solar system remains with the building and the monthly property rates are reduced, due to no PACE financing repayments. The disadvantage of the PACE financing mechanism is that it requires buy-in from the local municipality (PACENation, 2017).

The Pay As You Save (PAYS) financial model is a model largely used throughout Europe, the United Kingdom and Australia (The GreenAge, 2017). The PAYS mechanism operates exactly the same as a South African service procurement option with a PPA, in which the installer fully covers the cost of the system, sells the electricity to the client at a reduced rate and retains ownership of the solar photovoltaic system until the initial system cost has been fully paid off (The GreenAge, 2017).

3. Photovoltaic System Analysis

3.1. Introduction

For the analysis of the performance of ground-mounted and rooftop mounted solar photovoltaic systems, three separate solar photovoltaic systems were investigated: two ground-mounted systems and one rooftop mounted system. The two ground-mounted photovoltaic systems are located at South African Renewable Energy Business Incubator (SAREBI) and Stripform Packaging, whilst the rooftop mounted photovoltaic systems is located at SA Tyre Recyclers.

The SAREBI and the SA Tyre Recyclers systems are both located on the same premises but are electrically isolated with separate meters and distribution boards.

Figure 49 illustrates the distance between the photovoltaic system at Stripform Packaging, which is at a distance of 1.7 kilometres, and the photovoltaic systems at SAREBI and SA Tyre Recyclers. Since all the photovoltaic systems are located within a 5-kilometre radius, the metrological and environmental impacts affecting each photovoltaic system individually will be minimised. Thus, it can be assumed that each system is exposed to the same irradiation and metrological conditions.

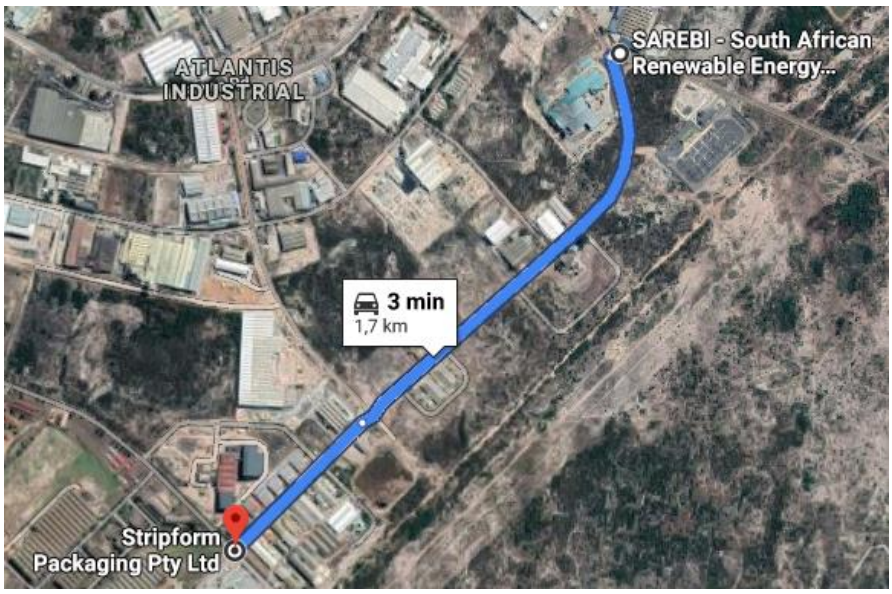

Figure 49: Distance between SAREBI and Stripform Packaging (GoogleEarth, 2019)

3.2. Solar photovoltaic site description

3.2.1. SAREBI photovoltaic system

The location of the ground-mounted photovoltaic solar system is at the South African Renewable Energy Business Incubator (SAREBI) which is situated in Atlantis, WC .

Figure 50: Aerial photo of SAREBI ground-mounted structure (Google Earth, 2019)

The site properties of the SAREBI location are the following:

Coordinates:	33° 35' 14.14" S, 18° 29' 31.58" E
Address:	9 Novel Building
	Cnr John Dreyer and Neil Hare Road
	Atlantis, 7349

Prior to the installation of the photovoltaic system at SAREBI, the property owner had the intention of building a carport for his tenants. However, SAREBI suggested that a carport consisting of photovoltaic panels be constructed instead of a carport consisting of shade cloth.

Due to the projects critical path, the construction of the photovoltaic system's structure had to be built first before the rest of the carport structure could be constructed. This was to ensure that the system would be generating energy before the entire carport was completed. Figure 51 illustrates the completed 10 kW_p carport ground-mounted photovoltaic system installation at SAREBI.

Figure 51: Completed installation of the photovoltaic system at SAREBI

It must be noted that at the area of the carport when the photovoltaic panels are situated, the panels act as the roofing structure, whereas the corrugated steel acts as the roofing structure for the rest of the carport.

Figure 52: Photovoltaic panel acting as the roofing structure

The installation and commissioning of the solar photovoltaic system at SAREBI was completed in December 2017.

3.2.2. SA Tyre Recyclers photovoltaic system

The location of the rooftop mounted photovoltaic solar system is at the South African Tyre Recyclers which is situated in Atlantis,WC.

Figure 53: Aerial photo of SA Tyre Recyclers (Google Earth, 2019)

The site properties of the SA Tyre Recyclers location are the following:

Coordinates:	33° 35' 09.04" S, 18° 29' 35.00" E
Address:	Novel Building
	Harry Alexander Cres
	Atlantis, 7349

The solar photovoltaic system installed at SA Tyre Recyclers is a rooftop mounted system, which was installed on 1 250 m^2 of SA Tyre Recyclers's available rooftop as seen in Figure 54.

Figure 54: Drone footage of the completed photovoltaic system at SA Tyre Recyclers

Figure 55 illustrates a closer view of the rooftop mounted photovoltaic system.

Figure 55: Mounting of the photovoltaic modules at SA Tyre Recyclers

The installation and commissioning of the solar photovoltaic system at SA Tyre Recyclers was completed in June 2018.

3.2.3. Stripform Packaging photovoltaic system

The location of the ground-mounted photovoltaic solar system is at Stripform Packaging, which is situated in Atlantis, Western Cape.

Figure 56: Aerial photo of the Stripform Packaging solar photovoltaic system (Google Earth, 2019)

The site properties of the Stripform Packaging location are the following:

Coordinates:	33° 59' 90.02" S, 18° 48' 09.95" E
Address:	20-21 Neil Hare Rd
	Atlantis, 7349

Prior to the installation of the photovoltaic system at Stripform Packaging, the land was open and unused. Figure 57 illustrates the available area located behind the Stripform Packaging facility before the ground-mounted structure was constructed.

Figure 57: Before the solar photovoltaic system was constructed at Stripform Packaging

Figure 58 illustrates the completed 20 kW_p ground-mounted system at Stripform Packaging. It must be noted that the ground underneath the photovoltaic system is paved to prevent future erosion from occurring as the soil in Atlantis is very sandy and Atlantis is prone to regular windy conditions.

Figure 58: Completed installation of the solar photovoltaic system at Stripform Packaging

The installation and commissioning of the solar photovoltaic system at Stripform Packaging was completed in July 2018.

3.3. Solar photovoltaic system specifications

3.3.1. SAREBI photovoltaic system

3.3.1.1. Photovoltaic modules

The ground-mounted solar photovoltaic system consists of 30 Canadian Solar CS6U-325P modules. The key features of the Photovoltaic panel is that Canadian solar is a Tier 1 manufacturer, the panel is designed for high voltage systems up to 1 500 V_{DC}, Saving on BoS costs, cell efficiency of up to 18.8%, outstanding performance at low irradiance averaging relative efficiency of 96% form an irradiance of 100W/m^2 to 200 W/m^2 (AM 1.5, 25^{o}C).

Table 3: Canadian Solar CS6U-325P datasheet (Canadian Solar, 2018)

CS6U-325P Photovoltaic Panel				
General Specification	**Technical Data**		**Electrical Data (STC*)**	**Technical Data**
Cell Type	Poly-crystalline		Nominal Max. Power (Pmax)	325 W
Dimensions, Weight	1960 x 992 x 40 mm, 22.4 kg		Opt. Operating Voltage (Vmp)	37.0 V
Linear power output warranty	25 years		Opt. Operating Current (Imp)	8.78 A
Product warranty	10 years		Open Circuit Voltage (Voc)	45.5 V
Temperature Characteristics			Short Circuit Current (Isc)	9.34 A
Temperature Coefficient (Pmax)	-0.41 % / °C		Module Efficiency	16.72 %
			Operating Temperature	-40°C ~ +85°C
Temperature Coefficient (Voc)	-0.31 % / °C		Max. System Voltage	1500 V (IEC) or 1500 V (UL)
Temperature Coefficient (Isc)	0.053 % / °C		Max. Series Fuse Rating	15 A
Nominal Operating Cell Temperature	45 ± 2 °C		Application Classification	Class A
			Power Tolerance	0 ~ + 5 W

*Under Standard Test Conditions (STC) of irradiance of 1000 W/m2, spectrum AM 1.5 and cell temperature of 25°C.

3.3.1.2. Photovoltaic system configuration

The ground-mounted solar photovoltaic system was designed to have the following angular inclination and orientation:

Table 4: Summary of SAREBI photovoltaic module configuration

Details	Technical Data
Tilt	15^{o}
Azimuth	-19^{o}
Photovoltaic surface area	59.5 m^2

3.3.1.3. Inverter

The inverter used for the ground-mounted photovoltaic system is a Schneider 20 kW Conext TL 20000E inverter.

Figure 59: Schneider Contex TL 20000E Inverter (Schneider Electric, 2018)

The key features of the 20 kW inverter is that it delivers high yields, has high conversion efficiencies of greater the 98% and offers design flexibility and compatibility with many photovoltaic modules. This is due to its multi-string capabilities and wide input voltage range.

Table 5: Schneider Contex TL 20000E datasheet (Schneider Electric, 2018)

Schneider Contex TL 20000E Inverter	Technical Data
General Specifications	
Product dimensions (h x w x d), weight	96.0 x 61.2 x 27.8 cm, 67.2 kg
Warranty (Standard/Optional	5 / 10 years
Input (DC)	
MPPT voltage range	350 - 800 V
Operating voltage range	200 - 1000 V
Max. input voltage, open circuit	1000 V
Nominal input power	20.8 kW

Output (AC)	
Nominal output power	20 kVA
Max. AC output power	21.0 kVA
Nominal output voltage	230 / 400 V, three-phase
AC voltage range	184 - 276 V
Frequency, Frequency range	50 / 60 Hz, +/- 3 Hz
Max. output current	32.0 A
Total harmonic distortion	< 3 %
Power factor (adjustable)	0.8 lead to 0.8 lag
Efficiency	98.0 %

The reasoning for the installation of the 20 kW Schneider inverter instead of a 10 kW inverter is to allow for future expansion to the SAREBI system.

3.3.1.4. Cabling

The selected cabling for both the DC of the solar photovoltaic systems was KBE Solar cables. KBE Solar cables were selected due to their ease of install capability as well as their use indoors, outdoors, in commercial and industrial as well as agricultural installations and locations. The cables are suitable for use in applications and devices containing protective insulation (safety class II) (KBE Elektrontechnik, 2018).

Table 6: KBE Solar Cable datasheet (KBE Solar, 2018)

KBE Solar 730600015003UU	Technical Data
Conductor	E-Cu tinned acc. IEC 60228, Class 5
Insulation Material	Crosslinked Special Polyolefin
Temperature range, Max	-40°C to 90°C, 126°C
Voltage range, Max	U_0/U = 600 / 1 000 V_{AC}, 1 800 V_{DC}
Resistance	3.390 mΩ / m
Cross sectional area	6 mm^2
Insulation thickness	0.5 mm
Jacket thickness	0.5 mm
Outer diameter	5.60 mm
Weight	80 kg/km

The selected cabling for both the AC side of the solar photovoltaic systems was Aberdare SWA 4mm^2 4 core copper cable

Figure 60: Aberdare SWA 4mm^2 4 core cable (Aberdare Cables, 2018)

Table 7: Aberdare SWA 4mm^2 4 core cable datasheet (Aberdare, 2018)

Aberdare SWA 4mm2 4 core cable	Technical Data
Conductor	4 core tinned stranded copper, Class 5
Insulation Material	PVC sheathed
Temperature range	-15°C to 70°C
Voltage range,	600 / 1 000 V_{AC}
Resistance	5.52 Ω / km

Cross sectional area	4 mm^2
Insulation thickness	2.91 mm
Outer diameter	18.39 mm
Weight	762 kg/km

3.3.1.5. Wiring Diagram

Figure 61 displays the ground-mounted solar photovoltaic system installed at SAREBI, consisting of two separate strings, each consisting of fifteen (15) solar photovoltaic panels, which are both connected to the Schneider inverter.

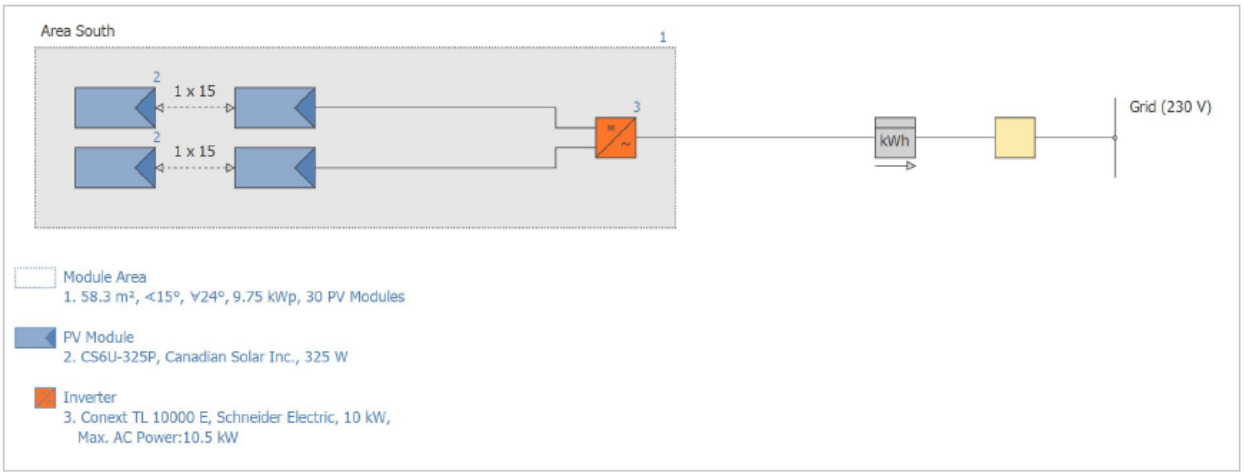

Figure 61: Wiring Diagram of the SAREBI ground-mounted solar photovoltaic system (PVSol, 2017)

3.3.1.6. Ground-mounted structure

The structure of the ground-mounted solar photovoltaic system is made up of galvanised S275 mild steel. Figure 62 illustrates the side view of the carport structure.

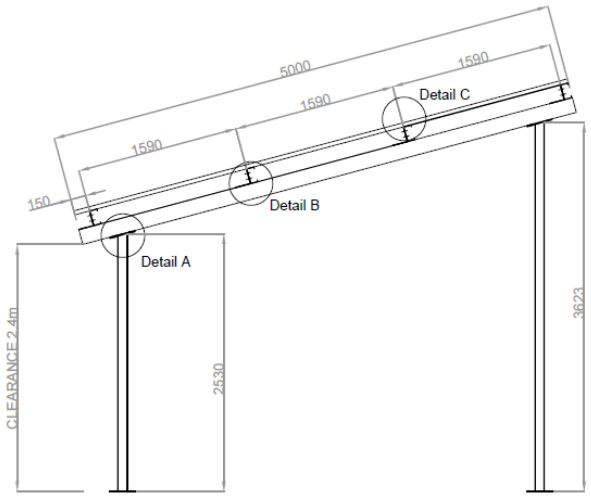

Figure 62: Side view of the ground-mounted structure

Figure 63 illustrates the front view of the carport structure, with a South facing orientation.

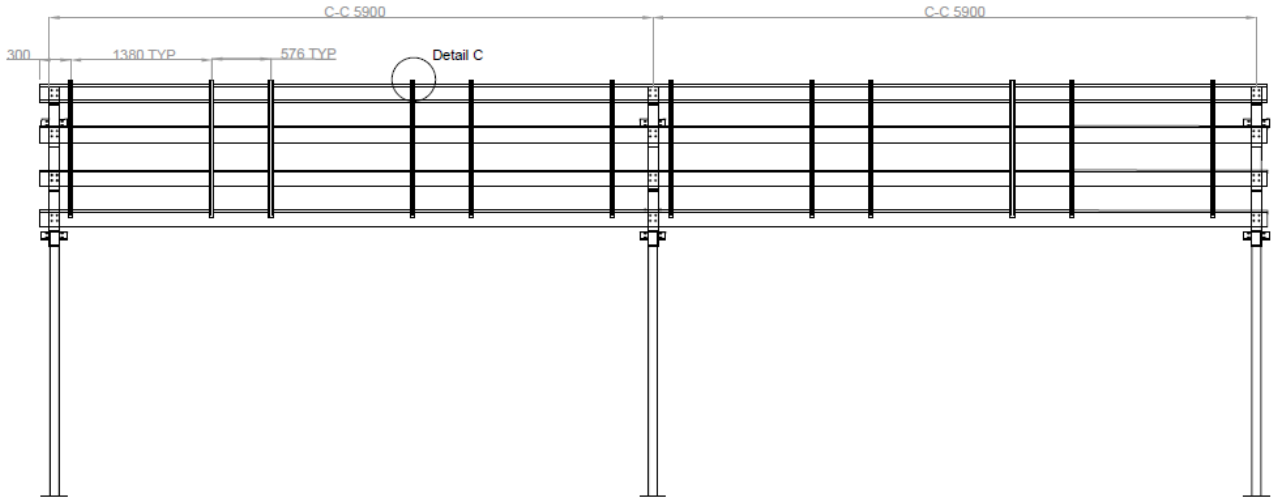

Figure 63: Front view of the ground-mounted structure (facing south)

3.3.1.7. Mounting system

The mounting system used in the ground-mounted solar photovoltaic system was the Renusol mounting system.

Figure 64: Renusol MS+ mounting system (Rensol, 2018)

Renusol mounting system consists of non-penetrative, mounting brackets, fastening material and module clamps, all made of stainless-steel material with a 10-year product guarantee.

Figure 65: Renusol RS Clamp and Rensol MS mount (Renusol, 2018)

The clamps, as shown in Figure 65, are specifically designed to cause no damage to the photovoltaic modules and to have a sound connection.

3.3.1.8. Monitoring

The web-based monitoring of the solar photovoltaic system's performance is accomplished by the use of a Solar-Log 1200 and the online web-based platform caller Solar-Log WEB Enerest as depicted in Figure 66.

Figure 66: Solar- Log 1200 (Solar-Log, 2018) and Solar-Log Enerest (Solar-Log, 2018)

The Solar-Log 1200 is specifically designed for small domestic installations and medium-sized solar photovoltaic plants, perfect for the 10 kWp photovoltaic system.

The onsite metering is recorded by municipal approved Elster A1140 energy meters, which are used to monitor and record the total energy consumed by the SAREBI building as well as the excess energy fed back into the grid.

3.3.2. SA Tyre Recyclers photovoltaic system

3.3.2.1. Photovoltaic modules

The rooftop mounted solar photovoltaic system at SA Tyre Recyclers consists of 700 JA Solar JAP72S-01-330-SC modules.

Table 8: JA Solar JAP72S-10-330-SC Solar datasheet (JA Solar, 2018)

JAP72S-10-330-SC Photovoltaic Panel				
General Specification	**Technical Data**		**Electrical Data (STC*)**	**Technical Data**
Cell Type	Poly-crystalline		Nominal Max. Power (Pmax)	330 W
Dimensions, Weight	2015 x 996 x 40 mm, 22.7 kg		Opt. Operating Voltage (Vmp)	37.72 V
Linear power output warranty	25 years		Opt. Operating Current (Imp)	8.75 A
Product warranty	10 years		Open Circuit Voltage (Voc)	43.54 V
Temperature Characteristics			Short Circuit Current (Isc)	9.26 A
Temperature Coefficient (Pmax)	-0.37 % / °C		Module Efficiency	16.4 %
			Operating Temperature	-40°C ~ +85°C
Temperature Coefficient (Voc)	-0.30 % / °C		Max. System Voltage	1500 V (IEC) or 1500 V (UL)
Temperature Coefficient (Isc)	0.054 % / °C		Max. Series Fuse Rating	20 A
Nominal Operating Cell Temperature	45 ± 2 °C		Application Classification	Class A
			Power Tolerance	0 ~ + 5 W

*Under Standard Test Conditions (STC) of irradiance of 1000 W/m2, spectrum AM 1.5 and cell temperature of 25°C.

3.3.2.2. Photovoltaic system configuration

The rooftop mounted solar photovoltaic system was designed to have the following angular inclination and orientation:

Table 9: Summary of SA Tyre Recyclers photovoltaic module configuration

Details	Technical Data
Tilt	13°
Azimuth	22°
Photovoltaic surface area	1 238 m^2

3.3.2.3. Inverter

The inverter used for the rooftop mounted photovoltaic system at SA Tyre Recyclers is a SolarEdge SE27.6K Three Phase inverter as depicted in Figure 67. The SolarEdge inverter complies with all City of Cape Town specifications and standards, therefore allowing for feedback of excess generated energy.

Figure 67: SolarEdge SE27.6k inverter (SolarEdge, 2018)

The key features of the SE27.6k inverter is that it offers built in smart energy management control and is the smallest and lightest inverter in its class.

Table 10: SolarEdge SE 27.6k datasheet, (SolarEdge, 2018)

SolarEdge SE27.6K Inverter	Technical Data
General Specifications	
Product dimensions (h x w x d), weight	54.0 x 31.5 x 26.0 cm, 45.0 kg
Warranty (Standard/Optional	5 / 10 years
Input (DC)	
Operating voltage range	200 - 900 V
Max. input voltage, open circuit	900 V
Nominal input power	37.25 kW
Output (AC)	
Nominal output power	27.6 kVA
Max. AC output power	27.6 kVA
Nominal output voltage	230 / 400 V, three-phase
AC voltage range	184 – 264.5 V
Frequency, Frequency range	50 / 60 Hz, +/- 5 Hz

Max. output current	40.0 A
Efficiency	98.3 %

3.3.2.4. Cabling

The cabling installed for both the DC and the AC side of the photovoltaic system at SA Tyre Recyclers is the same as the cabling installed at the SAREBI photovoltaic system.

3.3.2.5. Wiring Diagram

In Figure 68, the rooftop mounted photovoltaic system installed at SA Tyre Recyclers consists of seventeen separate strings connected to the seven SolarEdge inverters.

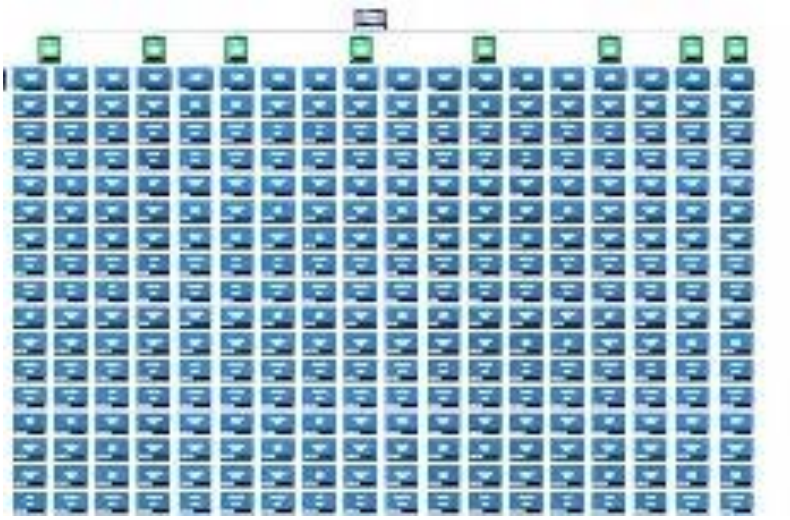

Figure 68: Wiring Diagram of the SA Tyre Recyclers solar photovoltaic system (SolarEdge, 2018)

The labelling of the photovoltaic modules follow the inverter, string and module numbering principle. Therefore module 3.2.5 represents the fifth photovoltaic module in the second string connected to inverter 3. The reasoning for this method of labelling is so that faults can be detected and corrected as rapidly as possible.

3.3.2.6. Mounting system

For the photovoltaic system installed at SA Tyre Recyclers, the same Renusol mounting system was used as noted in the SAREBI photovoltaic system.

The reasoning for using the Renusol mounting system was due to the non-penetrative mounting bracket and module clamps. The clamps are specifically designed to not cause any damage to the rooftop.

3.3.2.7. Monitoring

The web-based monitoring of the solar photovoltaic system's performance is accomplished by the use of SolarEdge's online solar PV web-based monitoring platform.

Figure 69: SolarEdge online solar PV monitoring platform (SolarEdge, 2018)

3.3.3. Stripform Packaging photovoltaic system

3.3.3.1. Photovoltaic modules

The ground-mounted solar photovoltaic system at Stripform Packaging consists of 60 Canadian Solar CS6U-335P modules.

Table 11: Canadian Solar CS6U-335P datasheet (Canadian Solar, 2018)

CS6U-335P Photovoltaic Panel				
General Specification	**Technical Data**		**Electrical Data (STC*)**	**Technical Data**
Cell Type	Poly-crystalline		Nominal Max. Power (Pmax)	335 W
Dimensions, Weight	1960 x 992 x 40 mm, 22.4 kg		Opt. Operating Voltage (Vmp)	37.2 V
Linear power output warranty	25 years		Opt. Operating Current (Imp)	8.88 A
Product warranty	10 years		Open Circuit Voltage (Voc)	45.6 V
Temperature Characteristics			Short Circuit Current (Isc)	9.45 A
Temperature Coefficient (Pmax)	-0.41 % / °C		Module Efficiency	16.97 %
			Operating Temperature	-40°C ~ +85°C
Temperature Coefficient (Voc)	-0.31 % / °C		Max. System Voltage	1500 V (IEC) or 1500 V (UL)
Temperature Coefficient (Isc)	0.053 % / °C		Max. Series Fuse Rating	15 A
Nominal Operating Cell Temperature	45 ± 2 °C		Application Classification	Class A

*Under Standard Test Conditions (STC) of irradiance of 1000 W/m2, spectrum AM 1.5 and cell temperature of 25°C.

3.3.3.2. *Photovoltaic system configuration*

The ground-mounted solar photovoltaic system was designed to have the following angular inclination and orientation:

Table 12: Summary of Stripform Packaging photovoltaic module configuration

Details	Technical Data
Tilt	15°
Azimuth	46°
Photovoltaic surface area	117 m^2

3.3.3.3. *Inverter*

The inverter used for the ground-mounted photovoltaic system is an SMA STP 20000 TL-20 inverter as illustrated inFigure 70. The SMA inverter complies with all City of Cape Town specifications and standards, therefore allowing for feedback of excess generated energy.

Figure 70: SMA STP 20000 TL-20 inverter (SMA Solar, 2018)

The key features of the 20 kW SMA inverter is that it delivers high yields with an extraordinary efficiency of 98.4%, offers enormous design flexibility and compatibility with many photovoltaic modules, offers integration of a free web-based management system (Sunny Portal) and a 24-hour reactive power provision on demand.

Table 13: SMA STP 20000 TL-20 datasheet (SMA, 2018)

SMA STP 20000 TL-20 inverter	Technical Data
General Specifications	
Product dimensions (h x w x d), weight	66.1 x 68.2 x 26.4cm, 61 kg
Warranty (Standard/Optional	5 / 10 years
Input (DC)	
MPPT voltage range	320 - 800 V
Operating voltage range	200 - 1000 V
Max. input voltage, open circuit	1 000 V
Nominal input power	20.44 kW
Output (AC)	
Nominal output power	20 kW
Max. AC apparent output power	20 kVA
Nominal output voltage	230 V, three-phase
Frequency, Frequency range	50 Hz, 44 - 50 Hz
Max. output current	33 A
Total harmonic distortion	< 3 %
Efficiency	98.4 %

3.3.3.4. Cabling

The selected cabling for both the DC side of the solar photovoltaic system was Aberdare SOLARDAC PV 4mm^2 cable depicted in Figure 71. Due to the low Amperage and the very short distances from the photovoltaic system to the inverter, a 4mm^2 cable was selected.

Figure 71: Aberdare SOLARDAC PV 4mm2 (Aberdare Cables, 2018)

Single-core, Class 5 tinned stranded copper wires bunched together to SANS 1411-1, polyolefin insulated and polyolefin sheathed LSOH FR construction.

Table 14: SOLARDAC PV cable datasheet (SOLARDAC, 2018)

SOLARDAC PV GPEE4.0T01TCXX1GC1	Technical Data
Conductor	Single core tinned stranded copper, Class 5
Insulation Material	Crosslinked Polyolefin
Temperature range	-15°C to 90°C
Voltage range,	1500 V_{DC} , 600 / 1 000 V_{AC}
Resistance	5.09 Ω / km
Cross sectional area	4 mm^2
Insulation thickness	2.0 mm
Outer diameter	6.60 mm
Weight	83.1 kg/km

The selected cabling for both the AC side of the solar photovoltaic system was Aberdare SWA 4mm^2 4 core copper cable that was also used for both SAREBI and SA Tyre Recyclers.

3.3.3.5. Wiring Diagram

Figure 72 details the ground-mounted solar photovoltaic system installed at Stripform Packaging consisting of four separate strings, each consisting of fifteen solar photovoltaic panels, which are both connected to the SMA inverter.

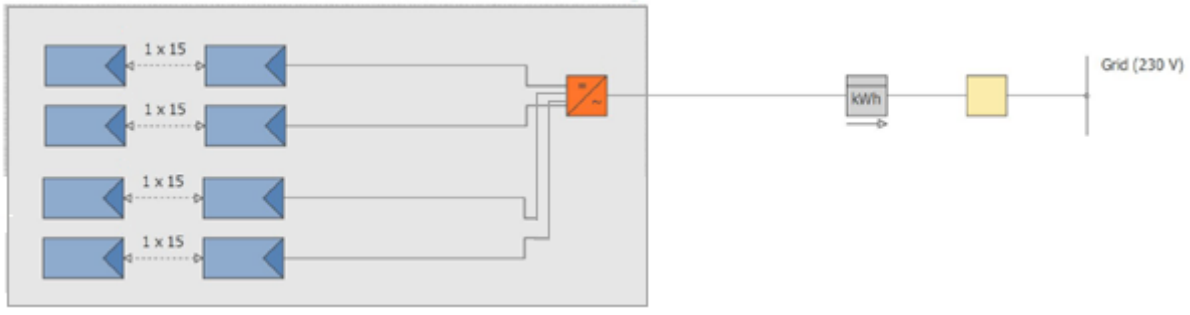

Figure 72: Wiring Diagram of the Stripform Packaging solar photovoltaic system (SEM Solutions, 2018)

3.3.3.6. Ground-mounted structure

The structure of the ground-mounted solar photovoltaic system is made up of galvanised S275 mild steel and is illustrated below in Figure 73 and Figure 74.

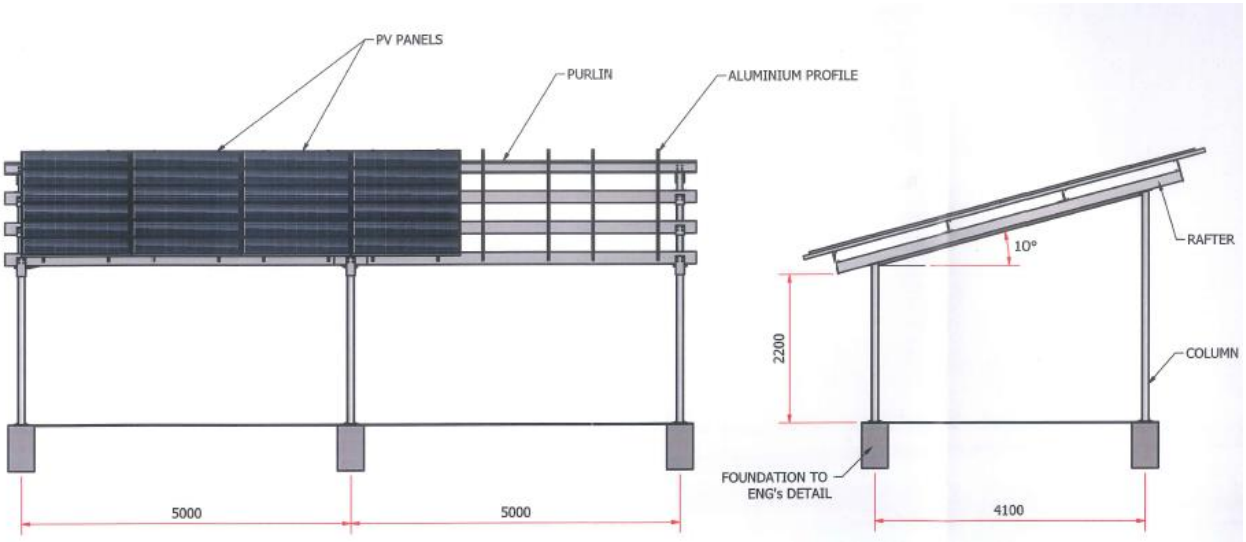

Figure 73: Side view of the ground-mounted structure

Figure 74: Isometric view of the ground-mounted structure

3.3.3.7. Mounting system

The mounting system used in the ground-mounted photovoltaic system at Stripform Packaging was the Clenergy solar mounting system depicted in Figure 75 and Figure 76, due to its durability under strong wind conditions and its quick mounting times.

Figure 75: Clenergy mounting system (Clenergy, 2018)

The Clenergy mounting system consists of a module clamp and mounting rail, both consisting of stainless-steel material with a 10-year product guarantee.

Figure 76: Clenergy module clamp (left) and mounting rail (right), (Clenergy, 2018)

3.3.3.8. Monitoring

The web-based monitoring of the solar photovoltaic system's performance was accomplished by the use of SMA Solar's Sunny Portal (SMA Solar Technology, 2018).

Figure 77: SMA Solar Sunny Portal (SMA Solar Technology, 2018)

The onsite metering was recorded by municipal approved Elster A1140 energy meters, which was used to monitor and record the total energy consumed by the Stripform Packaging building as well as the excess energy fed back into the grid.

4. Meteorological Dataset Analysis

4.1. Introduction

Section 2.4 showed that important variables needed to be considered in order to fully understand the effects on the performance of photovoltaics. To accurately analyse the performance of the photovoltaic systems, this chapter examines the different meteorological variables that could influence the performance of photovoltaic systems.

4.2. Meteorological variables

This section describes the key meteorological variables that could influence the performance of a photovoltaic system (Saglam, 2010).

Global Horizontal Irradiance (GHI):

The Global horizontal irradiation (GHI) is the amount of irradiance that makes contact with a surface horizontal to the surface of the earth (Stein, 2017). The GHI is measured in Watt-hours per square meter (Wh/m^2).

Ambient temperature:

The ambient temperature is the outside air temperature that the solar photovoltaic system is exposed to and is measured in degrees Celsius (^oC).

Module surface temperature:

The module surface temperature is the temperature of the actual photovoltaic module itself and is measured in degrees Celsius (^oC).

Standard Test Conditions (STC) of photovoltaic modules are designed for operation at 25^oC, however, real working conditions are frequently at ambient temperatures above and below 25^oC, therefore lowering the module's performance (Dash et al., 2015). At the STC, the surface module temperature ranges between 15^oC and 35^oC at which the photovoltaic module is at its most efficient point of production. However, in certain ambient conditions, the photovoltaic surface temperature can range from below 0^oC to 65^oC, at which point the module becomes impeded (Jäger et al., 2014).

Wind speed and direction:

As wind speed increases so does the rate at which temperature is exchanged over a surface and cooling occurs. Since the performance of photovoltaic modules is sensitive to temperature, the wind plays a

significant role in the output efficiency of a solar photovoltaic system. The phenomenon of lowing the temperature of a body by wind blowing on a surface is known as wind chill (Schwingshackl et al., 2013). The unit of measurement for the wind speed is kilometres per hour (km/h) or metres per second (m/s).

A significant factor to consider is the direction of the wind. Not only does the direction of the wind influence the weather, but it also affects the rate at which surface cooling occurs. Since the photovoltaic modules are installed at a fixed orientation, the level of exposure to the wind will affect the performance of the solar photovoltaic system.

Rain intensity:

The rain intensity and rain frequency also contribute to the performance of a solar photovoltaic system. The greatest impact is the removal of soiling on the surface of the photovoltaic modules (Elamri et al., 2018).

Overtime soiling occurs, which reduces the quantity of solar radiation from penetrating the photovoltaic material. However, after a significant amount of rain exposure, the modules are washed by removing the soiling from the surface of the modules (Elamri et al., 2018).

Relative humidity:

The relative humidity affects the rate of degradation of photovoltaic modules. This is due to the variation in moisture inside the photovoltaic modules, particularly in the encapsulant region where the encapsulant is used to provide adhesion between the solar cells (Honsberg et al., 2019).

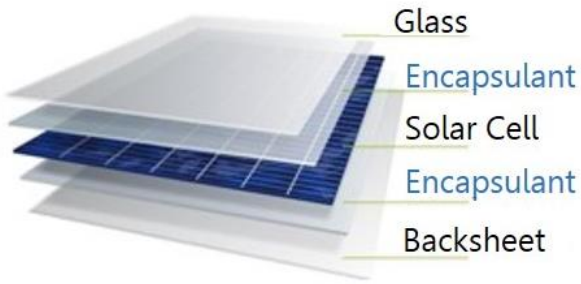

Figure 78: Encapsulant material of a solar photovoltaic module (Honsberg et al., 2019)

The degradation effects from the relative humidity do not significantly impact the performance of the solar photovoltaic system during the early stages of the photovoltaic system's lifespan, however, it does over time affect the performance (Park et, al. 2013).

Atmospheric air pressure:

As the air pressure increases, so does the short circuit current and the open circuit voltage of a solar photovoltaic system, and thus affects the performance of a solar photovoltaic system. The reasoning for the change is due to the quantity of photons that can penetrate photovoltaic material (Amajama, 2016). The atmospheric air pressure is measured in hectopascals (hPA), where 1 hPa is equivalent to 1 millibar.

4.3. Meteorological data sources

To fully analyse the correlation between the photovoltaic systems performance and the meteorological impact, data from all of the variables discussed in Section 4.2 have to be recorded and analysed. However, the ambient sensors installed at the photovoltaic systems do not measure and record the wind, rain, humidity, and air pressure data. Therefore, the meteorological data had to be obtained from a third-party weather data source, measured and recorded at hourly intervals.

For the meteorological analysis, two sources of data was utilised, namely Weather Underground (WU) data obtained from weather station IWESTERN216 and data from the Solar Radiation Data (SoDa) which is based on the Modern-Era Retrospective analysis for Research and Applications, Version 2 (MERRA-2) (GMAO, 2019). However, the various meteorological databases differ in methodology, time intervals, resolution and coverage area.

To determine which weather database to use in this study, each data source was validated by comparing to the onsite measurements. This was to ensure that the chosen weather source had a database that had the closest readings to the onsite measurements. The reasoning behind this was to ensure that the most suitable and accurate meteorological data sources were used in the analysis.

4.4. Results and Conclusion

The two data sources, SoDA and WU, were both validated by comparing them to the known onsite measurements. Table 15 below summarises the differences in data in comparison to the onsite measured data.

Table 15: Summary table of differences between data sources

Meteorological Factors	**Differences**	
	SoDa	**WU**
Global Horizontal Irradiation	- 6 %	-
Ambient Temperature	+ 2%	- 3 %
Average Difference	**- 2 %**	**-3 %**

From the values in Table 15, it is evident that the data source that is the most accurate in comparison to the measured onsite data is the SoDa data source.

5. Solar Photovoltaic System Simulations

5.1. Introduction

The most crucial step in installing any solar photovoltaic system is to first design and simulate the solar photovoltaic system performance. This can be done using simulation software. During this initial design process, the system's output losses, shading, sun orientation and energy generation yield is compiled using data and parameters supplied from the component manufactures, in addition to the local meteorological data.

This section introduces the software used to simulate the performance of the photovoltaic systems and presents the simulated results for each photovoltaic system.

5.2. Simulation Software

The simulation software used in this study is PVsyst. PVsyst is a Swiss developed solar photovoltaic software tool used by architects, engineers and researchers to accurately analyse different photovoltaic system design configurations, evaluate the predicted generated energy yield results and identify the solar photovoltaic system that gives the best possible performance (Ramoliya, 2015).

The reason why PVsyst was used for this study is due to its ease of use, the fact that it is commonly used throughout the solar photovoltaic industry, and its accuracies in its meteorological database and simulated results.

PVsyst makes use of the Perez model[1] for simulating each part of a photovoltaic system, as seen in Appendix A – PVsyst Simulations.However, the parameters that are entered by the user are the main sources of uncertainty.

The simulated result obtained from a PVsyst simulation have a reported accuracy of 1 - 2% Mean Bias Error (MBE) over one year and has a meteorological annual variability of approximately ± 5% in comparison to actual data (PVsyst, 2019).

[1] The Perez model is an applied mathematical analysis on the sky's diffusion components. The Perez Model divides diffuse radiation into three components: isotropic background, circumsolar and horizontal zones (PVsyst, 2019).

5.3. Simulation Input and Output Parameters

To determine the simulation results for each of the photovoltaic systems, the following input parameters were used:

Table 16: Simulation input parameters

Input Parameter	SAREBI	SA Tyre Recyclers	Stripform Packaging
Tilt Angle	15 °	13 °	15 °
Azimuth Angle	-19 °	22 °	46 °
Geographical Site	Atlantis	Atlantis	Atlantis
Meteo Data	Meteonorm 7.2	Meteonorm 7.2	Meteonorm 7.2
PV Modules	Canadian Solar (CS6U – 325P)	JA Solar (JAP72S-10-330-SC)	Canadian Solar (CS6U-335P)
No.of Modules	30	700	60
Inverter	Schneider Electric Conext CL 20000E	SolarEdge SE27.6k	SMA (STP 20000 TL-20)
No. of Inverters	1	7	1

Once each of the photovoltaic systems had been simulated, the key output parameters used to analyse the results were the following:

Table 17: Simulation output parameters

Output Parameter	Unit
Sysytem Production (MWh/year)	(MWh/year)
Specific Annual Production (kWh/kWp/year)	(kWh/kWp/year)
Performance Ratio (PR)	(%)

5.4. Simulation Results

The simulation results are presented separately for each system, results presented in this section include input parameters, the graphic and tabulated monthly energy production and therefore show the annual specific yield of each photovoltaic system which will allow for the photovoltaic systems' performance to be equally compared.

5.4.1. SAREBI Simulated system

Simulating the SAREBI solar photovoltaic system using the PVsyst software gives the following:

Table 18: SAREBI photovoltaic system simulation parameters

Main System Parameters				
System Type	Grid-Connected			
PV Field Orientation	Tilt	15^{o}	Azimuth	-19^{o}
PV Modules	Model	CS6U – 325P - Maxpower	Pnom	325 Wp
PV Array	No. of Modules	30	Pnom Total	9.75 kWp
Inverter	Model	Schneider 20 kW TL 20000E	Pnom	20.00 kW ac

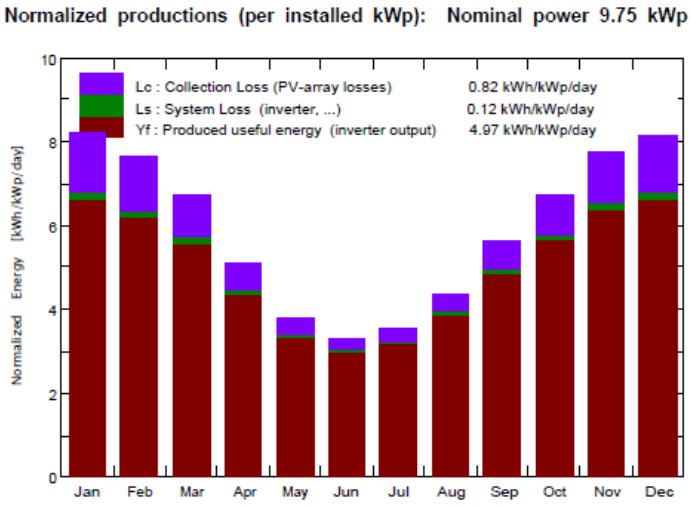

Figure 79: Solar photovoltaic system production (PVsyst, 2017)

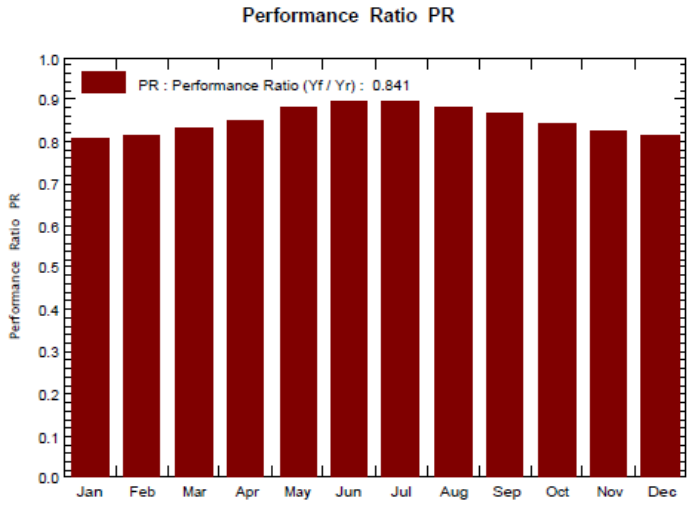

Figure 80: Solar photovoltaic system performance ratio (PVsyst, 2017)

Table 19: Summary of SAREBI photovoltaic system simulation results

Main Simulation Results		
System Production	17.70	MWh/year
Specific annual production	1 815	kWh/kWp/year
Performance Ratio (PR)	84.14	%

Table 20: SAREBI PVSyst simulation balances and results

	GHI (kWh/m²)	DHI (kWh/m²)	T Amb (°C)	G Inc (kWh/m²)	G Eff (kWh/m²)	EArray (MWh)	E_Grid (MWh)	PR
January	255.1	66.3	21.78	2542	248.6	2.053	2.002	0.808
February	205.5	56.1	21.81	213.6	209.0	1.735	1.694	0.814
March	188.9	50.46	20.16	209.2	204.9	1.731	1.69	0.829
April	130.3	38.51	17.36	153.3	149.8	1.303	1.273	0.852
May	93.7	35.38	14.87	117.4	114.5	1.032	1.009	0.881
June	76.1	29.05	12.39	99.8	97.3	0.893	0.873	0.897
July	85.7	33.21	11.98	110.7	107.8	0.991	0.969	0.897
August	110.9	33.99	12.52	135.5	132.3	1.194	1.168	0.883
September	149.0	45.61	14.18	168.7	165.1	1.454	1.422	0.865
October	197.5	60.35	17.03	209.2	205.0	1.755	1.714	0.840
November	231.7	66.41	18.72	232.7	227.6	1.919	1.875	0.826
December	257.7	66.76	20.83	252.7	246.9	2.055	2.006	0.814
Year	**1 982.1**	**582.13**	**16.94**	**2 157.1**	**2 108.8**	**18.118**	**17.706**	**0.841**

Legend:	GHI	Horizontal global irradiation	G Eff	Effected Global, corr for IAM and shading
	D	Horizontal Diffuse irradiation	EArray	Effective energy at the output of the array
	T Amb	Ambient Temperature	E_Grid	Energy injected into grid
	G Inc	Global incident in coll. Plane	PR	Performance Ratio

5.4.2. SA Tyre Recyclers Simulated system

Simulating the SA Tyre Recyclers solar photovoltaic system using the PVsyst software gives the following results:

Table 21: SA Tyre Recyclers photovoltaic system simulation parameters

Main System Parameters				
System Type	Grid-Connected			
PV Field Orientation	Tilt	13°	Azimuth	22°
PV Modules	Model	JAP72S-10-330-SC	Pnom	330 Wp
PV Array	No. of Modules	700	Pnom Total	231 kWp
Inverter	Model	SolarEdge SE27.6k	Pnom	27.6 kW ac

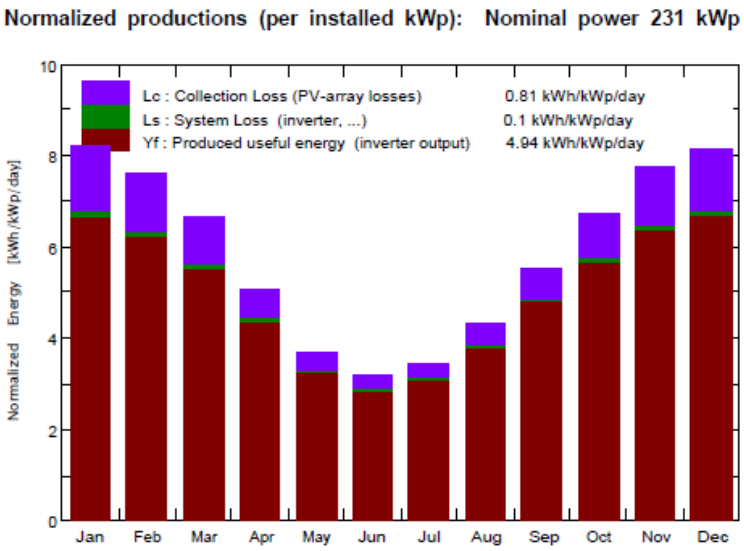

Figure 81: Solar photovoltaic system production (PVsyst, 2018)

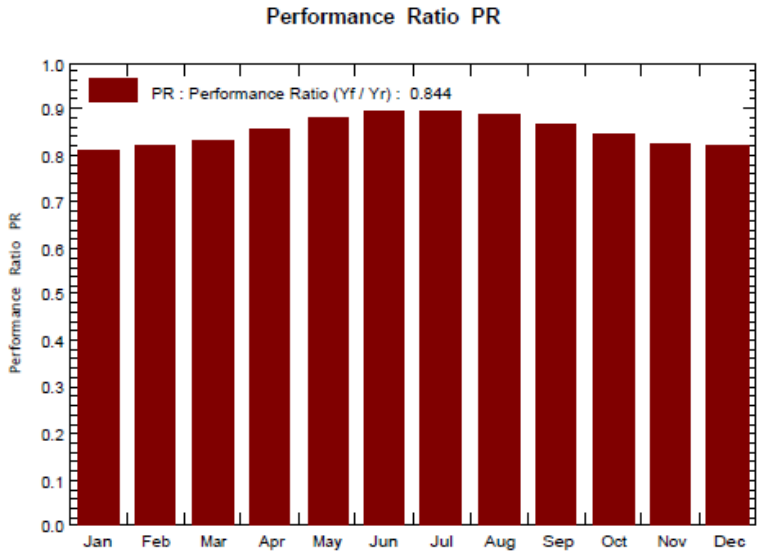

Figure 82: Solar photovoltaic system performance ratio (PVsyst, 2018)

Table 22: Summary of SA Tyre Recyclers photovoltaic system simulation results

Main Simulation Results		
System Production	416.3	MWh/year
Specific annual production	1802	kWh/kWp/year
Performance Ratio (PR)	84.43	%

Table 23: SA Tyre Recyclers PVsyst simulation balances and results

	GHI (kWh/m²)	DHI (kWh/m²)	T Amb (°C)	G Inc (kWh/m²)	G Eff (kWh/m²)	EArray (MWh)	E_Grid (MWh)	PR
January	255.1	66.3	21.78	254.4	247.5	48.66	47.72	0.812
February	205.5	56.1	21.81	212.5	206.5	41.06	40.27	0.82
March	188.9	50.46	20.16	205.8	199.5	40.38	39.6	0.833
April	130.3	38.51	17.36	152.8	147.9	30.86	30.27	0.858
May	93.70	35.38	14.87	114.4	110.0	23.74	23.29	0.881
June	76.10	29.05	12.39	96.0	92.1	20.23	19.85	0.894
July	85.70	33.21	11.98	106.7	102.3	22.49	22.06	0.895
August	110.9	33.99	12.52	133.1	128.5	27.79	27.26	0.886
September	149.0	45.61	14.18	165.8	160.6	33.90	33.25	0.868
October	197.5	60.35	17.03	208.3	202.5	41.49	40.69	0.846
November	231.7	66.41	18.72	231.9	225.0	45.14	44.27	0.826
December	257.7	66.76	20.83	252.9	245.7	48.78	47.83	0.819
Year	**1 982.3**	**582.13**	**16.94**	**2 134.6**	**2 086.7**	**426.39**	**416.36**	**0.844**

Legend:				
	GHI	Horizontal global irradiation	G Eff	Effected Global, corr for IAM and shading
	D	Horizontal Diffuse irradiation	EArray	Effective energy at the output of the array
	T Amb	Ambient Temperature	E_Grid	Energy injected into grid
	G Inc	Global incident in coll. Plane	PR	Performance Ratio

5.4.3. Stripform Packaging Simulated system

Simulating the Stripform Packaging solar photovoltaic system using the PVsyst software gives the following results:

Table 24: Stripform Packaging photovoltaic system simulation parameters

Main System Parameters				
System Type	Grid-Connected			
PV Field Orientation	Tilt	15°	Azimuth	46°
PV Modules	Model	CS6U – 335P - Maxpower	Pnom	335 Wp
PV Array	No. of Modules	60	Pnom Total	20.1 kWp
Inverter	Model	Sunny Tripower 10000TL-20	Pnom	20.00 kW ac

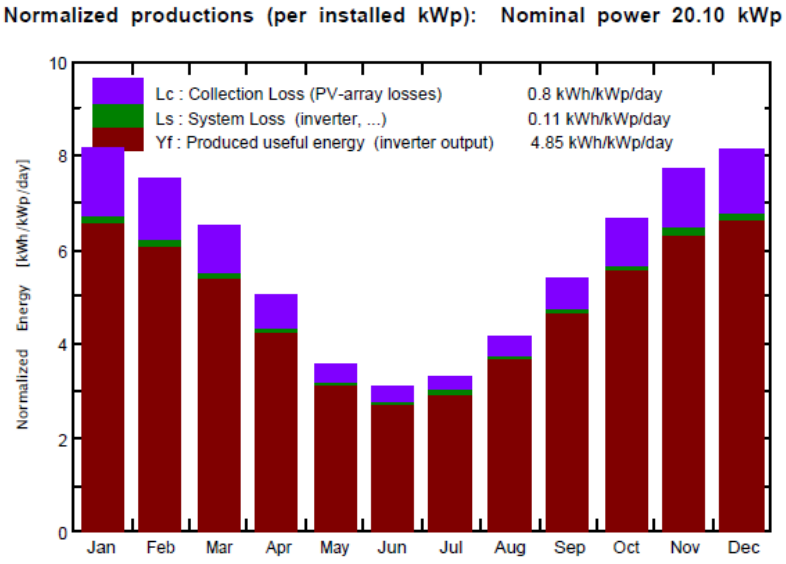

Figure 83: Solar photovoltaic system production and Performance Ratio (PVsyst, 2018)

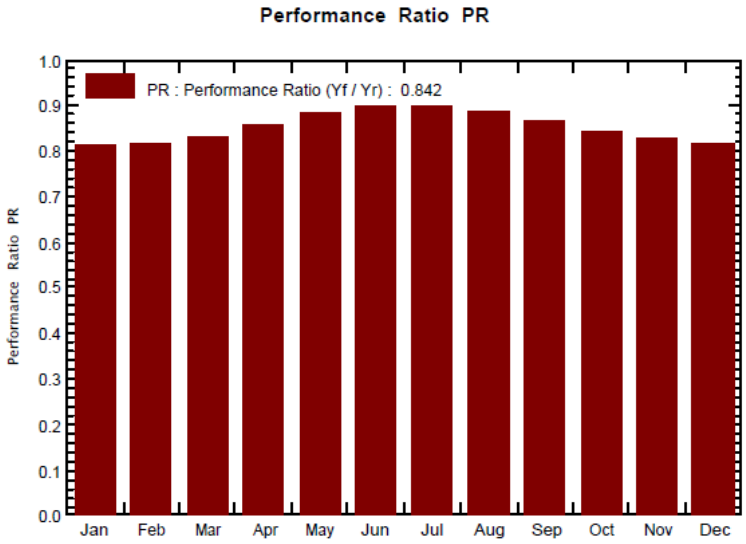

Figure 84: Solar photovoltaic system performance ratio (PVsyst, 2018)

Table 25: Summary of Stripform Packaging photovoltaic system simulation results

Main Simulation Results		
System Production	35.551	MWh/year
Specific annual production	1 769	kWh/kWp/year
Performance Ratio (PR)	84.19	%

Table 26: Stripform Packaging PVsyst simulation balances and results

	GHI (kWh/m²)	**DHI (kWh/m²)**	**T Amb (°C)**	**G Inc (kWh/m²)**	**G Eff (kWh/m²)**	**EArray (MWh)**	**E_Grid (MWh)**	**PR**
January	255.1	66.30	21.78	252.5	247.3	4.201	4.104	0808
February	205.5	56.10	21.81	209.7	205.5	3.516	3.437	0.815
March	188.9	50.46	20.16	201.9	197.7	3.466	3.372	0.831
April	130.3	38.51	17.36	150.5	147.0	2.643	2.588	0.855

May	93.7	35.38	14.87	111.0	107.8	2.004	1.963	0.880
June	76.1	29.05	12.39	92.4	89.7	1.698	1.665	0.896
July	85.7	33.21	11.98	102.8	99.8	1.889	1.851	0.895
August	110.9	33.99	12.52	129.9	126.5	2.359	2.312	0.885
September	149.0	45.61	14.18	162.1	158.6	2.884	2.825	0.867
October	197.5	60.35	17.03	205.7	201.4	3.554	3.476	0.841
November	231.7	66.41	18.72	230.4	225.4	3.920	3.834	0.828
December	257.7	66.76	20.83	251.8	246.5	4.221	4.126	0.815
Year	**1 982.1**	**582.13**	**16.94**	**2 100.7**	**2 053.2**	**36.336**	**35.551**	**0.842**

Legend:				
	GHI	Horizontal global irradiation	G Eff	Effected Global, corr for IAM and shading
	D	Horizontal Diffuse irradiation	EArray	Effective energy at the output of the array
	T Amb	Ambient Temperature	E_Grid	Energy injected into grid
	G Inc	Global incident in coll. Plane	PR	Performance Ratio

5.5. Conclusion

Comparing the specific production of each of the systems in Table 27 illustrates that the photovoltaic system at SAREBI (1 815 kWh/kWp/year) is the best performing, the system at SA Tyre Recyclers (1 802 kWh/kWp/year) is second best and the system at Stripform Packaging (1 769 kWh/kWp/year) is the worst performing system.

Table 27: Simulated Data Summary

PV System	System Production (MWh)	Specific prod (kWh/kWp/year)	Performance Ratio (%)
SAREBI	17.70	1 815	84.14
Stripform Packaging	35.551	1 769	84.19
SA Tyre Recyclers	416.3	1 802	84.43

This reveals an interesting observation that the best performing system and the worst performing system were both ground-mounted systems. According to previously published literature (Malagnino, 2015), ground-mounted systems are likely to outperform rooftop mounted systems. However, these results were not noted for the photovoltaic system at Stripform Packaging.

6. Solar Photovoltaic System Performance

6.1. Introduction

In the first part of this chapter, the actual and simulated performance for each of the photovoltaic systems are analysed in addition to how each of the systems performed in comparison to each other.

The second part of this chapter investigates how the environmental factors which the photovoltaic systems were exposed to correlate with the performance of the photovoltaic systems.

6.2. Solar photovoltaic system yield performance

In this section of the study, the performance of the photovoltaic systems are examined to see how the actual measured yield compares to the simulated yields, in addition to how the performance of each of the photovoltaic systems compares to one another.

6.2.1. SAREBI solar PV system performance

In Table 28 the actual energy generated by the solar photovoltaic system at SAREBI is compared to the simulated generation yield. Figure 85 illustrates the graphical representation of the actual and simulated energy yield of the solar photovoltaic system at SAREBI.

Table 28: Performance of the solar PV system at SAREBI

Month	Actual (kWh)	Simulated (kWh)	Achieved (%)
Aug-18	1 039	1 168	89%
Sep-18	1 232	1 422	87%
Oct-18	1 733	1 714	101%
Nov-18	1 826	1 875	97%
Dec-18	1 861	2 006	93%
Jan-19	1 973	2 002	99%
Feb-19	1 495	1 694	88%
Mar-19	1 245	1 690	74%
Apr-19	1 159	1 273	91%
May-19	941	1 009	93%
Jun-19	821	873	94%
Jul-19	720	969	74%
Total	**16 045**	**17 695**	**90,7%**

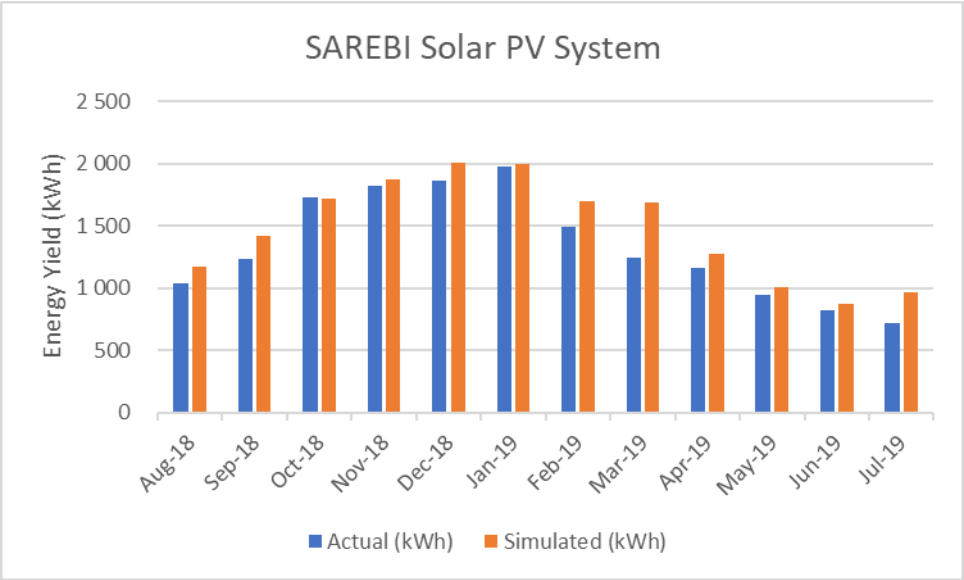

Figure 85: SAREBI Solar photovoltaic system energy yield

Table 29: Summary of SAREBI photovoltaic system performance

Actual Annual Yield (kWh)	16 045
Simulated Annual Yield (kWh)	17 695
Yield Achieved (%)	90.7 %
Performance Ratio (%)	84.14 %

Comparing the actual and simulated yields of the SAREBI photovoltaic system, the annual actual yield achieved is 90.7% of the simulated energy yield, which is greater than the predicted performance ratio of 84.14%.

6.2.2. SA Tyre Recyclers solar PV system performance

In Table 30 the actual energy generated by the solar photovoltaic system at SA Tyre Recyclers is compared to the simulated generation yield. Figure 86 illustrates the graphical representation of the actual and simulated energy yield of the solar photovoltaic system at SA Tyre Recyclers.

Table 30: Performance of the solar PV system at SA Tyre Recyclers

Month	Actual (kWh)	Simulated (kWh)	Achieved (%)
Aug-18	25 511	27 260	94%
Sep-18	31 884	33 250	96%
Oct-18	42 521	40 690	104%
Nov-18	44 289	44 270	100%
Dec-18	45 410	47 830	95%
Jan-19	48 311	47 720	101%
Feb-19	36 518	40 270	91%
Mar-19	31 759	39 600	80%
Apr-19	28 720	30 270	95%
May-19	21 997	23 290	94%

Jun-19	20 403	19 850	103%
Jul-19	18 165	22 060	82%
Total	**395 488**	**416 360**	**95,0%**

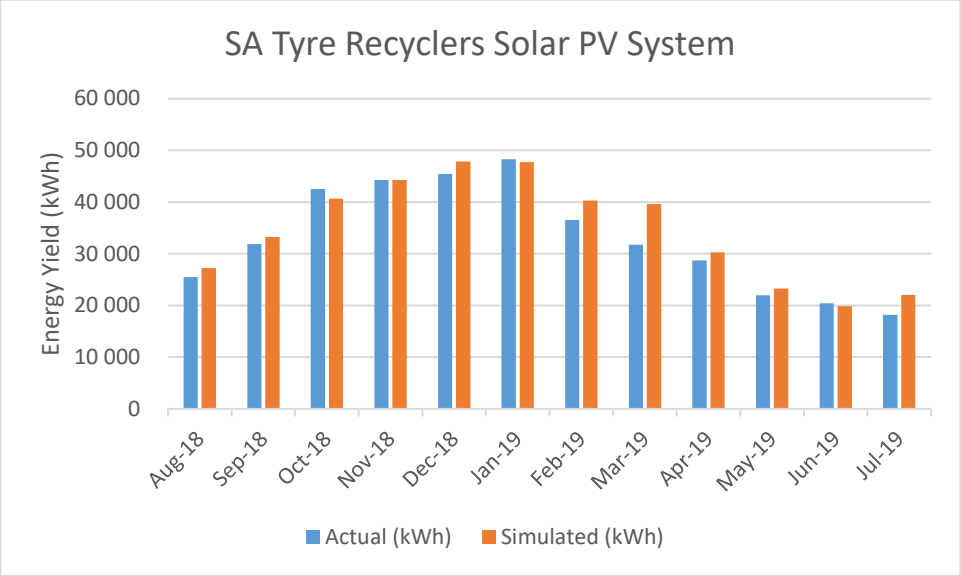

Figure 86: SA Tyre Recyclers solar PV system energy yield

Table 31: Summary of SA Tyre Recyclers photovoltaic system performance

Actual Annual Yield (kWh)	395 488
Simulated Annual Yield (kWh)	416 360
Yield Achieved (%)	95 %
Performance Ratio (%)	84.43 %

Comparing the actual and simulated yields of the SA Tyre Recyclers photovoltaic system, the annual actual yield achieved is 95% of the simulated energy yield, which is greater than the predicted performance ratio of 84.43 %.

6.2.3. Stripform Packaging solar PV system performance

In Table 32 the actual energy generated by the solar photovoltaic system at Stripform Packaging is compared to the simulated generation yield. Figure 87 illustrates the graphical representation of the actual and simulated energy yield of the solar photovoltaic system at SA Tyre Recyclers.

Table 32: Performance of the solar PV system at Stripform Packaging

Month	Actual (kWh)	Simulated (kWh)	Achieved (%)
Aug-18	2 345	2 312	101%
Sep-18	2 801	2 825	99%
Oct-18	3 800	3 476	109%
Nov-18	4 033	3 834	105%
Dec-18	4 360	4 126	106%
Jan-19	4 543	4 104	111%

Feb-19	3 479	3 437	101%
Mar-19	2 438	3 372	72%
Apr-19	2 191	2 588	85%
May-19	2 037	1 963	104%
Jun-19	1 743	1 665	105%
Jul-19	1 616	1 851	87%
Total	**35 387**	**35 553**	**99.5%**

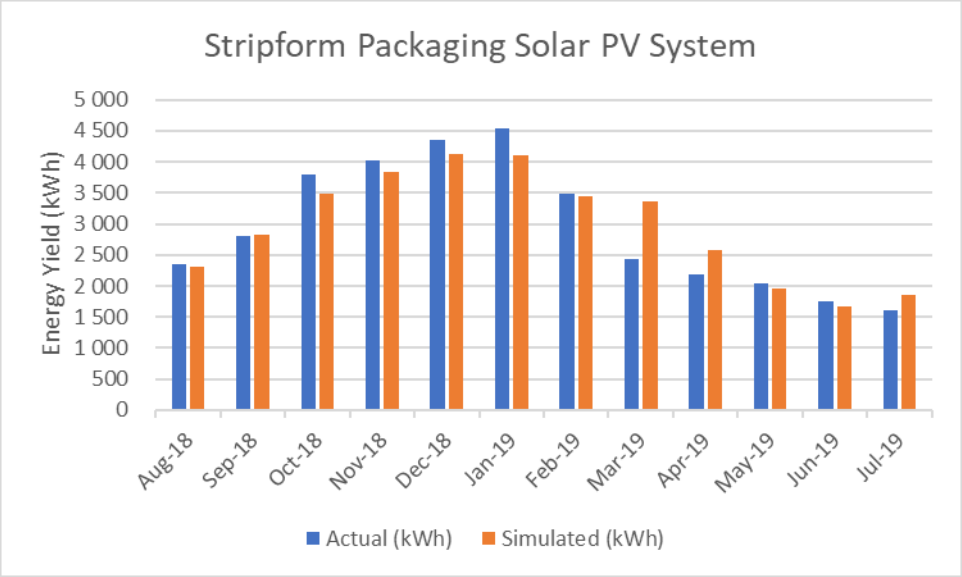

Figure 87: Stripform Packaging solar PV system energy yield

Table 33: Summary of Stripform Packaging photovoltaic system performance

Actual Annual Yield (kWh)	35 387
Simulated Annual Yield (kWh)	35 551
Yield Achieved (%)	99.5 %
Performance Ratio (%)	84.19 %

Comparing the actual and simulated yields of the Stripform Packaging photovoltaic system, the annual actual yield achieved is 99.5% of the simulated energy yield, which is greater than the predicted performance ratio of 84.19%.

6.2.4. Solar PV system performance and correlation

Due to the different sized solar photovoltaic systems, the specific yield (kWh/kWp) of each system has to be used to compare and analyse 'like with like'. The specific yield is a unit of measurement that is used to measure the quantity of energy produced for every kWp of photovoltaic model capacity. Table 34 and Figure 88 illustrates the different actual specific yields of each of the solar photovoltaic systems.

Table 34: Solar PV system energy yield comparisons

Month	SAREBI (kWh/kWp)	SA Tyre (kWh/kWp)	Stripform Packaging (kWh/kWp)
Aug-18	106.52	110.44	116.66
Sep-18	126.39	138.03	139.33
Oct-18	177.77	184.07	189.08
Nov-18	187.30	191.73	200.65
Dec-18	190.86	196.58	216.89
Jan-19	202.31	209.14	226.04
Feb-19	153.37	158.09	173.11
Mar-19	127.64	137.49	121.28
Apr-19	118.89	124.33	108.99
May-19	96.53	95.23	101.35
Jun-19	84.15	88.32	86.74
Jul-19	73.87	78.64	80.42
Total	**1 645.62**	**1 712.07**	**1 760.53**

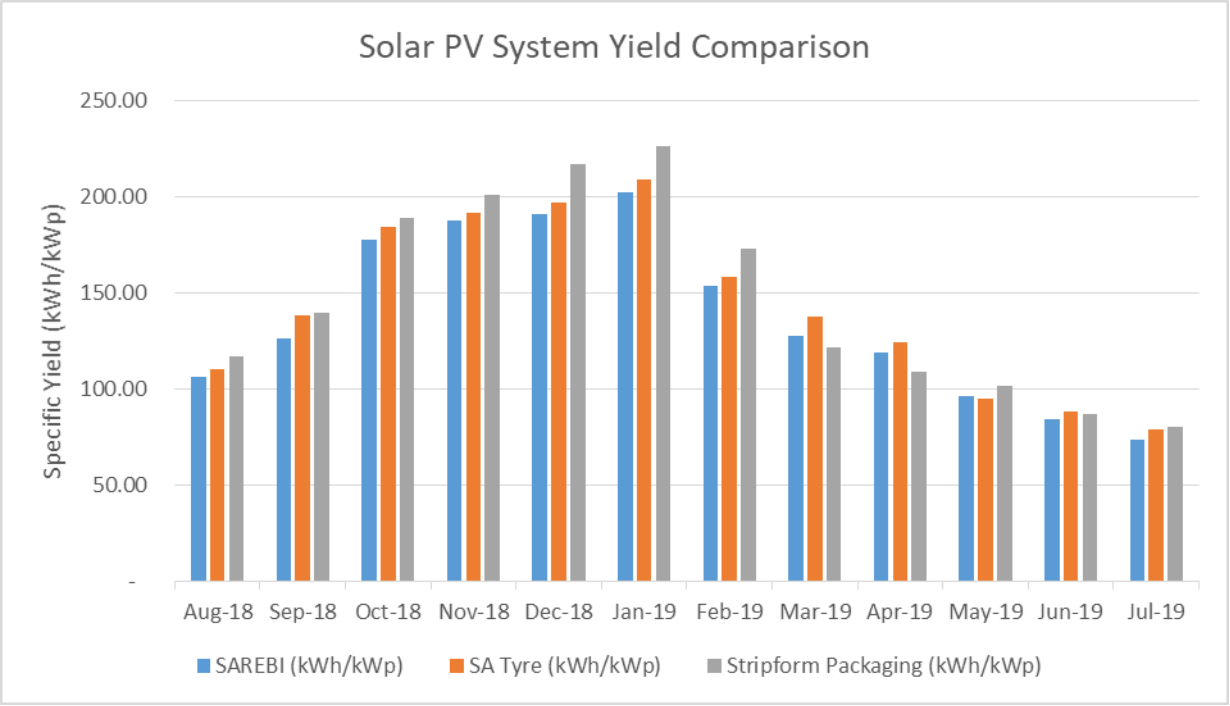

Figure 88: Solar PV specific yield comparisons

From Figure 88, all three of the photovoltaic systems have the highest specific yield values during the Summer months, which corresponds with the high GHI levels during Summer. Table 35 illustrates the differences in annual specify yield of each of the solar photovoltaic systems. The least efficient system was the ground-mounted system at SAREBI, whilst the photovoltaic system that generated the greatest yield was the ground-mounted system at Stripform Packaging.

Table 35: Comparison of the annual specific yield of the solar photovoltaic systems

Solar PV System	kWh/kWp	Difference		
		SAREBI	SA Tyre	Stripform
SAREBI	1 645.62	-	-4%	-7%
SA Tyre Recyclers	1 712.07	4%	-	-3%
Stripform Packaging	1 760.53	7%	3%	-

An additional comparison tool to consider is to examine the correlation between the solar photovoltaic systems. Correlation analysis is a statistical method used to evaluate the strength and linear relationship between two quantitative variables (Boston University, 2013).

To determine the correlation strength of two variables, the values for r range between 0 and 1, in which values of 0 result in no correlation, values less than 0.3 result in a weak correlation, values between 0.3 and 0.6 result in a medium correlation and values greater than 0.6 result in a strong correlation (Boston University, 2013).

Since the SAREBI and the SA Tyre Recyclers photovoltaic systems are located at the same facility, the correlation between the two annual specific yields are examined and represented in Figure 89, resulting in a strong positive linear correlation of 0.9296. The readings are for the entire annual period from August 2018 to July 2019 and consist of data recorded in hourly intervals.

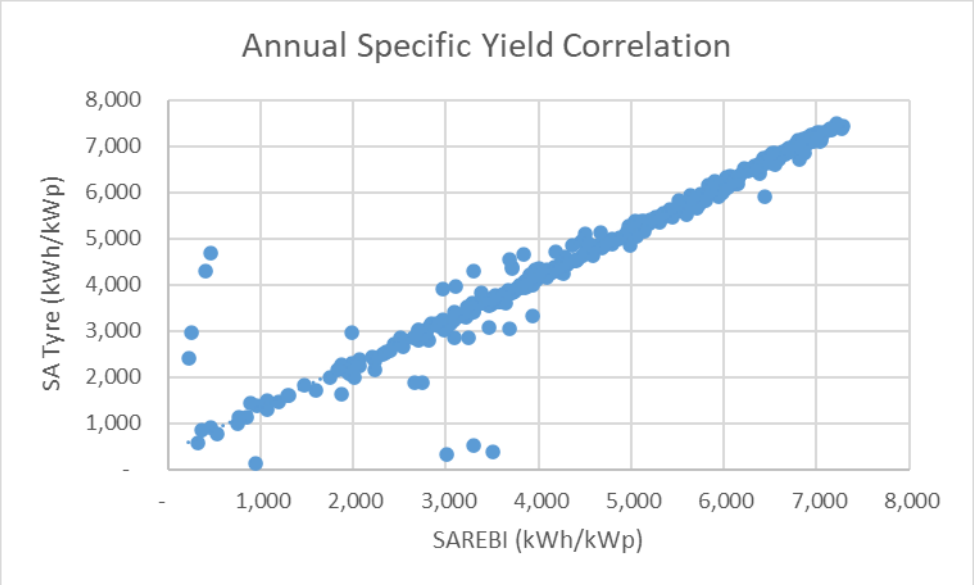

Figure 89: Annual specific yield correlation of the SAREBI and SA Tyre PV systems

Additionally, Figure 89 illustrates that as the specific yield of the system increases, so does the correlation between the two photovoltaic systems. However, this is not true when the specific yield decreases, resulting in less correlation between the two systems. This observation could be due to one of the photovoltaic systems performing worse during days of poor irradiation, resulting in one system not consistently

performing better than the other. However, the difference in performance is smaller when the yield is greater.

Since the photovoltaic systems at SAREBI and Stripform Packaging are both ground-mounted systems, they too should be analysed to see if there is a correlation in their specific yields.

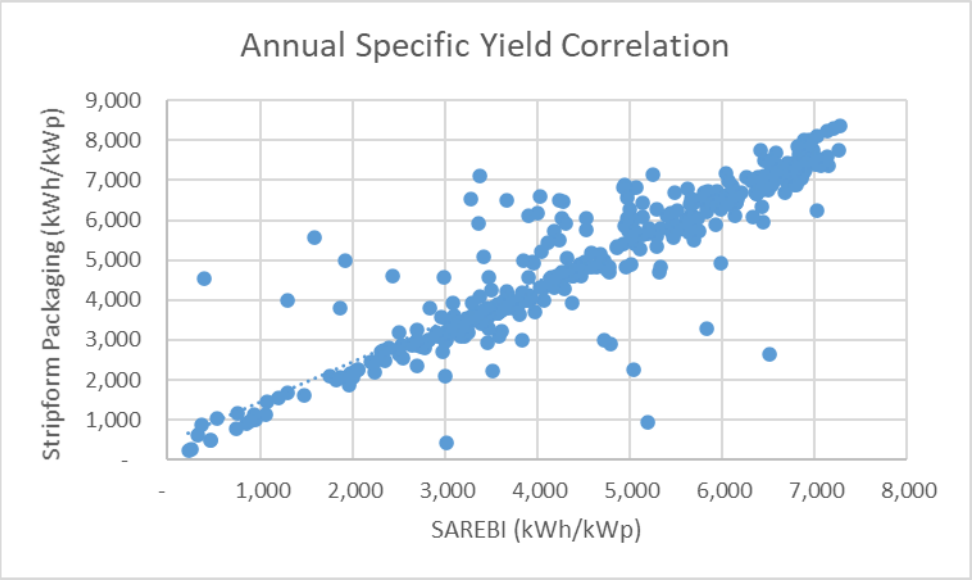

Figure 90: Annual specific yield correlation of ground-mounted PV systems

In Figure 90, the two ground-mounted systems have a strong positive linear correlation of 0.8179. even though the correlation is less than the correlation between the SAREBI and the SA Tyre Recyclers systems, it still illustrates a strong correlation. Reasoning for the weaker correlation in comparison to the correlation in Figure 89 could be due to the two ground-mounted systems being situated in different locations.

6.2.5. Conclusion

Analysing the performance of the annual simulated yield and the actual measured yield showed that all three photovoltaic systems underperformed in comparison to their simulated yields. The Stripform Packaging system achieved 99.5%, the SA Tyre Recyclers system achieved 95.0% and the SAREBI system achieved the worst percentage yield of 90.7%.

A factor that must be considered that effected the actual performance of all the three photovoltaic systems is the effects of Load shedding [2] that took place during the months of March 2019. Due to the inverters anti-islanding features, the photovoltaic systems were automatically shut down due to grid failure, thus preventing the systems from generating energy for approximately three hours per day. Another key factor

[2] Load shedding is done countrywide as a controlled option to respond to unplanned events to protect the electricity power system from a total blackout (Eskom, 2014)

to consider is that the degradation of the photovoltaic modules was omitted due to all three photovoltaic systems being in operation for less than a year.

Comparison of the annual specific yield (kWh/kWp) of the photovoltaic systems, reveals that the best performing system was Stripform Packaging while the worst performing system was the SAREBI system. This raises an interesting observation since both systems are ground-mounted systems and according to literature (Malagnino, 2015), ground-mounted systems will outperform rooftop mounted systems. This was not seen in this study where the rooftop mounted system at SA Tyre Recyclers outperformed the ground-mounted system at SAREBI by 4%.

However, to establish a full understanding of the photovoltaic systems' performance, the effects of the meteorological variables to the systems' performance must be examined.

6.3. Photovoltaic performance correlation to meteorological parameters

In this section, the performance of the photovoltaic systems are examined to see the extent to which the performance of each of the systems correlates with the meteorological variables mentioned in Section 4.2.

6.3.1. Photovoltaic system production and global horizontal irradiation (GHI)

In this section the annual specific yield of each of the photovoltaic systems and the annual global horizontal irradiation (GHI) (kW/m^2) were analysed to determine if there was a strong correlation between the two variables. The correlation graphs are listed in the Appendix B – Correlation Graphs.

Table 36 tabulates the correlation between the global horizontal irradiation (GHI) and each of the solar photovoltaic system's annual specific yield. Literature notes that, without irradiation, there will be no generation of energy since photovoltaic cells require photons to generate electricity (Jäger et al., 2014).Therefore, it is no surprise that there is a strong positive correlation between the photovoltaic system's yield and the GHI. However, the interesting observation is that, given that there is a strong positive correlation, there is an average correlation of only 0.8030. A reason for this could be due to the effects of the loss parameters, discussed further in Section 7.3, reducing the levels of annual specific yield throughout the annual period.

Table 36: Annual specific yield and GHI correlation

PV System	GHI Correlation (r)
SAREBI	0.7974
Stripform Packaging	0.8068
SA Tyre Recyclers	0.8073

6.3.2. Photovoltaic system production and ambient temperature

In this section the annual specific yield of each of the photovoltaic systems and the annual ambient temperature were analysed to determine the extent to which temperature influences performance. The correlation graphs are listed in Appendix B – Correlation Graphs.

Throughout the annual period, there was a maximum recorded temperature of 26° C, a minimum of 9° C and an average of 17° C.

Table 37 tabulates the correlation between the ambient temperature and each of the solar photovoltaic system's annual specific yield. The data revealed that there is a positive correlation between the photovoltaic systems yield and the ambient temperature, but a medium correlation strength, with an average correlation between the three photovoltaic systems being 0.5705.

Table 37: Annual specific yield and ambient temperature correlation

PV System	Ambient Temperature Correlation (r)
SAREBI	0.5547
Stripform Packaging	0.5906
SA Tyre Recyclers	0.5661

6.3.3. Photovoltaic system production and wind speed and direction

In this section the annual specific yield of each of the photovoltaic systems and the annual wind speed (m/s) and direction (°) were analysed to determine if there was a strong correlation between these two variables. The correlation graphs are listed in Appendix B – Correlation Graphs.

Table 38 tabulates the correlation between the wind speed, wind direction and each of the solar photovoltaic system's annual specific yield. The data revealed that there is a positive correlation between the photovoltaic systems yield and the wind speed and a negative correlation between the photovoltaic systems yield and the wind direction. However, both correlations are very close to zero.

Table 38: Annual specific yield and wind speed and direction correlation

PV System	Wind Speed Correlation (r)	Wind Direction Correlation (r)
SAREBI	0.1265	0.0812
Stripform Packaging	0.1616	0.0755
SA Tyre Recyclers	0.1356	0.1034

6.3.4. Photovoltaic system production and humidity

In this section, the annual specific yield of each of the photovoltaic systems and a years' worth of humidity data (%) were analysed to determine if there was a strong correlation between the two variables. The correlation graphs are listed in Appendix B – Correlation Graphs.

Table 39 tabulates the correlation between the humidity and each of the solar photovoltaic system's annual specific yield. The data revealed that there is a weak negative correlation between the photovoltaic system's yield.

Table 39: Annual specific yield and humidity correlation

PV System	Humidity Correlation (r)
SAREBI	0.4347
Stripform Packaging	0.4574
SA Tyre Recyclers	0.4424

Previous research states that, humidity affects the degradation of the photovoltaic modules, which over long periods of time will affect the yield of the photovoltaic system (Park et,al. 2013). However, from the correlation data over the annual period, the humidity did not affect the yield of the photovoltaic system. If, however, the correlation was determined over a range of several years, then potentially there would have been an improved level of correlation.

6.3.5. Photovoltaic system production and atmospheric pressure

In this section, the annual specific yield of each of the photovoltaic systems and a years' worth of atmospheric pressure data were analysed to determine if there was a strong correlation between the two variables.

Table 40 tabulates the correlation between the atmospheric pressure and each of the solar photovoltaic system's annual specific yield. The data revealed that there is a weak negative correlation between the photovoltaic systems yield and the atmospheric pressure.

Table 40: Annual specific yield and atmospheric pressure correlation

PV System	Atmospheric Pressure Correlation (r)
SAREBI	0.3382
Stripform Packaging	0.3428
SA Tyre Recyclers	0.3622

6.3.6. Photovoltaic system production and rainfall

In this section, the annual specific yield of each of the photovoltaic systems and a years' worth of rainfall data (mm/day) were analysed to determine if there was a strong correlation between these two variables. The correlation graphs are listed in Appendix B – Correlation Graphs.

Table 41 tabulates the correlation between the rainfall and each of the solar photovoltaic system's annual specific yield. The data revealed that there was a weak negative correlation between the photovoltaic systems yield and the rainfall.

Table 41: Annual specific yield and rainfall correlation

PV System	Rainfall Correlation (r)
SAREBI	0.2844
Stripform Packaging	0.2903
SA Tyre Recyclers	0.2941

A point to note is that the local Cape Town drought could not have played a role in affecting the performance of the photovoltaic systems performance. This is due to the drought occurring between the months of July 2015 to June 2018 and the data collected during this study took place from August 2018 (Zue and Begbie, 2019).

6.3.7. Photovoltaic system production and module temperature

In this section, the annual specific yield of each of the photovoltaic systems and the module temperature were analysed to determine if there was a strong correlation between these two variables.

Table 42 tabulates the correlation between the module temperature and each of the solar photovoltaic system's annual specific yield. The data revealed that there was a very strong positive correlation between the photovoltaic systems yield and the module temperature, with an average correlation value of 0.8792.

Table 42: Annual specific yield and module temperature correlation

	Correlation (r)		
Month	**SA Tyre Recyclers**	**SAREBI**	**Stripform Packaging**
January	0.9413	0.9289	0.9388
February	0.9035	0.9410	0.9541
March	0.8407	0.9215	0.9457
April	0.8458	0.8649	0.8821
May	0.8642	0.8368	0.8683
June	0.8418	0.7914	0.8304
July	0.8059	0.7892	0.8287
August	0.8201	0.8264	0.8445
September	0.8238	0.8925	0.9138
October	0.8969	0.8620	0.8653
November	0.9337	0.9109	0.9297
December	0.8853	0.9354	0.9458

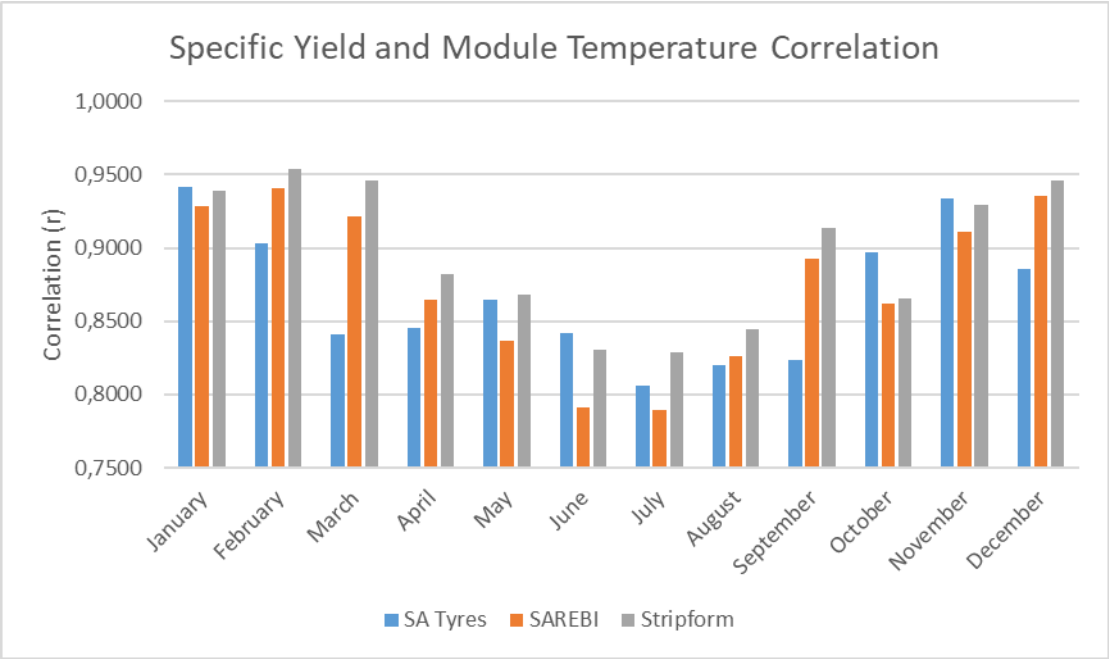

Figure 91: Monthly specific yield and module temperature correlation

Figure 91 and Table 43 illustrate the correlation seasonal trend in which the correlation is stronger during the summer months in comparison to the winter months. Therefore, the resulting effect is that the module temperature affects the photovoltaic system's yield more in the summer months than during the winter months, which agrees with published literature.

Another point to mention is that the photovoltaic systems that have the Canadian Solar photovoltaic modules are more susceptible to module temperature change, as discussed in Section 7.1.1. This is due to Canadian Solar modules having a greater temperature coefficient for the maximum power rating of -0.41 %/°C in comparison to the JA Solar Moules of -0.37 %/°C.

This factor would have a small effect on the performance of each of the photovoltaic systems, but it is very difficult to quantify as the changes in the recorded data was not collected under strict and restricted laboratory conditions.

Table 43: Seasonal specific yield and module temperature correlation

Season	Months	Correlation (r)		
		SA Tyre Recyclers	SAREBI	Stripform Packaging
Summer	Jan - May, Sep-Dec	0.8730	0.8953	0.9100
Winter	June, July and Aug	0.8247	0.8055	0.8359
Annual		0.8669	0.8768	0.8940

6.3.8. Conclusion

Table 44 and Table 45 provides a summary of the correlation of each of the meteorological parameters for the three photovoltaic systems. From the tables, the global horizontal irradiation (GHI) and the modular

temperature were the only parameters that had a strong positive correlation with the specific annual yield of the photovoltaic systems.

Table 44: Summary of positive annual specific yield and meteorological correlations

PV System	Positive Correlation (r)			
	GHI	Ambient Temperature	Wind Speed	Module Temperature
SAREBI	0.7974	0.5547	0.1265	0.8768
Stripform Packaging	0.8068	0.5906	0.1616	0.8940
SA Tyre Recyclers	0.8073	0.5661	0.1356	0.8669

Table 45: Summary of negative annual specific yield and meteorological correlations

PV System	Negative Correlation (r)			
	Wind Direction	Pressure	Humidity	Rainfall
SAREBI	0.0812	0.3382	0.4347	0.2844
Stripform Packaging	0.0755	0.3428	0.4574	0.2903
SA Tyre Recyclers	0.1034	0.3622	0.4424	0.2941

7. Technical Analysis

7.1. Photovoltaic System Equipment

As discussed in Section 2.3, the core components of a solar photovoltaic system are the solar modules, the inverters, the batteries and the tracking system. However, since all three photovoltaic systems do not have battery storage and are fixed axis systems, the core components of these systems are the photovoltaic modules and the inverters.

7.1.1. Photovoltaic modules

In Table 46 the photovoltaic modules from each of the photovoltaic systems are tabulated, illustrating that SAREBI and Stripform Packaging both consist of Canadian Solar's CS6U range, whilst the SA Tyre Recyclers consist of JA Solar's P72 range of modules.

All the photovoltaic modules have almost identical mechanical and temperature characteristics, but slightly different electrical characteristics represented in Table 47.

Table 46: Summary of modules from each of the photovoltaic systems

Photovoltaic System	No. of Modules	Photovoltaic Modules			
		Manufacturer	Range	Cell Type	Capacity
SAREBI	30	Canadian Solar	CS6U-325P	Poly-crystalline	325 Wp
SA Tyre Recyclers	700	JA Solar	JAP72S-10-330-SC	Poly- crystalline	330 Wp
Stripform Packaging	60	Canadian Solar	CS6U-335P	Poly- crystalline	335 Wp

Table 47: Photovoltaic module electrical characteristics

	At standard temperature conditions (STC)		
	CS6U-325P	JAP72S-10-330-SC	CS6U-335P
Nominal Max. Power	325 W	330 W	335 W
Operating Voltage	37.0 V	37.72 V	37.4 V
Operating Current	8.78 A	8.75 A	8.96 A
Open Circuit Voltage	45.5 V	43.54 V	45.8 V
Short Circuit Current	9.34 A	9.26 A	9.54 A
Module Efficiency	16.72 %	16.4%	17.23 %

Besides having the greatest nominal maximum power of 335 W, the CS6U-335P module also is the photovoltaic module with the greatest efficiency of 17.23%. The increased module efficiency of 0.51% in comparison to the second greatest module efficiency from the CS6U-325 module, will result in the CS6U-335P module generating more energy under the same conditions as the CS6U-325P module.

Table 47 illustrates that the module with the greatest Nominal Power is also the same module that has the greatest efficiency. This corresponds with the recorded data from the solar photovoltaic system at Stripform Packaging which consists of CS6U-335P modules and is the best performing photovoltaic system for actual recorded data. However, is the worst performing system during the simulations, which could unlikely be due to inaccurate PVsyst modelling data supplied from Canadian Solar, since Canadian Solar is one of the world's leading photovoltaic manufactures in the industry and is greatly reliant on PVsyst simulation results.

From Section 6.3.8, it was proven that one of the compelling factors that affect the performance of a photovoltaic system is the modular temperature. Table 48 summarises the temperature characteristics of each of the three different photovoltaic modules, all of which are very similar, except for the temperature coefficient for the maximum power rating (Pmax). The temperature coefficient of Pmax is the amount of power that is lost for every °C that the panel is hotter than Standard Temperature Conditions (STC) of 25 °C. Thus, resulting in the Canadian Solar modules losing 0.41% for every °C above 25°C, whereas the JA Solar module will lose 0.04% less than the Canadian Solar modules since it has a rate of -0.37%/°C (Peacock, 2012).

Table 48: Photovoltaic module temperature characteristics

Temperature Characteristic	**CS6U-325P**	**JAP72S-10-330-SC**	**CS6U-335P**
Temperature Coefficient (Pmax)	-0.41 % / °C	-0.37 % / °C	-0.41 % / °C
Temperature Coefficient (Voc)	-0.31 % / °C	-0.30 % / °C	-0.31 % / °C
Temperature Coefficient (Isc)	0.053 % / °C	0.054 % / °C	0.053 % / °C
Nominal Operating Cell Temperature	45 ± 2 °C	45 ± 2 °C	45 ± 2 °C
Operating Temperature	-40°C ~ +85°C	-40°C ~ +85°C	-40°C ~ +85°C

The similarities in temperature characteristics are as expected as all three of the photovoltaic modules consist of half-cell technology in which the photovoltaic cells are cut from 6-inch lengths to two 3-inch lengths (Canadian Solar, 2018). This results in the photovoltaic module being split into two independent parts, as seen in Figure 92. The reasoning for halving the length of the cells is to simultaneously halve the current by halving the surface area per cell. By reducing the amount of current the module temperature, power losses and ohmic losses (quarter the power loss since I^2R) are reduced, significantly improving the overall performance of the photovoltaic modules.

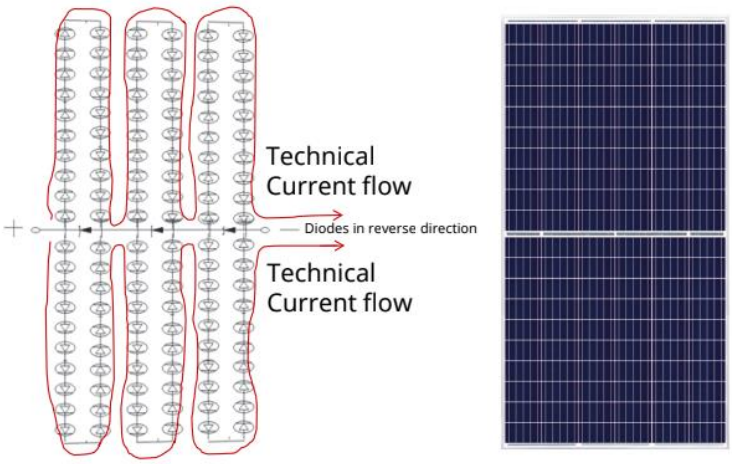

Figure 92: Current flow in half-cell technology

Even though the CS6U-335P photovoltaic module has the greatest nominal maximum power and efficiency, the other photovoltaic modules have similar characteristics which make it challenging to determine which may have the best performance. However, by making use of the PVsyst software, each of the photovoltaic systems can be modelled using each of the three different photovoltaic modules and compare the annual specific yield to determine which inverter performs best.

Table 49 illustrates the simulated annual specific yield of each of the photovoltaic systems if they had each of the photovoltaic modules. The findings obtained during the simulations revealed that according to PVsyst all three of the photovoltaic systems' performance could be improved by having different photovoltaic modules.

If the SAREBI system installed CS6U-335P modules instead of the CS6U-330P then the system would have an improved annual specific yield of 3 kWh/kWp. If the SA Tyre Recyclers system installed CS6U-325P modules instead of the JA Solar modules, then the system would have an improved annual specific yield of 13 kWh/kWp. If the Stripform Packaging system installed the JA Solar modules instead of the CS6U-335P modules, then the system would have an improved annual specific yield of 5 kWh/kWp.

Table 49: Specific annual yield comparison of the different photovoltaic modules

Photovoltaic System	CS6U-325P	JAP72S-10-330-SC	CS6U-335P
SAREBI	1 815 kWh/kWp	1 811 kWh/kWp	1 818 kWh/kWp
SA Tyre Recyclers	1 815 kWh/kWp	1 802 kWh/kWp	1 811 kWh/kWp
Stripform Packaging	1 719 kWh/kWp	1 774 kWh/kWp	1 769 kWh/kWp

Given the annual specific yield from Table 49, the results of installing different photovoltaic modules to the three different photovoltaic systems is inconclusive and unconvincing since these results do not correspond with the electrical characteristics mentioned in Table 47, in which the CS6U-335P module has the greatest nominal maximum power of 335 W and also the greatest efficiency of 17.23%.

A point to mention is that photovoltaic module manufactures ensure that all the modules operate as efficiently as possible when connected with different inverters. This is to prevent favouritism and allow the manufacturer to supply their modules to a greater market size.

7.1.2. Inverters

In Table 50 the inverters from each of the photovoltaic systems are tabulated illustrating that all three systems have different inverters. Even though they are all different inverter brands and output powers, they are almost identical in efficiency.

Table 50: Summary of inverters from each of the photovoltaic systems

Photovoltaic System	Inverters				
	Type	**Manufacturer**	**Output power**	**Output Current (AC)**	**Efficiency**
SAREBI	String	Schneider Electric	20 kW	32 A	98.0 %
SA Tyre Recyclers	String	SolarEdge	27.6 kW	40 A	98.3 %
Stripform Packaging	String	SMA	20 kW	33 A	98.4 %

Nowadays the inverter manufacturing market is extremely competitive. The key drivers for inverter choice are financial cost, remote monitoring software and the warranty since the most likely component in a solar photovoltaic system to fail is the inverter. Hence, it is no surprise that the Schneider, SolarEdge and SMA inverters have an almost identical efficiency (SolarQuotes, 2019).

Since all three of the inverters have similar properties, it is challenging to determine which inverter has the best performance. However, by making use of the PVsyst software, each of the photovoltaic systems can be modelled using each of the three different inverters and the annual specific yield compared, to determine which inverter performs best.

Table 51 illustrates the simulated annual specific yield of each of the photovoltaic systems if they had each of the inverters. The findings obtained during the simulations resulted in very similar specific yields for the Schneider Electric and SMA inverters, but a significant improvement in the specific yield when the photovoltaic systems had a SolarEdge inverter.

This observation does not come as a surprise as the photovoltaic system at SA Tyre Recyclers has a SolarEdge inverter and is the second best performing photovoltaic system for both the simulations and the actual recorded data.

Table 51: Specific annual yield comparison of the different inverters

Photovoltaic System	Schneider Electric	SolarEdge	SMA
SAREBI	1 815 kWh/kWp	1 851 kWh/kWp	1 818 kWh/kWp
SA Tyre Recyclers	1 793 kWh/kWp	1 802 kWh/kWp	1 797 kWh/kWp
Stripform Packaging	1 765 kWh/kWp	1 784 kWh/kWp	1 769 kWh/kWp

7.2. Photovoltaic System Configuration

Analysing the configuration of each of the photovoltaic systems, all three are configured in the same way. The photovoltaic modules are connected in series to form a string which is fed to an inverter, converted to AC and then fed directly to a busbar within a distribution board (DB). The only key differences between systems is the number of strings in each system, due to the size of the photovoltaic system, the azimuth angle of each of the systems and the tilt angle of the modules.

Discussed in Section 2.1, the ideal azimuth angle, in the Sothern Hemisphere, for a photovoltaic system is 0° North. However, this is not always possible due to constraints where the photovoltaic system is located. The constraints to the azimuth angle of the SAREBI and the Stripform Packaging systems were purely based on the available area. However, since the photovoltaic system at SA Tyre Recyclers is a rooftop mounted system, the azimuth angle is limited to the position of the building's roof.

The constraints to system's tilt angles are less complicated in comparison to the azimuth angle, in which since the SAREBI and Stripform Packaging systems are both ground-mounted systems, there is not a restriction to their tilt angles. However, the system at SA Tyre Recyclers is restricted to the pitch angle of the roof. Table 52 illustrates the different azimuth and tilt angles of each of the photovoltaic systems.

Table 52: Summary of azimuth and tilt angles

Photovoltaic System	Azimuth Angle	Tilt Angle
SAREBI	-19°	15°
SA Tyre Recyclers	22°	13°
Stripform Packaging	46°	15°

In Figure 93, the PVsyst software illustrated that ideal tilt angle for the systems, at their longitude and latitude locations, when simulated was 30°, which agrees with the literature (Jacobson and Jadhav, 2018).

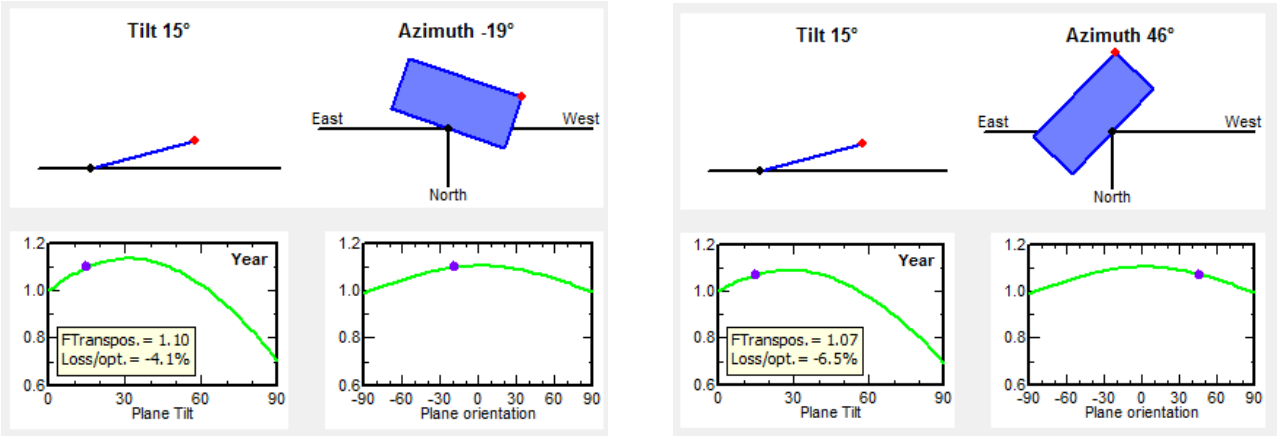

Figure 93: PVsyst simulation of azimuth and tilt angle for SAREBI and Stripform Packaging Systems

The simulations were then compiled again, but with different tilt angles. The results of which are represented in Table 53.

Table 53: Tilt angle simulation results

Tilt	SAREBI (kWh/kWp)	Difference (kWh/kWp)		Stripform Packaging (kWh/kWp)	Difference (kWh/kWp)
15°	1 815	-		1 769	-
20°	1 842	27		1781	12
25°	1 859	44		1786	17
30°	1 865	50		1 782	13
35°	1 860	45		1769	0
40°	1 845	30		1749	-20

From Table 53, the optimal angle that has the greatest specific yield for the SAREBI system is 30°, which agrees with the literature, but for the Stripform system the optimal angle in 25°. However, the difference between the 15° and 30° tilts for the SAREBI system, at 50 kWh/kWp, is far greater than the difference between the 15° and 25° tilts for the Stripform Packaging system, at 13 kWh/kWp.

Since the size of both the ground-mounted systems are relatively small in comparison to the rooftop mounted system at SA Tyre Recyclers, increasing the tilt angle from 15° to 30° would not make a significant impact to the annual generation yield. However, the increased tilt angle of the ground-mounted systems will have a significant impact to the cost of the steel structure because more steel is required to mount the models.

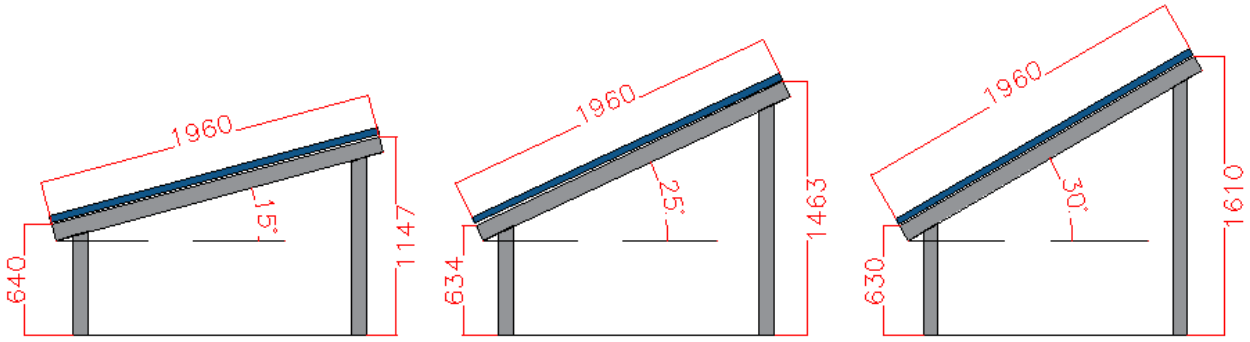

Figure 94: Ground-mounted steel structure dimensions

Figure 94, illustrates three ground-mounted structures all mounting a photovoltaic module with a length of 1 960 mm, at a 15° tilt, 25° tilt and at a 30° tilt. The total amount of steel required for the 15° tilted system is 3 747 mm, 4 057mm for the 25° tilt and 4 200 mm for the 30° tilted system. Thus, resulting in an additional requirement of 453 mm of steel to compensate for the increased tilt angle from 15° to 30°.

This is a compelling observation that must be considered when analysing the comparative cost of a ground-mounted solar photovoltaic system and was a factor that influenced the engineering, procurement and construction stages of the photovoltaic system. This is the resulting reason as to why the ground-mounted photovoltaic systems at SAREBI and Stripform Packaging were both installed at a tilt angle of 15° instead of the respective optimal tilt angle.

7.3. Photovoltaic System Technical Losses

7.3.1. Introduction

Before any solar photovoltaic system is installed it is carefully modelled on simulation software to forecast the quantity of energy yield it will produce over an annual period. As discussed in previous sections, many different factors influence the annual energy yield and the performance of a photovoltaic system. However, losses can play a significant role in affecting the performance of a photovoltaic system. In this section, the technical losses of the three installed systems will be discussed, namely the wiring losses and the soiling losses.

7.3.2. Simulation losses

During the PVsyst simulations the technical loss parameters were all set to the default parameters, as follows:

Thermal loss factor: $U = Uc + Uv \; x \, Wind \, Velocity$

Where,

Constant loss factor (W/m^{2}k): $Uc = 20$

Wind loss factor (W/m^{2}k): $Uv = 0$

DC Ohmic Losses: Loss fraction at STC = 1.5 %

AC Ohmic Losses: Loss fraction at STC = 0.0 %

Module Quality: Module Efficiency Loss = 3.0 %

Module Mismatch: Power Loss at MPP = 1.0 %

String Voltage Mismatch: Power Loss at MPP = 0.1 %

Soiling Loss: Yearly Soiling Loss Factor = 3%

It must be noted that the AC ohmic losses were set to 0.0 % due to the distances between the inverters and the tie-in points of each of the three photovoltaic systems vary from system to system. Therefore, to ensure that the simulations were as accurate as possible, the AC ohmic losses were set to the same value.

Table 54, summarises the key loss parameters from each of the photovoltaic system's loss diagrams. A loss diagram is a powerful tool that is used to identify the main sources of losses (PVsyst, 2020).

Table 54: Loss parameters from loss diagrams over a year

Photovoltaic System	PV Loss due to Temperature	Mismatch Loss, module & strings	Ohmic Losses	Inverter Losses
SAREBI	-9.78 %	-1.10 %	-1.17 %	-2.28 %
SA Tyre Recyclers	-9.84 %	0.00 %	-0.88 %	-1.92 %
Stripform Packaging	-9.89 %	-1.10 %	-1.16 %	-2.16 %

Table 54, presents an interesting finding in that the PV losses due to temperature is a combination of the losses due to the ambient temperature and the module temperature. An interesting point is that according to the literature the two ground-mounted systems should have the least amount of temperature losses due to their free-standing nature, allowing for improved airflow around the modules (USDOE, 2004). This is true for the SARBI system, having the least temperature losses, whilst the Stripform Packaging system has the greatest amount temperature losses out of the three photovoltaic systems. However, the ohmic losses for the two ground-mounted systems are almost identical in comparison to the rooftop-mounted system. The ohmic losses are the losses that occur due to the resistance of the wiring circuit between modules and the terminals of the sub-array.

The mismatch losses for both the SAREBI and Stripform Packaging systems are identical, which is expected since both the ground-mounted systems consist of Canadian Solar modules. The inverter losses of each of the photovoltaic systems are all different, which is expected since each system has a different inverter and all three correlates with each of their efficiency rating of 98%.

7.3.3. Soil losses

As mentioned in Section 2.4.2, soiling losses are due to dirt, dust and other forms of contamination that can cover the solar cells and prevent the photons from colliding with the silicon cells. Soiling losses are not a standard rate and will differ depending on the location of the photovoltaic system. This is due to a multitude of factors such as exposure to dust, road traffic, frequency of rain and the number of birds in the area.

According to the National Renewable Energy Laboratory (NREL), the industry standard for the typical soiling losses is suggested to be 5%. However, that value can range from 2% to 25% depending on the location of the photovoltaic system (Marion, *et.al*, 2005).

However, for this study, the soiling losses were very difficult to quantify and incorporate. What is certain is that all the photovoltaic systems were cleaned once every four months during the annual period that the energy generation measurements were obtained. However, it is uncertain at what dates the modules were cleaned, thus making it difficult to determine the effects of soiling on the performance of the photovoltaic systems.

7.3.4. Calculated DC Losses

To determine the DC voltage losses from the DC cables used in the photovoltaic systems the following equation must be used:

$$V\ drop = 2(Imp)(R)(l)$$

Where:

Length of the Cable = l

Operating current of the module = I_{mp}

Resistance of the cable per meter = R

In Table 55, the volt drop of each of the DC cable lengths are all less than the recommended maximum of 2%, recommended by the NREL (Marion, *et.al*, 2005), and will thus not affect the performance of each of the photovoltaic systems. A point to mention is that the cabling for the SAREBI photovoltaic system didn't have to be 6 mm^2, a 4 mm^2 cable would have been sufficient since the current generated from the photovoltaic system will be less than that generated from the Stripform Packaging system. However, the 6 mm^2 DC cabling could have been selected due to available supply in comparison to the 4 mm^2 cable.

Table 55: Summary of DC losses of the photovoltaic systems

Photovoltaic Systems	Cable	Cable Length (m)	R (mΩ/m)	Imp (A)	Volt Drop (V)	Volt Drop (%)
SAREBI	KBE Solar 6 mm^2	42	3.39	8.78	2.5	0.45

SA Tyre Recyclers	KBE Solar 6 mm^2	135	3.39	8.75	8.01	1.52
Stripform Packaging	KBE Solar 4 mm^2	50	5.09	7.17	3.65	0.71

7.3.5. Calculated AC Losses

To determine the AC voltage losses from the AC cables used in the photovoltaic systems the following equation must be used:

$$V\ drop = \frac{(Imp)(R)(l)}{\sqrt{3}(V)}$$

Where:

Length of the Cable = l

Operating current of the module = I_{mp}

Resistance of the cable per meter = R

AC Voltage = V

In Table 56, the voltage drop of each of the AC cable lengths are all less than the recommended maximum of 3%, recommended by the NRS 097-2-3:2014 (NRS, 2014), and will thus have a minimal effect on the performance of each of the photovoltaic systems. The NRS 097-2-3:2014 standard ensures that the maximum change in a Low Voltage (LV) cable from a voltage drop due to embedded generators is limited to 3 %.

The reasoning for such small voltage drops is due to the relatively short AC cable length since the inverters for the SA Tyre Recyclers and the Stripform Packaging photovoltaic systems are all mounted next to their tie-in points. The distance between the inverter and the tie-in point for the SAREBI photovoltaic system is far greater in length, but not long enough to affect the performance of the photovoltaic system.

Table 56: Summary of AC losses of the photovoltaic systems

Photovoltaic System	Inverter	Cable	Power (kW)	Length (m)	Voltage (V)	Current (A)	Volt Drop (V)	Volt Drop (%)
SAREBI	Inverter 1	SWA 4 mm^2 Cu 4 Core	20	20	400	28.9	0.87	0.45
SA Tyre Recyclers	Inverter 1	SWA 4 mm^2 Cu 4 Core	20.6	5	400	39.8	1.90	0.48
	Inverter 2	SWA 4 mm^2 Cu 4 Core	20.6	5	400	39.8	1.90	0.48
	Inverter 3	SWA 4 mm^2 Cu 4 Core	20.6	5	400	39.8	1.90	0.48
	Inverter 4	SWA 4 mm^2 Cu 4 Core	20.6	5	400	39.8	1.90	0.48
	Inverter 5	SWA 4 mm^2 Cu 4 Core	20.6	5	400	39.8	1.90	0.48
	Inverter 6	SWA 4 mm^2 Cu 4 Core	20.6	5	400	39.8	1.90	0.48
	Inverter 7	SWA 4 mm^2 Cu 4 Core	20.6	5	400	39.8	1.90	0.48
Stripform Packaging	Inverter 1	SWA 4 mm^2 Cu 4 Core	20	2	400	28.9	0.09	0.14

7.4. Ideal Photovoltaic System Design

7.4.1. Introduction

In this section of the study, an ideal photovoltaic system will be designed and simulated. In each case, the design will make use of the same components that were incorporated in the three photovoltaic systems in addition to the same geographic location and meteorological dataset. The reasoning for this is to have a realistic ideal system that the three photovoltaic systems can be compared to.

7.4.2. Solar photovoltaic system specifications

Analysis of the annual specific yield of the three different photovoltaic systems, both the simulated and the actual yield, resulted in the ground-mounted configuration outperforming the rooftop mounted configuration. Therefore, a ground-mounted system will be selected for the ideal photovoltaic system.

From Section 7.1.1 the best performing photovoltaic module out of the three was the CS6U-335P, due to its module efficiency and nominal maximum power, which were the modules installed in the Stripform Packaging photovoltaic system. From Section 7.1.2 the best performing inverter was the SolarEdge SE27.6k, which was installed at the SA Tyre recyclers photovoltaic system.

As discussed by Jacobson and Jadhav, the ideal tilt angle for a photovoltaic system in the Cape Town region is 30° (Jacobson and Jadhav, 2018) and from in Section 2.1, the ideal azimuth angle for a photovoltaic system in the Southern Hemisphere is 0° North. Therefore, the selected orientation for the ideal photovoltaic system was a 30° tilt and an azimuth angle of 0°

Since the SolarEdge SE27.6k inverter has three inputs for three separate strings, the optimal configuration is to connect 28 modules in series to each string. This would equate to a DC output power of 9.38 kWp per string and a maximum DC power output of 28.14 kWp. However, since the inverter is limited to 27.5 kW, the photovoltaic system will only be able to output a maximum of 27.6 kWp on the AC side of the system. Even though the inverter is slightly overloaded with the additional 540 Wp, there is still 0% overload losses and a nominal power ration of 0.96 as illustrated in Figure 95.

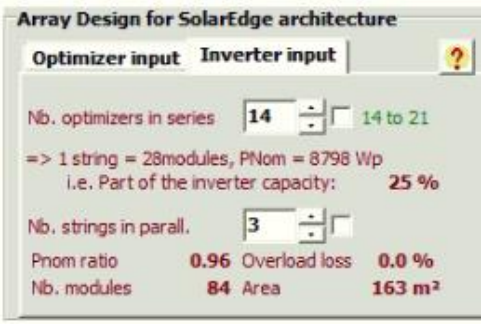

Figure 95: PVsyst simulation of an ideal PV system in Atlantis

7.4.3. Solar photovoltaic system performance

In Table 57 the results from modelling the ideal photovoltaic system in PVsyst and the results from the actual and simulated photovoltaic system at Stripform Packaging system are compared. It is expected that the ideal system will have a greater energy yield over the annual period since the ideal system is 8.14 kWp greater in capacity. However, to accurately compare the performance of the two photovoltaic systems, the annual specific yield of the two systems must be analysed. This analysis resulted in a significant difference in the yield generated.

Analysis of the ideal system's annual specific yield and the actual Stripform Packaging yield resulted in the ideal system's annual specific yield being 8 % (141 kWh/kWp/year) greater than the Stripform Packaging actual annual specific yield and 7.5 % (133 kWh/kWp/year) greater than the Stripform Packaging simulated annual specific yield. This result correlates with the difference between the simulated and the actual annual specific yield discussed in Section 6.2.3, in which the difference between the actual and the simulated annual specific yield is 0.5%.

Table 57: Comparison of Ideal system and the Stripform Packaging system

Parameters	Ideal System	Stripform Packaging (Actual)	Stripform Packaging (PVsyst)
Tilt / Azimuth	30° / 0°	15° / 46°	15° / 46°
Photovoltaic Modules	84 x CS6U - 335P	60 x CS6U - 335P	60 x CS6U - 335P
Maximum Nominal Power (DC)	28.14 kWp	20.1 kWp	20.1 kWp
Maximum Nominal Power (AC)	27.6 kW	20 kW	20 kW
Inverter	SolarEdge SE27.6k	SMA (20000 TL-20)	SMA (20000 TL-20)
Produced Energy (kWh/year)	53 520	35 387	35 550
Annual Specific Yield (kWh/kWp/year)	1 902	1 761	1 769

The only major differences between the ideal system and the Stripform Packaging system is the change in the tilt angle, the azimuth angle and the use of the SolarEdge inverter instead of the SMA inverter. Both systems are ground-mounted, and both consist of the CS6U-335P photovoltaic modules.

From Section 7.1.2, it was observed that modelling the Stripform Packaging system with the SolarEdge inverter instead of an SMA inverter resulted in improving the annual specific yield from 1769 kWh/kWp to 1784 kWh/kWp, an increase of only 0.8 % (15 kWh/kWp/year). However, if the only modification to the Stripform Packaging system is changing the tilt angle to 30° and the azimuth angle to 0°, as illustrated in Table 58, then the result is a 6% (114 kWh/kWp/year) increase in annual specific yield from 1769 kWh/kWp to 1883 kWh/kWp. This is a far greater improvement to the performance of the solar photovoltaic systems performance in comparison to changing the inverter from an SMA to a SolarEdge.

Table 58 compares the annual specific yield of the ideal system and the Stripform Packaging system which has been configured to a 30° tilt angle and an azimuth angle of 0°. The result of the comparison is that even though the ideal system still has a greater annual specific yield, the improvement has been reduced to only 1% (19 kWh/kWp/year) when compared to the performance of the ideal photovoltaic system.

Table 58: Comparison of Ideal system and the Stripform Packaging system at 30° tilt and azimuth of 0°

Parameters	**Ideal System**	**Stripform Packaging (30° / 0°)**
Tilt / Azimuth	30° / 0°	30° / 0°
Photovoltaic Modules	84 x CS6U - 335P	60 x CS6U - 335P
Maximum Nominal Power (DC)	28.14 kWp	20.1 kWp
Maximum Nominal Power (AC)	27.6 kW	20 kW
Inverter	SolarEdge SE27.6k	SMA (20000 TL-20)
Produced Energy (kWh/year)	53 520	37 840
Annual Specific Yield (kWh/kWp/year)	1 902	1 883

7.5. Conclusion

Technical analysis of the equipment used in the three different photovoltaic systems resulted in the Canadian Solar CS6U-335P module being the best performing photovoltaic module and the SolarEdge SE27.6k being the best performing inverter. From the actual and the simulated annual specific yields, the best performing photovoltaic system configuration was the ground-mounted configuration. However, when configuring a ground-mounted photovoltaic system, the most crucial factors to consider that affect the performance is the tilt angle and the azimuth angle, which is proven and discussed when the Stripform Packaging system's annual specific yield is compared to that of an ideal photovoltaic system with the same photovoltaic equipment and in the same geographical location.

In addition to a technical analysis of the photovoltaic equipment and the configuration of the photovoltaic system, the technical losses must also be analysed to determine their relationship with the performance of the photovoltaic systems. It was observed that it was very difficult to quantify the soiling losses in this study.

Analysis of the DC and AC cable voltage losses resulted in all three of the photovoltaic systems falling well within the recommended maximum voltage drop allowance range in which a maximum of 2% voltage drop is recommended by the NREL (Marion, *et.al*, 2005), and a maximum of 3%, recommended by the South African Standard NRS 097-2-3:2014 (NRS, 2014). Therefore, the selection of cable material and sizing is perfectly matched for the current ratings and the lengths of cable required to connect the photovoltaic system to their respective connection tie-in points.

8. Financial Analysis

8.1. Introduction

With the current under allocation of debt to finance solar photovoltaic systems in South Africa. Accurate budgeting and finance allocation for a solar photovoltaic system is extremely crucial.

This chapter will investigate the different component costing for a photovoltaic system and how they correspond to the three photovoltaic systems, the value of the energy generated by the three photovoltaic systems and how their payback periods will be affected due to the performance of the systems.

8.2. Photovoltaic System Capital Costing

The final stage of designing a photovoltaic system is to allocate the budget to procure the equipment and construction costs to install the system. Once the number of photovoltaic modules, inverters, cabling, circuit breakers and the remaining balance of system components have been determined, then they must be procured from the supplier. However, each component incurs a different cost, as does the construction of the system. Every photovoltaic system is different, due to its unique design, size, location and configuration.

Table 59, illustrates the approximate Rand/Wp costing obtained from New Southern Energy for each of the solar photovoltaic systems at different sizes. Since the majority of the photovoltaic system components are imported from international suppliers, the costs fluctuate relative to the Rand/ US Dollar exchange rate. An additional factor to consider is that EPC companies such as New Southern Energy procure their photovoltaic system components at bulk quantities to obtain a better purchase price, due to their economy of scales. Therefore, the larger the photovoltaic systems, the lower the Rand/Wp rate, which corresponds with GreenCape's analysis of the 2018 Western Cape solar photovoltaic market, illustrated in Table 60 (Radmore and Chilwan, 2018).

Table 59: Approximate photovoltaic system Costing breakdown (New Southern Energy, 2020)

Photovoltaic System Costing (R/Wp)	System Size		
	< 100 kWp	> 100 kWp and < 500 kWp	> 500 kWp
Cost breakdown (Ex storage)	14.00	13.00	12.30
Inverter	1.50	2.32	1.76
PV modules	5.30	4.79	5.10
Metering	0.18	0.19	0.03
Protection, switches, reticulation	2.72	1.29	1.82
Mounting and structures	1.65	1.98	1.67
Engineering	0.83	1.00	1.00
Construction	0.55	0.74	0.65

Other (transportation, rigging, P&Gs, equipment hire, contingency, etc)	1.28	0.69	0.27

Table 60: GreenCape analysis of the South African photovoltaic market (GreenCape, 2018)

System Size	Capital Cost of System (R/kWp)	Power Purchase Agreement Tariff (R/kWh)
< 100kWp	R 13.50 – R 16.00	R 1.20 – R1.45
> 100kWp and < 500kWp	R 11.50 – R 14.00	R 1.05 – R 1.25
> 500kWp	R 10.50 – R 13.00	R 0.90 – R 1.15

Unfortunately, the capital costs for each of the three photovoltaic systems are not available, due to non-disclosure agreements between the EPC installer and the client. Using the information from GreenCape's analysis in Table 60 the capital cost of each of the three photovoltaic systems can be determined and is illustrated below in Table 61.

Table 61: Estimated capital cost of the photovoltaic systems

Photovoltaic System	System Size (kWp)	R/kWp Rate	Estimated Capital Cost
SAREBI	10	R 16 000/kWp	R 160 000
Stripform Packaging	20.1	R 16 000/kWp	R 320 000
SA Tyre Recyclers	231	R 12 750/kWp	R 2 945 250

However, a point to note is that GreenCape's capital cost analysis is only based on rooftop mounted systems and not photovoltaic systems that are ground-mounted. This leaves for a level of uncertainty, but according to New Southern Energy, the capital cost difference between a ground-mounted system and a rooftop mounted system is an increased cost of approximately 8% for a ground-mounted system in comparison to a rooftop mounted system (New Southern Energy, 2020).

When installing a photovoltaic system on a roof consisting of asbestos roofing, the roof first must be removed, the asbestos safely disposed of and then replaced before a photovoltaic system can be installed. This has a significant impact to the capital cost of a photovoltaic system. According to GreenCape's analysis, there is a 13% increase in capital costing if the roof removal and replacement is included in the total capital cost of the photovoltaic system (GreenCape, 2019). These figures are based on market research and from interviews from Conrad Kok from EnviroServ, a South African waste management company with approved certification to safely remove and dispose of asbestos.

In Section 7.2 a correlation between the length of steel, required for ground-mounted systems, and the photovoltaic module tilt angle is evident and as the tilt angle of a photovoltaic module is increased, so does the length of the steel ground-mounted structure. However, from New Southern Energy's experience in

installing ground-mounted systems, for every 5° that the tilt angle is increased, the capital cost for the ground-mounted framing increases by 3.5% (New Southern Energy, 2020). This increase in cost is relatively low for a photovoltaic system with a similar size as the SAREBI or Stripform Packaging systems. However, this increase would have a significant impact to the capital costing of a photovoltaic system that is of a utility sized ground-mounted installation.

8.3. Capital Cost Recovery

To determine the capital cost recovery, a financial model for each of the photovoltaic systems must be developed to accurately determine the payback period and the levelized cost of energy (LCOE) for each of the systems. Each of the three financial models are illustrated in Appendix C. However, to accurately analyse the financials, the assumptions in Table 62 must be made.

Table 62: Financial modelling assumptions

Assumptions	Qty	Units
Capital cost of the SAREBI photovoltaic system	160 000	Rand
Capital cost of the Stripform Packaging photovoltaic system	320 000	Rand
Capital cost of the SA Tyre Recyclers photovoltaic system	2 945 250	Rand
Actual annual specific yield of the SAREBI system	1 646	kWh/kWp/year
Actual annual specific yield of the Stripform Packaging system	1 761	kWh/kWp/year
Actual annual specific yield of the SA Tyre Recyclers system	1 712	kWh/kWp/year
Lifetime of the photovoltaic systems	30	years
Duration of Operation and maintenance (O&M)	30	years
Module Degradation	0.07	%/ year
OPEX per annum as percentage of initial CAPEX	1.00	%
Inverter replacements in year 11 as percentage of initial CAPEX	5.00	%
Inflation	6.00	%
Discount rate (nominal)	10.0	%
City of Cape Town electricity tariff (Small Power User 1 (High consumption >1000 kWh/ Month)	1.79	R/kWh
City of Cape Town electricity tariff annual increase	8.00	%

The levelized cost of energy and the payback periods of each of the photovoltaic systems obtained from the financial models in Appendix are illustrated in Table 63 below.

Table 63: Photovoltaic system financial modelling results

Photovoltaic Systems	LCOE (R/kWh)	Payback Period (Years)
SAREBI	R 0.65	6.11
Stripform Packaging	R 0.60	5.64
SA Tyre Recyclers	R 0.50	4.56

From Table 63, the photovoltaic system with the lowest payback period and levelized cost of energy is the SA Tyre Recyclers photovoltaic system. While the highest levelized cost of energy and payback period is the SAREBI photovoltaic system.

8.4. Conclusion

From the market research obtained from GreenCape and New Southern Energy, accurate pricing and financial modelling was able to be developed for each of the three photovoltaic systems. This aided the financial analysis of each of the three systems which could result in a comparative financial analysis between them.

When encountering a rooftop that consists of asbestos roofing material, two options are available: replacing the asbestos roofing with a new and safe roofing material or installing a ground-mounted system. Both of which have an increased cost implication, but out of the two options, the cheapest and less hazardous is installing a ground-mounted system, due to an increased cost of only 8% in comparison to an increase of 13% to replace the asbestos roofing. However, before one goes ahead with a ground-mounted installation, the photovoltaic module tilt angle must be taken into account due to its correlation with the increased cost in ground-mounting framing, which will have a significant impact on a photovoltaic systems LCOE and payback period, should the system be of a large capacity.

9. Conclusion

PVsyst simulations of the three photovoltaic systems revealed that from a simulated specific annual yield perspective the best performing system and the worst performing system are both ground-mounted systems. Out of the two ground-mounted and one rooftop mounted systems, the SAREBI ground-mounted system was the best performing, whilst the worst performing was the ground-mounted Stripform Packaging system. Analysis of the performance of the photovoltaic systems from an actual specific annual yield perspective revealed a similar outcome as the simulated system performance. However, in this case, the SAREBI system was the worst performing and Stripform Packaging system was the best performing system.

Both the simulated and actual cases agree with the literature, in which it was found that a ground-mounted system has a greater annual specific yield and will thus outperform a rooftop mounted system. However, the reason for the discrepancy between the simulated and the actual performance of the two ground-mounted systems could relate to inaccuracies in the PVsyst modelling databases or evidence that load shedding had a far greater impact on the actual yield than was initially expected.

With regards to the actual performance of the photovoltaic systems, the only meteorological factors considered in this study that have a strong correlation with the generated yield of the photovoltaic systems are the global horizontal irradiation (GHI) and the modular temperature, both of which agree with the literature.

A potential cause of the SAREBI system's poor performance can be attributed to the effects of the module surface temperature, which could be due to the SAREBI system being a carport, wherein on a daily basis cars park directly underneath the exposed photovoltaic modules. This likely exposed the modules to heat radiating from the car's engines. In comparison, the area directly underneath the photovoltaic modules at Stripform Packaging are completely vacant without any cars or objects placed underneath the modules.

From the technical analysis of the three different photovoltaic systems, the Canadian Solar CS6U-335P module was the best performing photovoltaic module and the SolarEdge SE27.6k the best performing inverter. However, given that the findings noted the optimal performance was that of the ground-mounted system, the most crucial factors affecting the performance includes that of the tilt angle and the azimuth angle. Unfortunately, by configuring a ground-mounted system's tilt angle to the optimal angle of 30° the capital cost is increased and must be factored into financial models and debt financing of solar photovoltaic systems. Accurate budgeting and finance allocation is extremely critical.

From the financial analysis, the comparative cost of each of the three photovoltaic systems are determined by calculating the levelized cost of energy (LCOE) and each of the systems payback periods. Given the capital cost for all three of the photovoltaic systems, the system with the lowest payback period is the rooftop mounted system. In addition to the payback period and from the levelized cost of energy analysis for each of

the three systems, the rooftop mounted system again has the lowest value of the three photovoltaic systems. Thus, from a financial perspective, the rooftop mounted system is the most financially feasible. This result is in contrast to the findings from the 2004 study by The US Department of Energy, in which the ground-mounted system is the most financially feasible, due to the relatively lower payback period, in comparison to the rooftop mounted system. However, the USDOE study is 16 years old and since 2004 the pricing of photovoltaic components has significantly reduced over time. Therefore, it is unable to provide an accurate financial comparison to the current 2020 prices.

From an actual annual specific yield perspective, the best performing photovoltaic configuration is a ground-mounted system. However, over the lifetime of a photovoltaic system, the rooftop-mounted system comes at a much less capital cost and thus, more financially viable in comparison to a ground-mounted system. However, if a roof consists of asbestos material, the most financially feasible option is to install a ground-mounted system instead of replacing the asbestos roofing.

In conclusion, by fully understanding the performance, payback period and levelized cost of energy, a clear understanding of potential risk can be determined, thus making the installation of photovoltaic systems more appealing for financiers.

10. Limitations and Recommendations

The study has shown that from an annual specific yield perspective a ground-mounted photovoltaic system is a better performing system in comparison to a rooftop mounted photovoltaic system. However, from a financial perspective, the rooftop mounted system is a better performer. A significant portion of this research is based on the actual onsite specific yield data recorded from each of the photovoltaic systems, which inevitably has levels of uncertainty which could have affected the results and potentially the outcome of this study.

The data collected for this study was collected for a period of only one year, during which load shedding occurred and due to the inverters anti-islanding safety features, the photovoltaic systems stopped operating during these times, reducing the potential quantity that each system could generate. Since each of the photovoltaic systems consisted of different photovoltaic equipment, the measuring equipment for each system differed and could have affected the accuracy in recording the generate energy. Another factor that could have played a crucial role in affecting the performance of each of the photovoltaic systems, is the accurate recording of when operation and maintenance (O&M) procedures took place. If data had been collected during O&M procedures, then one would be able to ensure that each of the photovoltaic systems were clean and operating at their peak level of performance simultaneously.

However, a possible remedy to the inaccuracies in the data collection is to increase the sample size, by recording at least two years' worth of data instead of only one year. The reasoning for only one years of data is based solely on construction delays, which could have been prevented if construction began during the summer months, and contract negotiations which could have had occurred in a prompt manner. By obtaining a greater sample size of data, the effects of load shedding, meteorological irregularities and the potential O&M inaccuracies could potentially be omitted.

From a financial point of view, a key component to modelling the payback periods and the levelized costs of energy were the total capital costs of each of the photovoltaic system. Unfortunately, the actual capital costs for the three systems were unattainable and had to be assumed based on market research. These capital cost assumptions were within the market price range, but it does leave margin for error when determining the comparative costs for each of the systems.

It is recommended that the study be repeated in a manner in which each of the configurations of the photovoltaic systems are constructed consisting of all the same photovoltaic components, measuring equipment, tilt and azimuth angles. All of which would result in two identical photovoltaic systems where one is installed on a rooftop and the other installed on the ground. Once the two photovoltaic system configurations are equal in all manners, then it will be an accurate comparison to determine which configuration is the most optimal performer and which is the most financially viable.

References

Amajama, J. 2016. Effect of Air Pressure on the Output of Photovoltaic Panel and Solar Illuminance (or Intensity). International Journal of Scientific Engineering and Applied Science (IJSEAS) – Volume-2, Issue-8.

Available: http://www.solafuture.co.za/news/sola-completes-212kw-cape-quarter-project// [2017, June 10].

Available: http://www.solafuture.co.za/news/sola-completes-212kw-cape-quarter-project// [2017, June 10].

Basha, L. 2012. Analysis and evaluation tools development of photovoltaic modules and system performance. Master Thesis, Cairo University.

Bergmann, R, Werner, J. 2002. The Future of Crystalline Silicon Films on Foreign Substrates. Thin Solid Films. Elsevier.

Boston University School of Public Health. 2013. Introduction to Correlation and Regression Analysis. Boston University. Available: http://sphweb.bumc.bu.edu/otlt/mph-modules/bs/bs704_multivariable/bs704_multivariable5.html [2019, August 28].

Brent, A, van der Merwe, W. 2020. Evaluating the Energy Potential of Solar PV Located on Mining Properties in the Northern Cape Province of South Africa. Sustainability 2020. MDPI.

Canadian Solar. 2018. Canadian Solar KuModules. Powerpoint Presentation.

Canadian Solar. 2018. MAXPOWER CS6U-315|320|325|330P. Canadian Solar. Available: https://www.canadiansolar.com/fileadmin/user_upload/downloads/datasheets/v5.53/Canadian_Solar-Datasheet-MaxPower-CS6U-P-v5.53en.pdf [2018, March 05].

Census 2011. 2011. Atlantis. STATSSA. Available at: https://census2011.adrianfrith.com/place/199004 [2018, January 02].

Climate Data. 2018. Atlantis Climate. Climate Data.org. Available: https://en.climate-data.org/location/23404/ [2018, January 02].

Dabrowski, L. 2014. Advantages of Ground-Mounted Solar Systems. Renewable Energy Corporation. Available: https://renewableenergysolar.net/advantages-ground-mounted-solar-system/ [2020, October 22].

Dash, P, Gupta, N. 2015. Effect of Temperature on Power Output from Different Commercially available Photovoltaic Modules. International Journal of Engineering Research and Applications (IJERA). ISSN : 2248-9622, Vol. 5, Issue 1(Part 1).

Department of Environmental Affairs (DoEA). n.d. Asbestos: Know what it is and how you can protect yourself. Department of Environmental Affairs (DoEA). Available: https://www.environment.gov.za/sites/default/files/docs/asbestos_pamphlet.pdf [2017, March 27].

Derrick, A. 1998. Financing Mechanisms for Renewable Energy. Renewable Energy. Elsevier.

Dolara, A, Lazaraoiu, G, Leva. S. Manzolini, G, Votta, L. 2016. Snail Trails And Cell Microcrack Impact On PV Module Maximum Power And Energy Production. IEEE Journal of Photovoltaics.

DuPont. 2017. Mitigation Strategies for Hot Spots in Crystalline Silicon Solar Panels. DuPont. Available: http://www.dupont.com/content/dam/dupont/products-and-services/solar-photovoltaic-materials/solar-photovoltaic-materials-landing/documents/hot-spot-mitigation.pdf [2017, December 18].

ECOSMART. 2017. PV System Performance: GHI to PoA. ECOSMART. Available: https://ecosmartsun.com/pv-system-performance-3/pv-system-performance-ghi-to-poa/ [2017, August 01].

Elamri Y, Cheviron B, Mange A , Dejean C , Liron F and Belaud G. 2018. Rain concentration and sheltering effect of solar panels on cultivated plots. Hydrol. Earth Syst. Sci., 22, 1285–1298.

Eskom, 2014. Load Shedding Frequently Asked Questions (FAQ). Eskom. Available: http://www.eskom.co.za/documents/LoadSheddingFAQ.pdf [2019, August 28].

Foster, R., Ghassemi, M. and Cota, A., 2009. Solar energy: renewable energy and the environment. CRC Press.

Gaisma. Available: http://www.gaisma.com/en/location/cape-town.html [2016, August 23].

Gielen, D, Boshell, Francisco, Saygin, D, Brazilian, M, Wagner, N, Gorini, R. 2019. The role of renewable energy in the global energy transformation. Energy Strategy Review. Elsevier.

Global Modeling and Assimilation Office (GMAO) (2015), MERRA-2 tavg1_2d_slv_Nx: 2d,1-Hourly,Time-Averaged, Single-Level, Assimilation, Single-Level Diagnostics V5.12.4, Greenbelt, MD, USA, Goddard Earth Sciences Data and Information Services Center (GES DISC), Accessed [Atlantis South Africa, 2019, July25] DOI:10.5067/VJAFPLI1CSIV. Available: http://www.soda-pro.com/web-services/meteo-data/merra [2019, July 25].

Goetzberger, A, Luther, J, Willeke, G. 2002. Solar cells: past, present, future. Solar Energy Materials and Solar Cells Volume 74. Elsevier.

Goswami, D.Y., 2015. Principles of Solar Engineering. CRC Press.

GreenCape. 2017. Market Intelligence Report – Energy Services 2017. GreenCape.

GreenCape. 2017. Market Intelligence Report – Renewable Energy 2017. GreenCape.

Halliday, D, Resnick, R, Walk, J. 2011. Fundamentals of Physics. John Wiley & Sons.

Honsberg C, Bowden S. 2019. Module Materials. PVEducation.org. 2019. Available: https://www.pveducation.org/pvcdrom/modules-and-arrays/module-materials [2019, July 25].

Honsberg, C, Bowden, S. 2017. Standard Solar Spectra. PVEducation.org. Available: http://www.pveducation.org/pvcdrom/appendices/standard-solar-spectra [2017, August 01].

IRENA (2019), Future of Solar Photovoltaic: Deployment, investment, technology, grid integration and socio-economic aspects (A Global Energy Transformation: paper), International Renewable Energy Agency, Abu Dhabi.

Jacobson, M, Jadhav, V. 2018. World estimates of PV optimal tilt angles and ratios of sunlight incident upon tilted and tracked PV panels relative to horizontal panels. Elsevier. Solar Energy: Volume 169, 15 July 2018, Pages 55-66. Available: https://web.stanford.edu/group/efmh/jacobson/Articles/I/TiltAngles.pdf [2019, October 17].

Jäger, K, Isabella O,Smets, A, van Swaaij, R, Zeman, M. 2014. Solar Energy: Fundamentals, Technology and Systems. Delft University of Technology. 2014.

KBE Elektrontechnik. 2018. KBE Solar PV1-F – Datenblatt / Technical Data Sheet. Available: https://www.kbe-elektrotechnik.com/fileadmin/KBE_B/Broschueren/Solarbroschuere_1_Solar_TUEV_72dpi.pdf [2018, March 05].

Kernahan, K, Curzon, P, Stewart, M. 2012.Solar Cell Microcracks Are Inevitable, And idealPV FOZHS Makes Them Irrelevant. Ideal PV. Available: http://idealpv.com/Solar_Cell_Microcracks_Are_Inevitable_And_idealPV_FOZHS_Makes_Them_Irrelevant.pdf [2017, December 20].

Laughton, C., 2010. Solar domestic water heating: the earthscan expert handbook for planning, design and installation. Routledge.

Luque, A,Hegedus, S. 2011. Handbook of Photovoltaic Science and Engineering. Second Edition. John Wiley & Sons.Boyle, G. 2004. Renewable Energy: Power for a Sustainable Future. Second Edition. Oxford, UK: Oxford University Press.

Malagnino, R.A, 2015. Performance analysis of photovoltaic plants installed in dairy cattle farms. Journal of Agricultural Engineering 2015; volume XLVI:455. Department of Agricultural and Food Sciences, University of Bologna, Italy.

Marion, B, Adelstein, J, Boyle, K, Hayden, H, Hammond, B, Fletcher, T, Canada, B, Narang, B, Shugar, D, Wenger, H, Kimber, A, Mitchell, L, Rich, G, Townsend, T. 2005. Performance Parameters for Grid-Connected. PV Systems. National Renewable Energy Laboratory (NREL). Available: https://www.nrel.gov/docs/fy05osti/37358.pdf [2020, January 20].

Masters, G. 2004. Renewable and Efficient Electric Power Systems, 2nd ed. New Jersey: Wiley-IEEE Press. 2004.

Mishra, S. 2018. Poor Structures Trip Solar Plan. Telegraph India. Available: https://www.telegraphindia.com/odisha/poor-structures-trip-solar-plan/cid/1310611 [2020, October 22].

Muringathuparambil, R, Radmore, J. 2019. Financing Rooftop Solar PV Unlocking the energy potential for your business through innovative green finance. GreenCape. Available: https://www.greencape.co.za/assets/Uploads/GC-Finance-Brief-v7-WEB.pdf [2020, October 22].

National Oceanic and Atmospheric Administration (NOAA). Solar Position Calculator. Available: http://www.esrl.noaa.gov/gmd/grad/solcalc/azel.html [2016, August 23].

National Rationalised Specifications (NRS). 2014. GRID INTERCONNECTION OF EMBEDDED GENERATION - Part 2: Small-scale embedded generation - Section 3: Simplified utility connection criteria for low-voltage connected generators (NRS 097-2-3:2014). National Rationalised Specifications (NRS).

National Rationalised Specifications (NRS). 2017. GRID INTERCONNECTION OF EMBEDDED GENERATION - PART 2: SMALL-SCALE EMBEDDED GENERATION - SECTION 1: UTILITY INTERFACE (NRS 097-2-1:2017). National Rationalised Specifications (NRS).

National Renewable Energy Laboratory (NREL). 2015. Economic Analysis Case Studies of Battery Energy Storage with SAM. NREL. Available: http://www.nrel.gov/docs/fy16osti/64987.pdf [2017, May 23].

Nieuwlaar, E and Alsema, E. 1997. Energy Pay-Back Time (EPBT) and CO2 mitigation potential. Available: http://www.ecotopia.com/apollo2/pvepbtne.htm [2017, June 10].

PACENation. 2017. What is PACE? PACENation. Available: http://pacenation.us/what-is-pace/ [2017, June 10].

Park, N, Oh, W, D. Kim, D. 2013. Effect of Temperature and Humidity on the Degradation Rate of Multicrystalline Silicon Photovoltaic Module. International Journal of Photoenergy Volume 2013, Article ID 925280, 9 pages.

Peacock, F. 2012. How To Read A Solar Panel Specification: Part #1 Power & Temperature Specs.

PQRS. 2017. Solar Photovoltaic Database. PQRS [2017, February 15].

PVsyst, 2019, PVsyst Validations Available: https://www.pvsyst.com/help/validations.htm [2019, December 06].

Radmore, J-V, Chilwan, S. 2018. Solar PV for businesses in the Western Cape. GreenCape. Available: https://www.greencape.co.za/assets/Uploads/Industry-Brief-Solar-PV-FINAL-WEB-CORRECT.pdf [2020, January 20].

Ramoliya, J. 2015. Performance Evaluation of Grid-connected Solar Photovoltaic plant using PVSYST Software. Journal of Emerging Technologies and Innovative Research (JETIR). ISSN:2349-5162, Vol.2, Issue 2, page no.372-37. Available: http://www.jetir.org/papers/JETIR1502036.pdf [2020, October 21].

Renusol .2018 .RS1. Renusol. Available: http://www.renusol.com/fileadmin/downloads/montageanleitungen/rs1/RENUSOL_RS1_IM_150325.pdf [2018, March 20].

Rix, A, Kritzinger, K, Meyer, I, van Niekerk, J. 2016. Potential for distributed solar photovoltaic systems in the Western Cape Province. Centre for Renewable and Sustainable Energy Studies (CRSES).

Rome, N, Bosio, A, Romeo, A. 2010. An innovative process suitable to produce high efficiency CdTe/CdS thin film modules. Solar Energy Materials and Sola Cells.

Saglam, S. 2010. Meteorological parameters effects on solar energy power generation. WSEAS Transactions on Circuits and Systems.

Schmid, C, Ashmore, J, Mickiewicz, R, Meakin, D. 2015. The Influence of the PV back sheet on the FormaDon of Snail Trails. Fraunhofer Centre for Sustainable Energy Systems CSE. Available: https://www.nrel.gov/pv/assets/pdfs/2015_pvmrw_115_schmid.pdf [2017, December 18].

Schneider Electric. 2018. Conext TL Three-phase grid-tie solar inverters. Schneider Electric. Available: https://41j5tc3akbrn3uezx5av0jj1bgm-wpengine.netdna-ssl.com/wp-content/uploads/2014/10/conext-tl-15-20-datasheet-20141002_eng.pdf [2018, March 05].

Schwingshackl, C, Marcello Petitta, Jakob Birkedal Wagner, Giorgio Belluardo, David C. Moser, Marco Antonio Castelli, Marc Zebisch and Anke Tetzlaff. 2013. Wind effect on PV module temperature: Analysis of different techniques for an accurate estimation. Energy Procedia, Vol 40, Page 77-86, Elsevier, 2013.

Sharma, G. 2014. Snail Trail on your PV module: A disease or symptom?. Firstgreen Consulting. Available: http://www.firstgreen.co/2014/09/snail-trail-on-your-pv-module-a-disease-or-symptom/ [2017, December 18].

Skelton, P. 2012. Using thermal imagers to locate ‘hot spots’ on solar installations. Electrical Connection. Available: http://electricalconnection.com.au/using-thermal-imagers-locate-hot-spots-solar-installations/ [2017, December 18].

Solar Future Energy. 2017. SOLA Completes 212kW Cape Quarter Project. Solar Future Energy.

Solargis, 2017.World Solar Resource May. Available: http://solargis.com/products/maps-and-gis-data/free/download/world [2017, August 01].

SolarQuotes Blog. Available: https://www.solarquotes.com.au/blog/how-to-read-a-solar-panel-specification-part-1-power-temperature-specs/ [2020, January 20].

SolarQuotes, 2019, Inverter Comparison Chart. Peacock Media Group. Available: https://www.solarquotes.com.au/inverters/comparison/chart/ [2019, October 17th].

South African Bureau of Standards (SABS). 2014. The wiring of premises - Part 2: Medium-voltage installations above 1 kV a.c. not exceeding 22 kV a.c. and up to and including 3 MVA installed capacity (SANS 10142-2:2014). SABS.

South African Bureau of Standards (SABS). 2017. Programme of Work: Standards. SABS.

South African Bureau of Standards (SABS). 2017. The wiring of premises - Part 1: Low-voltage installations (SANS 10142-1:2017). SABS.

South African National Standard (SABS), 2014. NRS 097-2-3:2014 GRID INTERCONNECTION OF EMBEDDED GENERATION. South African National Standard (SABS).

Stein, J. 2017. PV Performance modelling collaborative. Sandia National Laboratories. Available: https://pvpmc.sandia.gov/modeling-steps/ [2017, July 31].

Sun Earth Tools. Sun Position. Available: http://www.sunearthtools.com/ [2016, August 23].

The GreenAge. 2017. Do Pay-As-You-Save Energy Saving Schemes Work? The GreenAge. Available: https://www.thegreenage.co.uk/do-pay-as-you-save-energy-saving-schemes-work/ [2017, June 10].

The Sun Exchange. 2017. What is the Sun Exchange?. The Sun Exchange. Available: https://thesunexchange.com [2017, June 10].

US Department of Energy (USDOE). 2004. What is Energy Payback for PV? US Department of Energy (USDOE). Available: http://www.nrel.gov/docs/fy04osti/35489.pdf [2017, June 10].

US Department of Energy (USDOE). 2004. What is Energy Payback for PV? US Department of Energy (USDOE). Available: http://www.nrel.gov/docs/fy04osti/35489.pdf [2017, June 10].

US Department of Energy (USDOE). 2014. On-Site Commercial Solar PV Decision Guide. US Department of Energy. Available: https://betterbuildingssolutioncenter.energy.gov/sites/default/files/attachments/On_Site_Solar_Decision_Guide.pdf [2017, June 10].

US Department of Energy (USDOE). 2014. On-Site Commercial Solar PV Decision Guide. US Department of Energy. Available: https://betterbuildingssolutioncenter.energy.gov/sites/default/files/attachments/On_Site_Solar_Decision_Guide.pdf [2017, June 10].

Vashishtha, S. 2012.Difference Between the DNI, DHI and GHI?. Firstgreen Consulting Private Limited. Available: https://firstgreenconsulting.wordpress.com/2012/04/26/differentiate-between-the-dni-dhi-and-ghi/ [2017, August 01].

Western Cape Government (WCG). 2016. Old mutual Makes History Twice In One Day. Western Cape Government. Available: https://www.westerncape.gov.za/110green/news/old-mutual-makes-history-twice-one-day [2017, June 10].

Western Cape Government (WCG). 2016. Old mutual Makes History Twice In One Day. Western Cape Government. Available: https://www.westerncape.gov.za/110green/news/old-mutual-makes-history-twice-one-day [2017, June 10].

Western Cape Government (WCG). 2016. Old mutual Makes History Twice In One Day. Western Cape Government. Available: https://www.westerncape.gov.za/110green/news/old-mutual-makes-history-twice-one-day [2017, June 10].

Zue, C, Begbie, N. City of Cape Town. Cape Town Drought. City of Cape Town. Available: http://www.capetowndrought.com/ [2019, August 28].

Appendix A – PVsyst Simulations

	PVSYST V6.84			Page 1/4

Grid-Connected System: Simulation parameters

Project : **SAREBI**

Geographical Site	**Atlantis**		Country	**South Africa**
Situation	Latitude	-33.59° S	Longitude	18.49° E
Time defined as	Legal Time	Time zone UT+2	Altitude	139 m
	Albedo	0.20		
Meteo data:	**Atlantis**	Meteonorm 7.2, Sat=35% - Synthetic		

Simulation variant : **orignial_simulation**

	Simulation date	17/01/20 09h40

Simulation parameters	System type	**No 3D scene defined, no shadings**		
Collector Plane Orientation	Tilt	15°	Azimuth	-19°
Models used	Transposition	Perez	Diffuse	Perez, Meteonorm
Horizon	Free Horizon			
Near Shadings	No Shadings			
User's needs :	Unlimited load (grid)			

PV Array Characteristics

PV module	Si-poly	Model	**CS6U - 325P**		
Original PVsyst database		Manufacturer	Canadian Solar Inc.		
Number of PV modules		In series	15 modules	In parallel	2 strings
Total number of PV modules		Nb. modules	30	Unit Nom. Power	325 Wp
Array global power		Nominal (STC)	**9.75 kWp**	At operating cond.	8.74 kWp (50°C)
Array operating characteristics (50°C)		U mpp	496 V	I mpp	18 A
Total area		Module area	**58.3 m²**	Cell area	52.6 m²
Inverter		Model	**Conext CL 20000E**		
Original PVsyst database		Manufacturer	Schneider Electric		
Characteristics		Operating Voltage	350-800 V	Unit Nom. Power	20.0 kWac
Inverter pack		Nb. of inverters	1 * MPPT 50 %	Total Power	10.0 kWac
				Pnom ratio	0.97

PV Array loss factors

Thermal Loss factor	Uc (const)	20.0 W/m²K	Uv (wind)	0.0 W/m²K / m/s
Wiring Ohmic Loss	Global array res.	474 mOhm	Loss Fraction	1.5 % at STC
Module Quality Loss			Loss Fraction	-0.4 %
Module Mismatch Losses			Loss Fraction	1.0 % at MPP
Strings Mismatch loss			Loss Fraction	0.10 %

Incidence effect (IAM): User defined profile

10°	20°	30°	40°	50°	60°	70°	80°	90°
0.998	0.998	0.995	0.992	0.986	0.970	0.917	0.763	0.000

Grid-Connected System: Main results

Project : SAREBI

Simulation variant : orignial_simulation

Main system parameters				
System type		**No 3D scene defined, no shadings**		
PV Field Orientation	tilt	15°	azimuth	-19°
PV modules	Model	CS6U - 325P	Pnom	325 Wp
PV Array	Nb. of modules	30	Pnom total	**9.75 kWp**
Inverter	Model	Conext CL 20000E	Pnom	20.00 kW ac
User's needs	Unlimited load (grid)			

Main simulation results				
System Production	**Produced Energy**	**17.70 MWh/year**	Specific prod.	1815 kWh/kWp/year
	Performance Ratio PR	84.14 %		

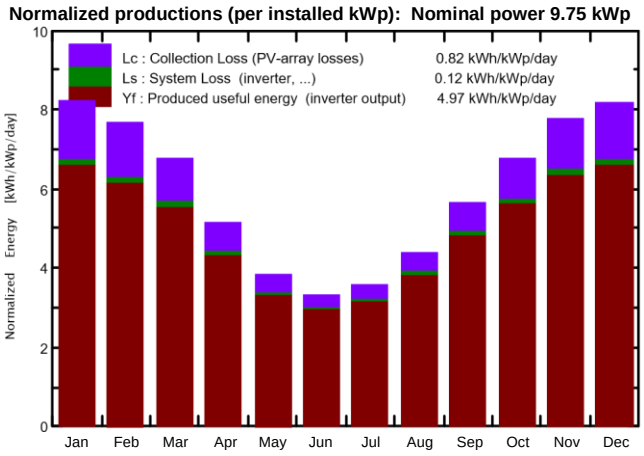

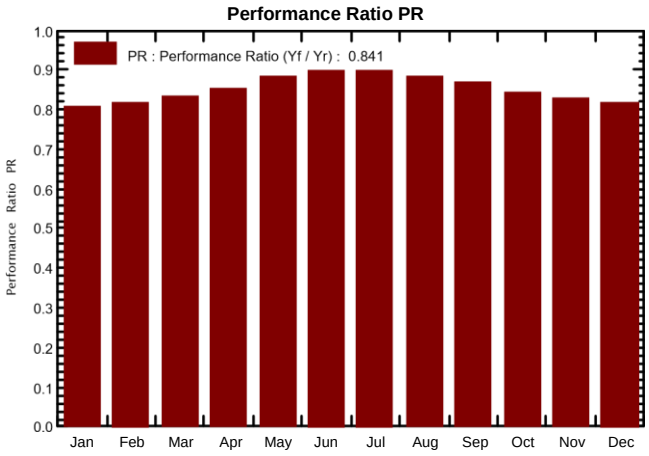

orignial_simulation

Balances and main results

	GlobHor kWh/m²	DiffHor kWh/m²	T_Amb °C	GlobInc kWh/m²	GlobEff kWh/m²	EArray MWh	E_Grid MWh	PR
January	255.1	66.30	21.78	254.2	248.6	2.053	2.002	0.808
February	205.5	56.10	21.81	213.6	209.0	1.735	1.694	0.814
March	188.9	50.46	20.16	209.2	204.9	1.731	1.690	0.829
April	130.3	38.51	17.36	153.3	149.8	1.303	1.273	0.852
May	93.7	35.38	14.87	117.4	114.5	1.032	1.009	0.881
June	76.1	29.05	12.39	99.8	97.3	0.893	0.873	0.897
July	85.7	33.21	11.98	110.7	107.8	0.991	0.969	0.897
August	110.9	33.99	12.52	135.5	132.3	1.194	1.168	0.883
September	149.0	45.61	14.18	168.7	165.1	1.454	1.422	0.865
October	197.5	60.35	17.03	209.2	205.0	1.755	1.714	0.840
November	231.7	66.41	18.72	232.7	227.6	1.919	1.875	0.826
December	257.7	66.76	20.83	252.7	246.9	2.055	2.006	0.814
Year	1982.3	582.13	16.94	2157.1	2108.8	18.115	17.695	0.841

Legends:
GlobHor Horizontal global irradiation
DiffHor Horizontal diffuse irradiation
T_Amb T amb.
GlobInc Global incident in coll. plane
GlobEff Effective Global, corr. for IAM and shadings
EArray Effective energy at the output of the array
E_Grid Energy injected into grid
PR Performance Ratio

Main system parameters	System type	**No 3D scene defined, no shadings**		
PV Field Orientation	tilt	15°	azimuth	-19°
PV modules	Model	CS6U - 325P	Pnom	325 Wp
PV Array	Nb. of modules	30	Pnom total	**9.75 kWp**
Inverter	Model	Conext CL 20000E	Pnom	20.00 kW ac
User's needs	Unlimited load (grid)			

Daily Input/Output diagram

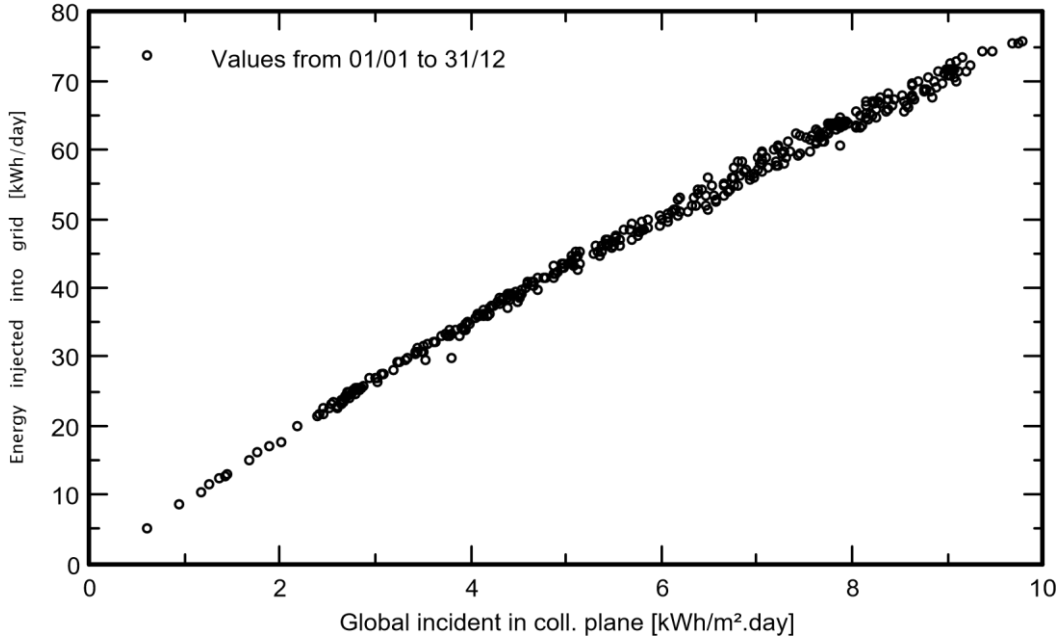

System Output Power Distribution

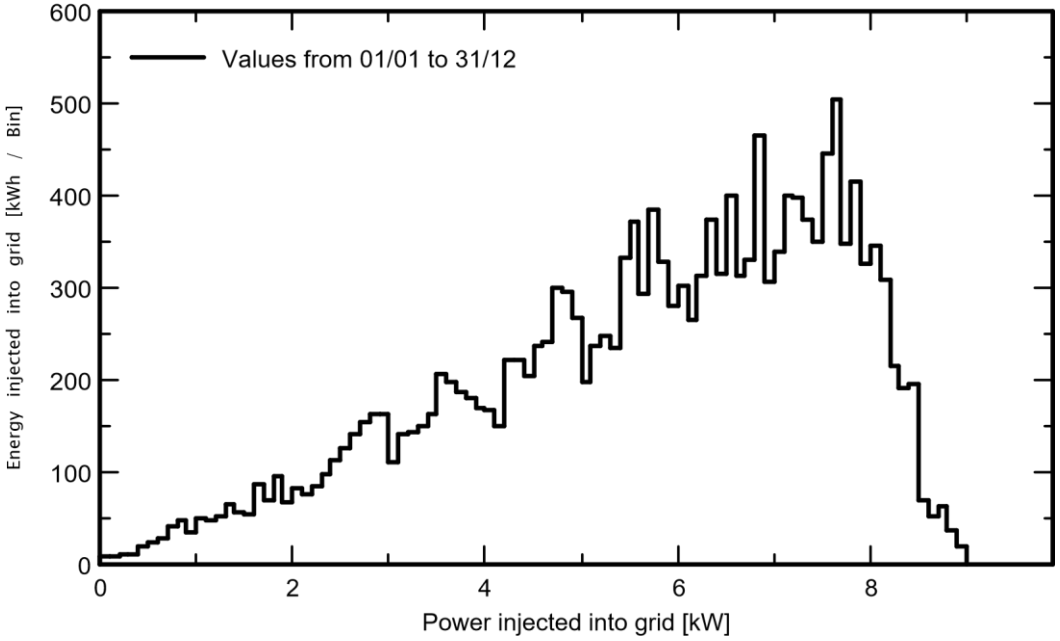

Grid-Connected System: Loss diagram

Project : **SAREBI**

Simulation variant : **orignial_simulation**

Main system parameters	System type	**No 3D scene defined, no shadings**		
PV Field Orientation	tilt	15°	azimuth	-19°
PV modules	Model	CS6U - 325P	Pnom	325 Wp
PV Array	Nb. of modules	30	Pnom total	**9.75 kWp**
Inverter	Model	Conext CL 20000E	Pnom	20.00 kW ac
User's needs	Unlimited load (grid)			

Loss diagram over the whole year

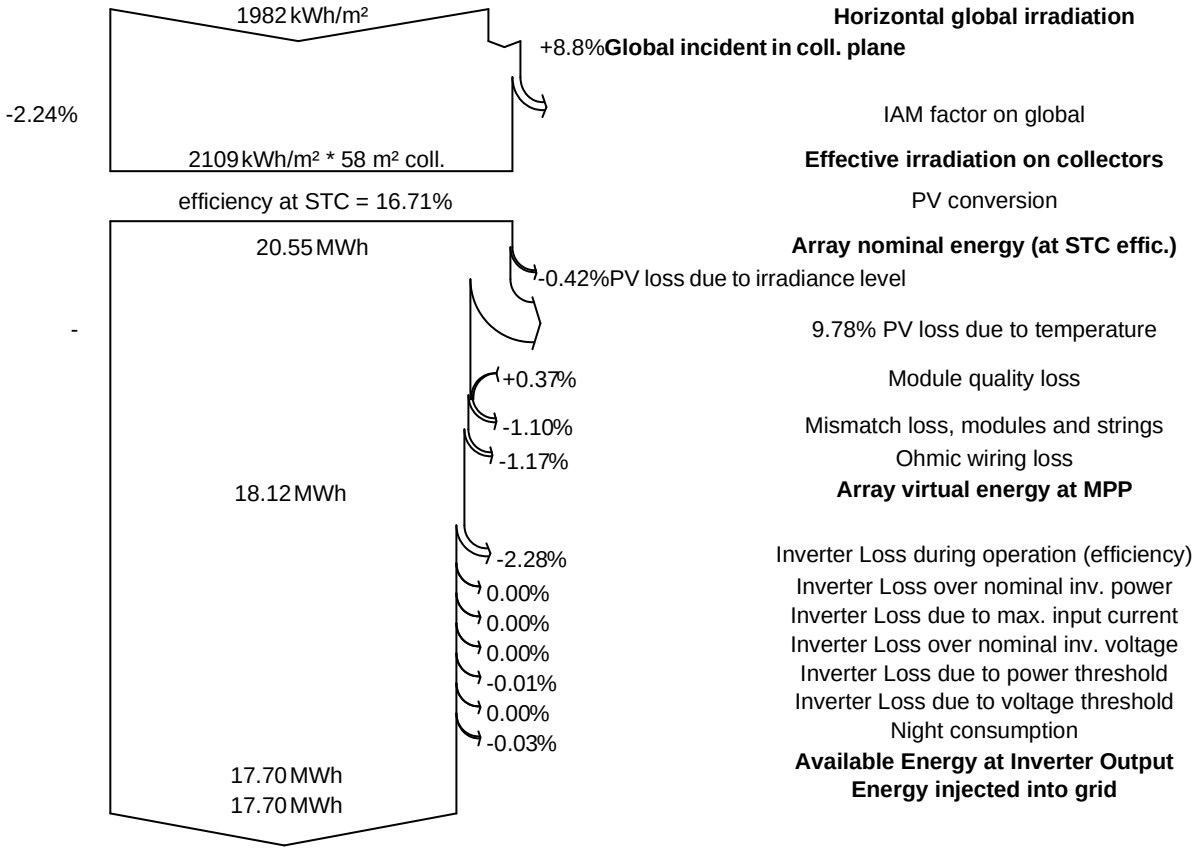

Grid-Connected System: Simulation parameters

Project : **Stripform**

Geographical Site	**Atlantis**		Country	**South Africa**
Situation	Latitude	-33.59° S	Longitude	18.49° E
Time defined as	Legal Time	Time zone UT+2	Altitude	139 m
	Albedo	0.20		
Meteo data:	**Atlantis**	Meteonorm 7.2, Sat=35% - Synthetic		

Simulation variant : **Stripform**

Simulation date 16/10/19 16h58

Simulation parameters	System type	**No 3D scene defined, no shadings**		
Collector Plane Orientation	Tilt	15°	Azimuth	46°
Models used	Transposition	Perez	Diffuse	Perez, Meteonorm
Horizon	Free Horizon			
Near Shadings	No Shadings			
User's needs :	Unlimited load (grid)			

PV Array Characteristics

PV module	Si-poly	Model	**CS6U - 335P**		
Original PVsyst database		Manufacturer	Canadian Solar Inc.		
Number of PV modules		In series	15 modules	In parallel	4 strings
Total number of PV modules		Nb. modules	60	Unit Nom. Power	335 Wp
Array global power		Nominal (STC)	**20.10 kWp**	At operating cond.	18.04 kWp (50°C)
Array operating characteristics (50°C)		U mpp	501 V	I mpp	36 A
Total area		Module area	**117 m²**	Cell area	105 m²

Inverter		Model	**Sunny Tripower 20000TL-30**		
Original PVsyst database		Manufacturer	SMA		
Characteristics		Operating Voltage	320-800 V	Unit Nom. Power	20.0 kWac
Inverter pack		Nb. of inverters	2 * MPPT 50 %	Total Power	20 kWac
				Pnom ratio	1.01

PV Array loss factors

Thermal Loss factor	Uc (const)	20.0 W/m²K	Uv (wind)	0.0 W/m²K / m/s
Wiring Ohmic Loss	Global array res.	234 mOhm	Loss Fraction	1.5 % at STC
Module Quality Loss			Loss Fraction	-0.4 %
Module Mismatch Losses			Loss Fraction	1.0 % at MPP
Strings Mismatch loss			Loss Fraction	0.10 %

Incidence effect (IAM): User defined profile

10°	20°	30°	40°	50°	60°	70°	80°	90°
0.998	0.998	0.995	0.992	0.986	0.970	0.917	0.763	0.000

Grid-Connected System: Main results

Project : **Stripform**

Simulation variant : **Stripform**

Main system parameters				
System type	**No 3D scene defined, no shadings**			
PV Field Orientation	tilt	15°	azimuth	46°
PV modules	Model	CS6U - 335P	Pnom	335 Wp
PV Array	Nb. of modules	60	Pnom total	**20.10 kWp**
Inverter	Model	Sunny Tripower 20000TL-30		20.00 kW ac
User's needs	Unlimited load (grid)			

Main simulation results				
System Production	**Produced Energy**	**35.55 MWh/year**	Specific prod.	1769 kWh/kWp/year
	Performance Ratio PR	84.19 %		

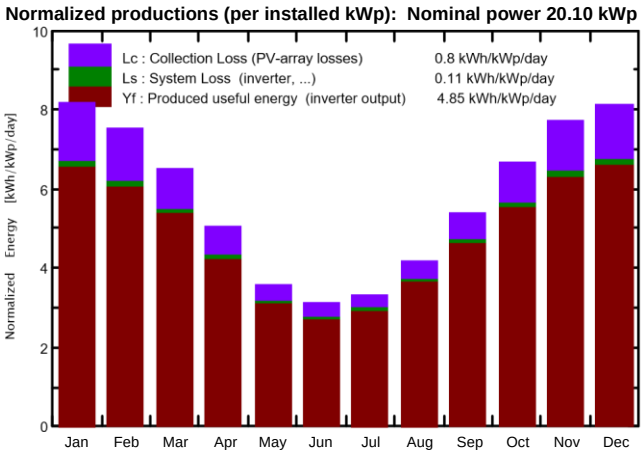

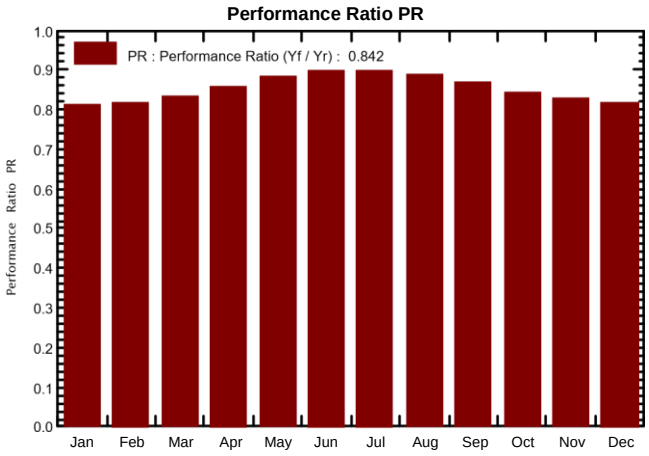

Stripform

Balances and main results

	GlobHor kWh/m²	DiffHor kWh/m²	T_Amb °C	GlobInc kWh/m²	GlobEff kWh/m²	EArray MWh	E_Grid MWh	PR
January	255.1	66.30	21.78	252.5	247.3	4.201	4.104	0.808
February	205.5	56.10	21.81	209.7	205.5	3.516	3.437	0.815
March	188.9	50.46	20.16	201.9	197.7	3.446	3.372	0.831
April	130.3	38.51	17.36	150.5	147.0	2.643	2.588	0.855
May	93.7	35.38	14.87	111.0	107.8	2.004	1.963	0.880
June	76.1	29.05	12.39	92.4	89.7	1.698	1.665	0.896
July	85.7	33.21	11.98	102.8	99.8	1.889	1.851	0.895
August	110.9	33.99	12.52	129.9	126.5	2.359	2.312	0.885
September	149.0	45.61	14.18	162.1	158.6	2.884	2.825	0.867
October	197.5	60.35	17.03	205.7	201.4	3.554	3.476	0.841
November	231.7	66.41	18.72	230.4	225.4	3.920	3.834	0.828
December	257.7	66.76	20.83	251.8	246.5	4.221	4.126	0.815
Year	1982.3	582.13	16.94	2100.7	2053.3	36.336	35.551	0.842

Legends:
GlobHor Horizontal global irradiation
DiffHor Horizontal diffuse irradiation
T_Amb T amb.
GlobInc Global incident in coll. plane
GlobEff Effective Global, corr. for IAM and shadings
EArray Effective energy at the output of the array
E_Grid Energy injected into grid
PR Performance Ratio

Grid-Connected System: Special graphs

Project : **Stripform**

Simulation variant : **Stripform**

Main system parameters	System type	**No 3D scene defined, no shadings**		
PV Field Orientation	tilt	15°	azimuth	46°
PV modules	Model	CS6U - 335P	Pnom	335 Wp
PV Array	Nb. of modules	60	Pnom total	**20.10 kWp**
Inverter	Model	Sunny Tripower 20000TL-30		20.00 kW ac
User's needs	Unlimited load (grid)			

Daily Input/Output diagram

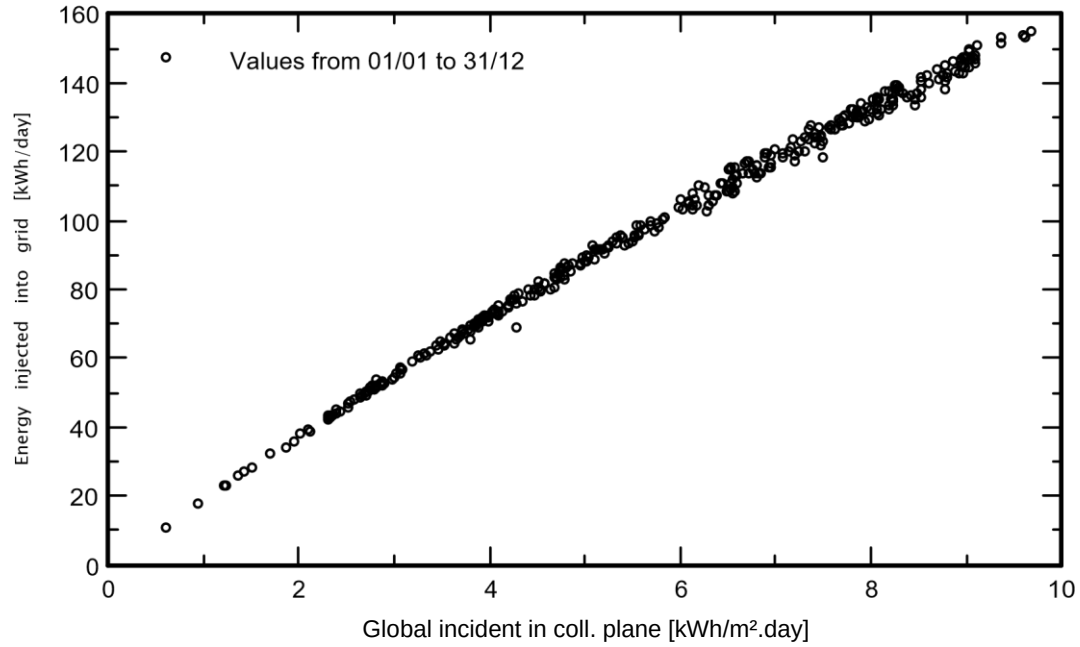

System Output Power Distribution

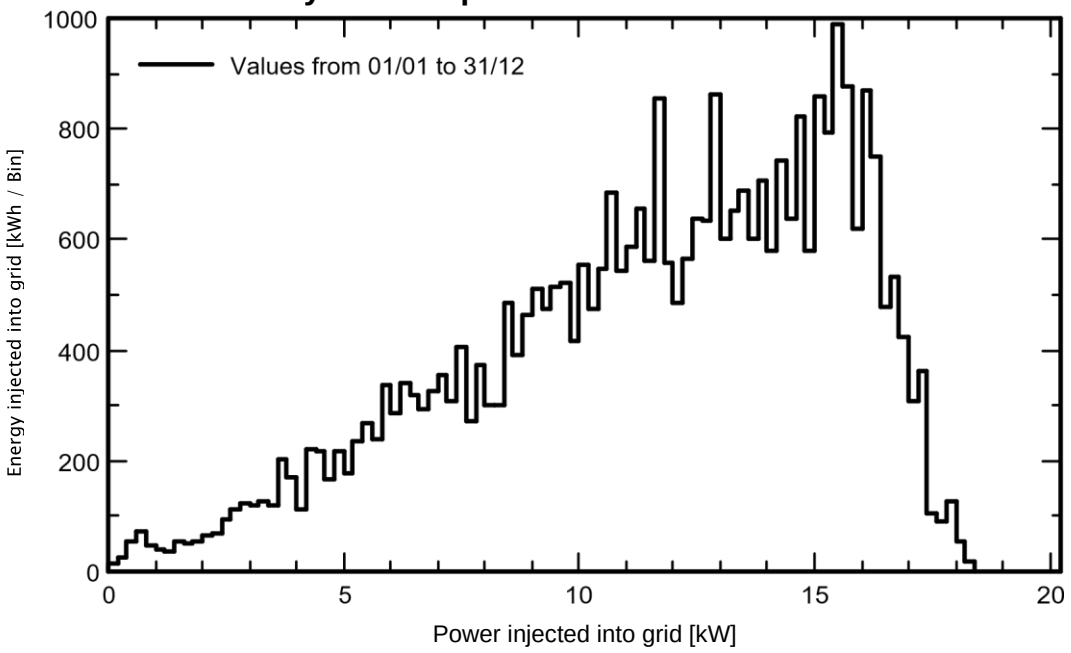

Grid-Connected System: Loss diagram

Project : **Stripform**

Simulation variant : **Stripform**

Main system parameters	System type	**No 3D scene defined, no shadings**		
PV Field Orientation	tilt	15°	azimuth	46°
PV modules	Model	CS6U - 335P	Pnom	335 Wp
PV Array	Nb. of modules	60	Pnom total	**20.10 kWp**
Inverter	Model	Sunny Tripower 20000TL-30		20.00 kW ac
User's needs	Unlimited load (grid)			

Loss diagram over the whole year

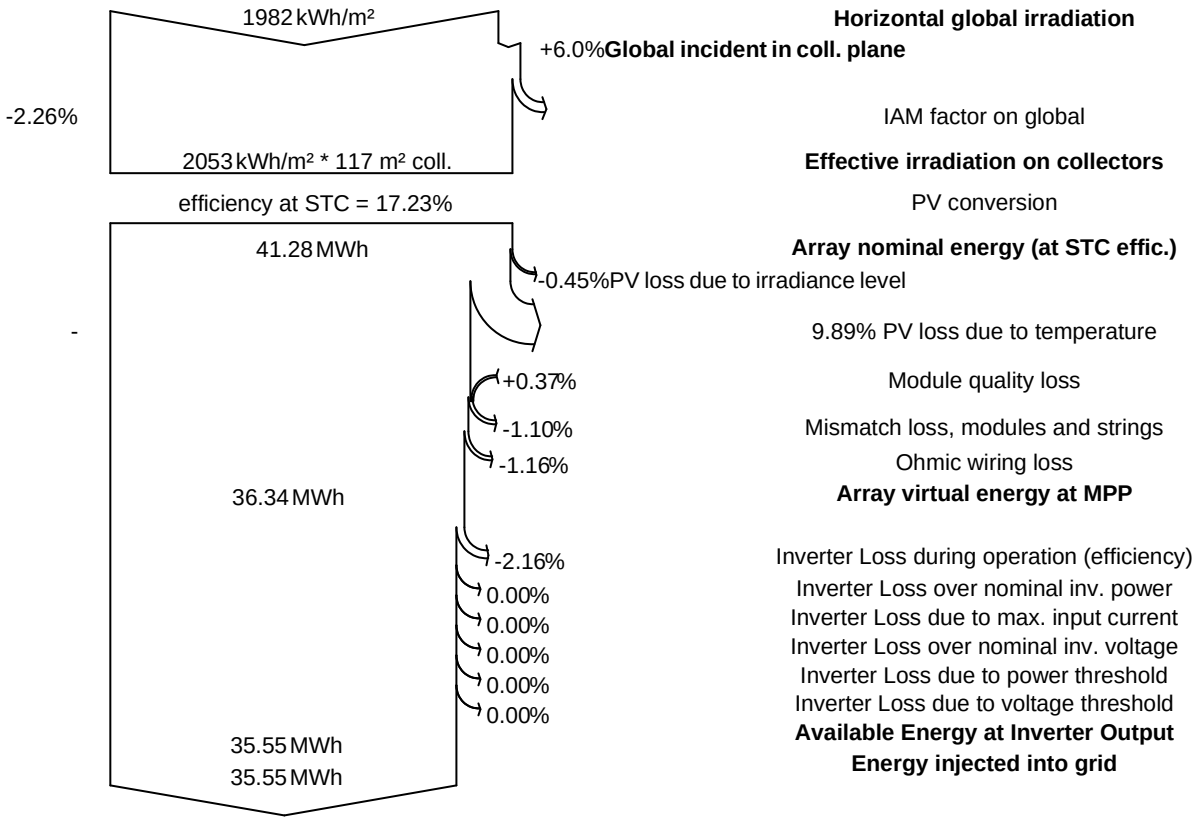

Grid-Connected System: Simulation parameters

Project : **SATyres**

Geographical Site	**Atlantis**		Country	**South Africa**
Situation	Latitude	-33.59° S	Longitude	18.49° E
Time defined as	Legal Time	Time zone UT+2	Altitude	139 m
	Albedo	0.20		
Meteo data:	**Atlantis**	Meteonorm 7.2, Sat=35% - Synthetic		

Simulation variant : SATyres_Original Design_JA-modules Simulation date 17/01/20 09h46

Simulation parameters	System type	**No 3D scene defined, no shadings**		
Collector Plane Orientation	Tilt	13°	Azimuth	22°
Models used	Transposition	Perez	Diffuse	Perez, Meteonorm
Horizon	Free Horizon			
Near Shadings	No Shadings			
User's needs :	Unlimited load (grid)			

PV Array Characteristics

PV module	Si-poly	Model	**JAP6-72-330/3BB**	
Original PVsyst database		Manufacturer	JA Solar	

SolarEdge Power Optimizer Model **P730 Worldwide** Unit Nom. Power 730 W PV modules on one Power Optimizer in series 2 in parallel 1

Nb. of optimizers	In series	14	In parallel	25 strings
Total number of PV modules	Nb. modules	700	Unit Nom. Power	330 Wp
Array global power	Nominal (STC)	**231 kWp**	At operating cond.	207 kWp (50°C)
Output of optimizers	U oper	750 V	I at Poper	276 A
Total area	Module area	**1357 m²**	Cell area	1227 m²

Inverter		Model	**SE27.6K-EU-APAC/AUS**	
Original PVsyst database		Manufacturer	SolarEdge	
Characteristics	Operating Voltage	750 V	Unit Nom. Power	27.6 kWac
Inverter pack	Nb. of inverters	7 units	Total Power	193 kWac
			Pnom ratio	1.14

Physical inverters

SE27.6K-EU-APAC/AUS	6 units, 4 strings	4 strings of 14 optimizers P730 Worldwide
SE27.6K-EU-APAC/AUS	1 units, 1 strings	1 strings of 14 optimizers P730 Worldwide

PV Array loss factors				
Thermal Loss factor	Uc (const)	20.0 W/m²K	Uv (wind)	0.0 W/m²K / m/s
Wiring Ohmic Loss	Global array res.	37 mOhm	Loss Fraction	1.5 % at STC
Module Quality Loss			Loss Fraction	-0.8 %
Module Mismatch Losses			Loss Fraction	0.0 % (fixed voltage)
Incidence effect, ASHRAE parametrization	IAM =	1 - bo (1/cos i - 1)	bo Param.	0.05

Grid-Connected System: Main results

Project : SATyres

Simulation variant : SATyres_Original Design_JA-modules

Main system parameters				
System type		**No 3D scene defined, no shadings**		
PV Field Orientation	tilt	13°	azimuth	22°
PV modules	Model	JAP6-72-330/3BB	Pnom	330 Wp
PV Array	Nb. of modules	700	Pnom total	**231 kWp**
Inverter	Model	SE27.6K-EU-APAC/AUS	Pnom	27.60 kW ac
Inverter pack	Nb. of units	7.0	Pnom total	**193 kW ac**
User's needs	Unlimited load (grid)			

Main simulation results				
System Production	**Produced Energy**	**416.3 MWh/year**	Specific prod.	1802 kWh/kWp/year
	Performance Ratio PR	84.43 %		

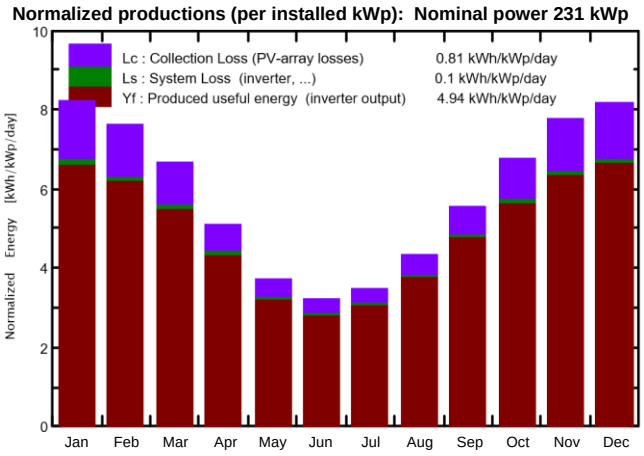

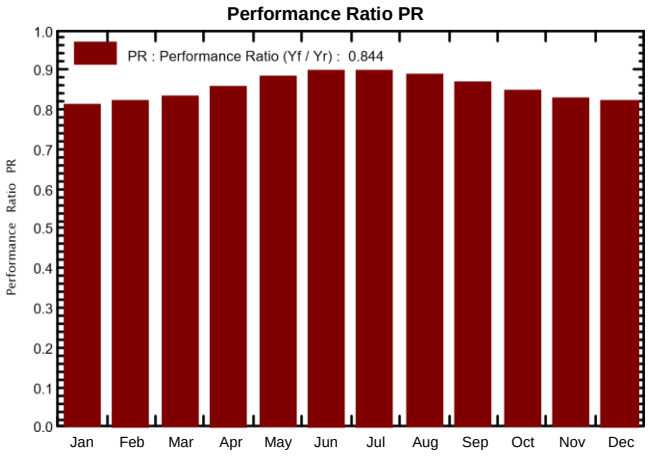

SATyres_Original Design_JA-modules

Balances and main results

	GlobHor kWh/m²	DiffHor kWh/m²	T_Amb °C	GlobInc kWh/m²	GlobEff kWh/m²	EArray MWh	E_Grid MWh	PR
January	255.1	66.30	21.78	254.4	247.5	48.66	47.72	0.812
February	205.5	56.10	21.81	212.5	206.5	41.06	40.27	0.820
March	188.9	50.46	20.16	205.8	199.5	40.38	39.60	0.833
April	130.3	38.51	17.36	152.8	147.9	30.86	30.27	0.858
May	93.7	35.38	14.87	114.4	110.0	23.74	23.29	0.881
June	76.1	29.05	12.39	96.0	92.1	20.23	19.85	0.894
July	85.7	33.21	11.98	106.7	102.3	22.49	22.06	0.895
August	110.9	33.99	12.52	133.1	128.5	27.79	27.26	0.886
September	149.0	45.61	14.18	165.8	160.6	33.90	33.25	0.868
October	197.5	60.35	17.03	208.3	202.5	41.49	40.69	0.846
November	231.7	66.41	18.72	231.9	225.0	45.14	44.27	0.826
December	257.7	66.76	20.83	252.9	245.7	48.78	47.83	0.819
Year	1982.3	582.13	16.94	2134.6	2068.0	424.52	416.35	0.844

Legends:
GlobHor Horizontal global irradiation
DiffHor Horizontal diffuse irradiation
T_Amb T amb.
GlobInc Global incident in coll. plane
GlobEff Effective Global, corr. for IAM and shadings
EArray Effective energy at the output of the array
E_Grid Energy injected into grid
PR Performance Ratio

Main system parameters	System type	**No 3D scene defined, no shadings**		
PV Field Orientation	tilt	13°	azimuth	22°
PV modules	Model	JAP6-72-330/3BB	Pnom	330 Wp
PV Array	Nb. of modules	700	Pnom total	**231 kWp**
Inverter	Model	SE27.6K-EU-APAC/AUS	Pnom	27.60 kW ac
Inverter pack	Nb. of units	7.0	Pnom total	**193 kW ac**
User's needs	Unlimited load (grid)			

Daily Input/Output diagram

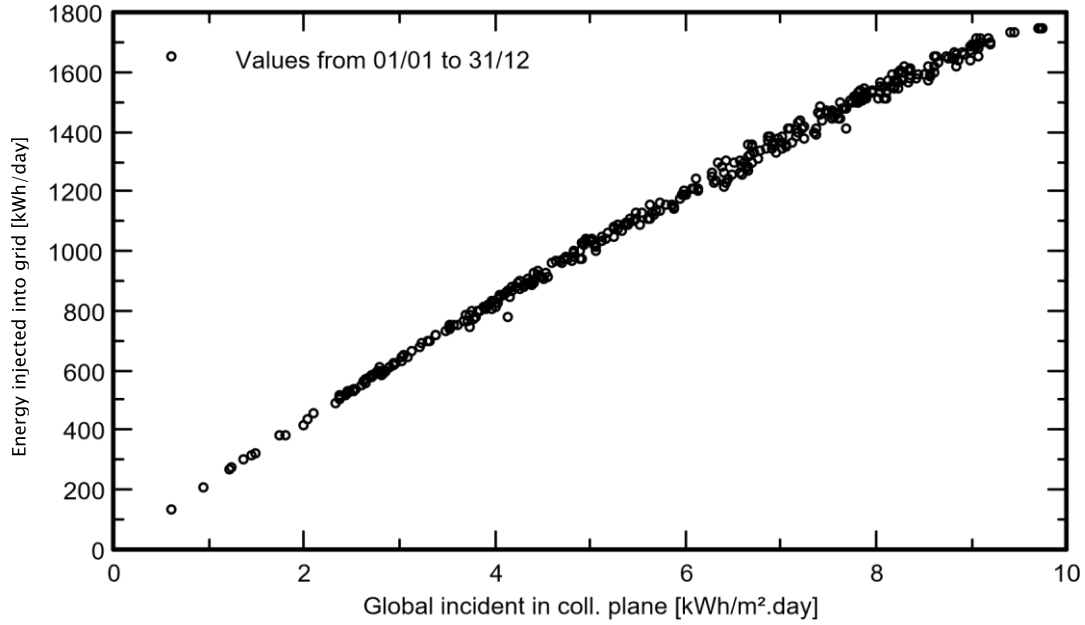

System Output Power Distribution

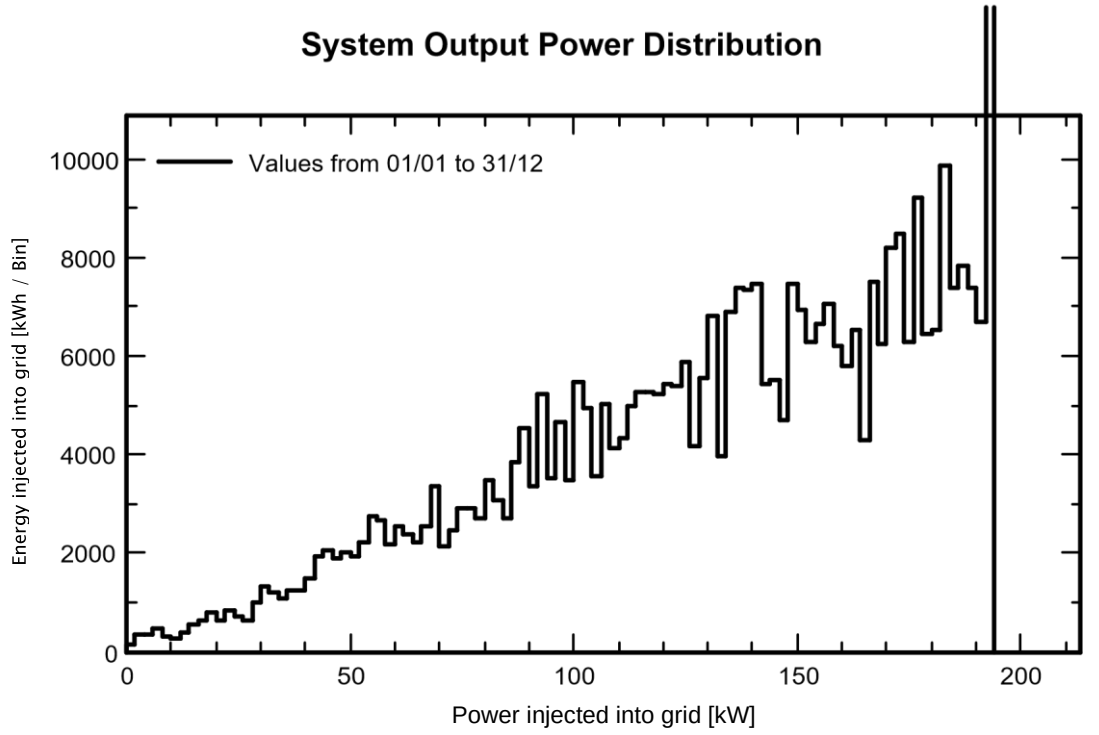

Grid-Connected System: Loss diagram

Project : **SATyres**

Simulation variant : **SATyres_Original Design_JA-modules**

Main system parameters	System type	**No 3D scene defined, no shadings**			
PV Field Orientation	tilt	13°	azimuth	22°	
PV modules	Model	JAP6-72-330/3BB	Pnom	330 Wp	
PV Array	Nb. of modules	700	Pnom total	**231 kWp**	
Inverter	Model	SE27.6K-EU-APAC/AUS	Pnom	27.60 kW ac	
Inverter pack	Nb. of units	7.0	Pnom total	**193 kW ac**	
User's needs	Unlimited load (grid)				

Loss diagram over the whole year

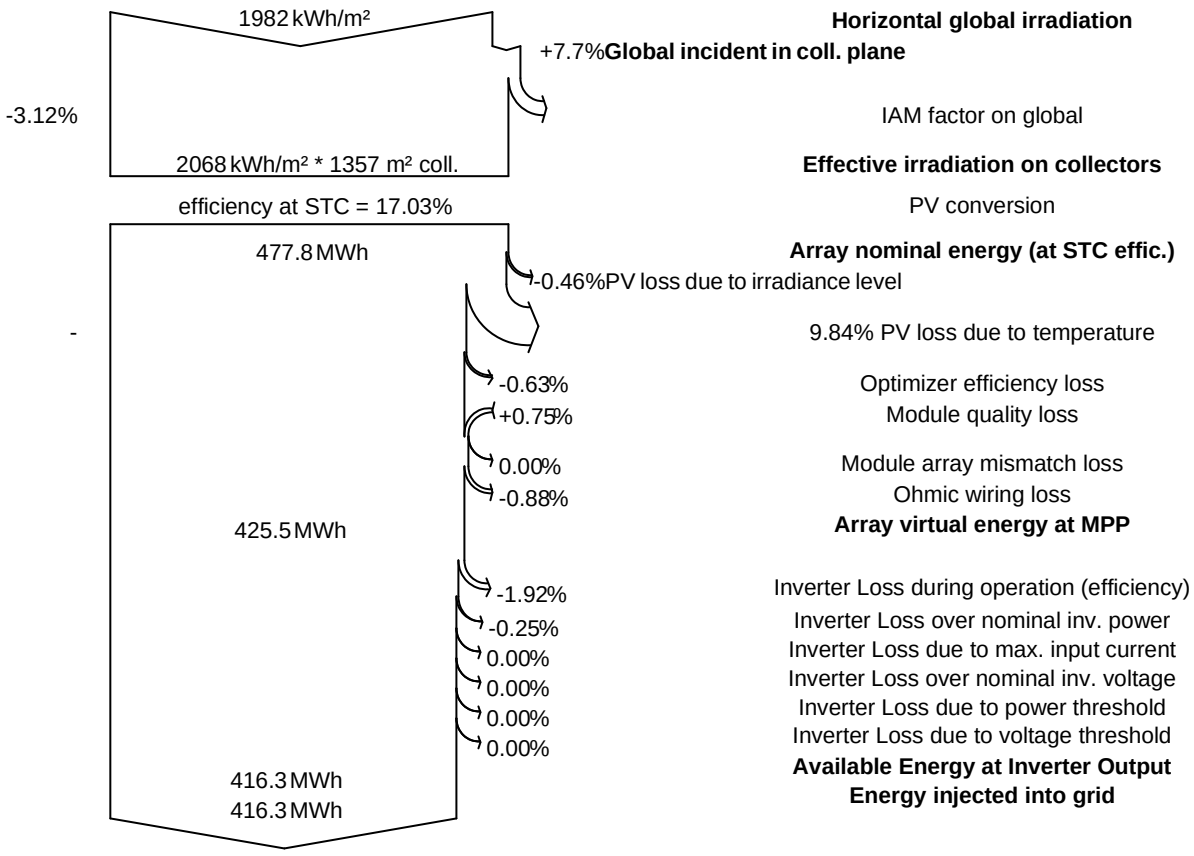

Grid-Connected System: Simulation parameters

Project : **Atlantis_Ideal System**

Geographical Site	**Atlantis**		Country	**South Africa**
Situation	Latitude	-33.59° S	Longitude	18.49° E
Time defined as	Legal Time	Time zone UT+2	Altitude	139 m
	Albedo	0.20		
Meteo data:	**Atlantis**	Meteonorm 7.2, Sat=35% - Synthetic		

Simulation variant : **Atlantis_Ideal System**

Simulation date 31/01/20 13h46

Simulation parameters	System type	**No 3D scene defined, no shadings**		
Collector Plane Orientation	Tilt	30°	Azimuth	0°
Models used	Transposition	Perez	Diffuse	Perez, Meteonorm
Horizon	Free Horizon			
Near Shadings	No Shadings			
User's needs :	Unlimited load (grid)			

PV Array Characteristics

PV module	Si-poly	Model	**CS6U - 335P**	
Original PVsyst database		Manufacturer	Canadian Solar Inc.	
SolarEdge Power Optimizer Model **P850 Worldwide** Unit Nom. Power 850 W PV modules on one Power Optimizer in series 2 in parallel 1				
Nb. of optimizers		In series	14	In parallel 3 strings
Total number of PV modules		Nb. modules	84	Unit Nom. Power 335 Wp
Array global power		Nominal (STC)	**28.14 kWp**	At operating cond. 25.25 kWp (50°C)
Output of optimizers		U oper	750 V	I at Poper 34 A
Total area		Module area	**163 m²**	Cell area 147 m²

Inverter		Model	**SE27.6K-EU-APAC/AUS**	
Original PVsyst database		Manufacturer	SolarEdge	
Characteristics		Operating Voltage	750 V	Unit Nom. Power 27.6 kWac
Inverter pack		Nb. of inverters	1 units	Total Power 28 kWac
				Pnom ratio 0.96

PV Array loss factors

Thermal Loss factor	Uc (const)	20.0 W/m²K	Uv (wind)	0.0 W/m²K / m/s
Wiring Ohmic Loss	Global array res.	300 mOhm	Loss Fraction	1.5 % at STC
Module Quality Loss			Loss Fraction	-0.4 %
Module Mismatch Losses			Loss Fraction	0.0 % (fixed voltage)

Incidence effect (IAM): User defined profile

10°	20°	30°	40°	50°	60°	70°	80°	90°
0.998	0.998	0.995	0.992	0.986	0.970	0.917	0.763	0.000

Grid-Connected System: Main results

Project : **Atlantis_Ideal System**

Simulation variant : **Atlantis_Ideal System**

Main system parameters				
	System type	**No 3D scene defined, no shadings**		
PV Field Orientation	tilt	30°	azimuth	0°
PV modules	Model	CS6U - 335P	Pnom	335 Wp
PV Array	Nb. of modules	84	Pnom total	**28.14 kWp**
Inverter	Model	SE27.6K-EU-APAC/AUS	Pnom	27.60 kW ac
User's needs	Unlimited load (grid)			

Main simulation results				
System Production	**Produced Energy**	**53.52 MWh/year**	Specific prod.	1902 kWh/kWp/year
	Performance Ratio PR	85.19 %		

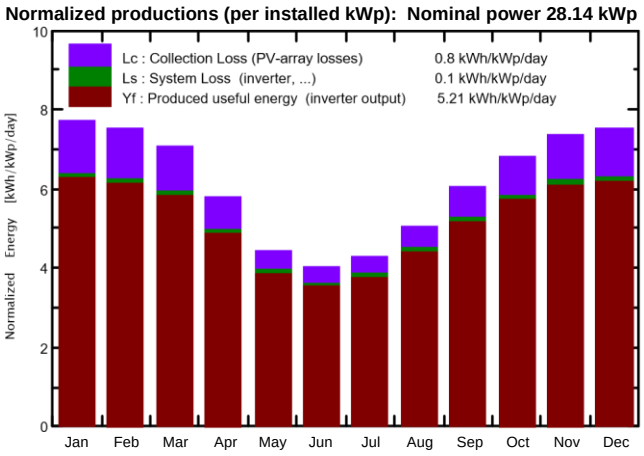

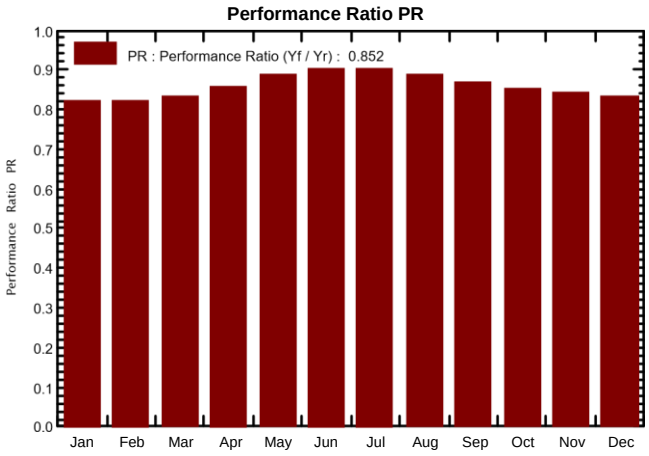

Atlantis_Ideal System

Balances and main results

	GlobHor kWh/m²	DiffHor kWh/m²	T_Amb °C	GlobInc kWh/m²	GlobEff kWh/m²	EArray MWh	E_Grid MWh	PR
January	255.1	66.30	21.78	238.7	233.1	5.631	5.522	0.822
February	205.5	56.10	21.81	210.4	205.7	4.966	4.871	0.823
March	188.9	50.46	20.16	219.1	214.7	5.236	5.136	0.833
April	130.3	38.51	17.36	173.2	170.4	4.256	4.175	0.856
May	93.7	35.38	14.87	137.8	135.5	3.498	3.431	0.885
June	76.1	29.05	12.39	120.3	118.3	3.108	3.049	0.901
July	85.7	33.21	11.98	132.0	129.8	3.411	3.346	0.901
August	110.9	33.99	12.52	156.5	154.0	3.982	3.906	0.887
September	149.0	45.61	14.18	181.1	177.9	4.509	4.422	0.868
October	197.5	60.35	17.03	211.0	207.1	5.141	5.041	0.849
November	231.7	66.41	18.72	219.8	215.0	5.293	5.191	0.839
December	257.7	66.76	20.83	232.5	227.0	5.533	5.426	0.829
Year	1982.3	582.13	16.94	2232.3	2188.5	54.564	53.516	0.852

Legends: GlobHor Horizontal global irradiation
DiffHor Horizontal diffuse irradiation
T_Amb T amb.
GlobInc Global incident in coll. plane
GlobEff Effective Global, corr. for IAM and shadings
EArray Effective energy at the output of the array
E_Grid Energy injected into grid
PR Performance Ratio

Grid-Connected System: Special graphs

Project : **Atlantis_Ideal System**

Simulation variant : **Atlantis_Ideal System**

Main system parameters	System type	**No 3D scene defined, no shadings**		
PV Field Orientation	tilt	30°	azimuth	0°
PV modules	Model	CS6U - 335P	Pnom	335 Wp
PV Array	Nb. of modules	84	Pnom total	**28.14 kWp**
Inverter	Model	SE27.6K-EU-APAC/AUS	Pnom	27.60 kW ac
User's needs	Unlimited load (grid)			

Daily Input/Output diagram

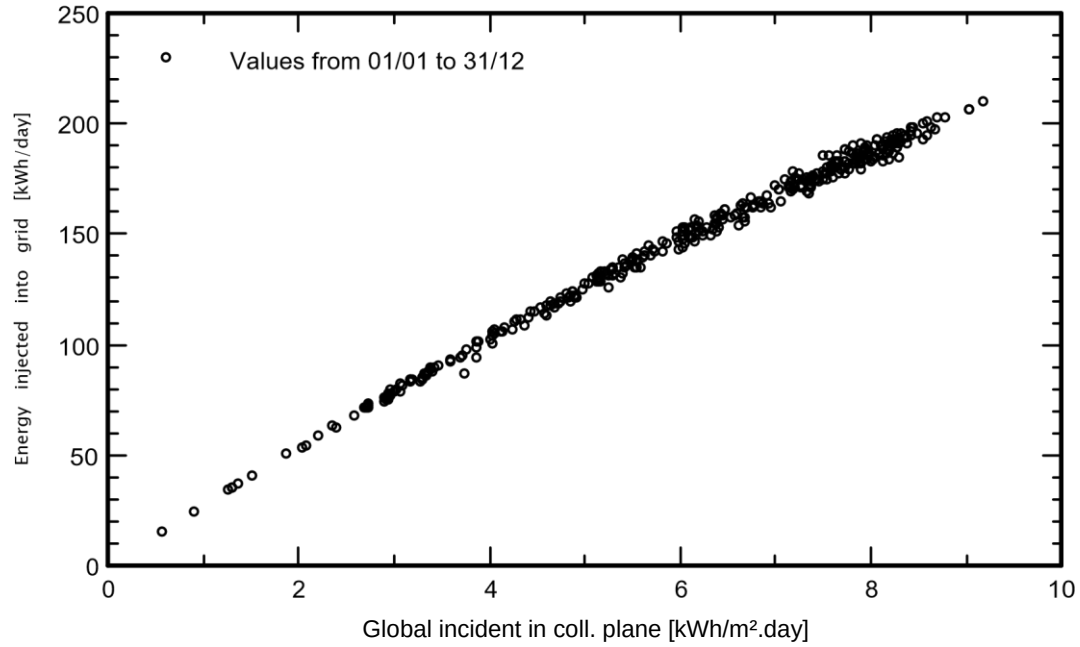

System Output Power Distribution

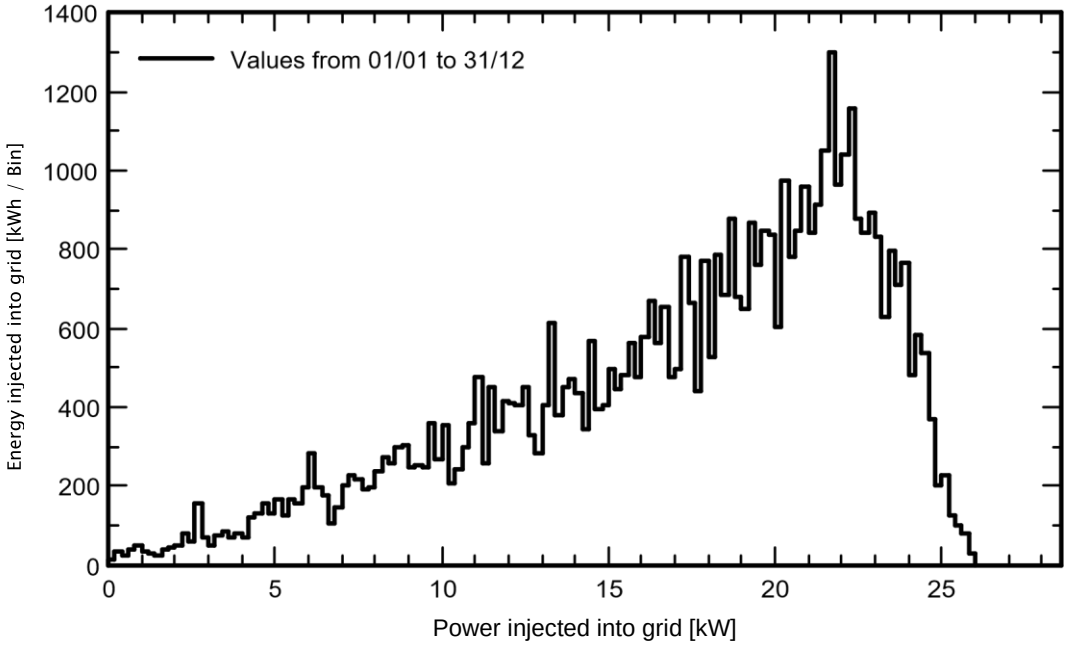

Grid-Connected System: Loss diagram

Project : **Atlantis_Ideal System**

Simulation variant : **Atlantis_Ideal System**

Main system parameters	System type	**No 3D scene defined, no shadings**			
PV Field Orientation	tilt	30°	azimuth	0°	
PV modules	Model	CS6U - 335P	Pnom	335 Wp	
PV Array	Nb. of modules	84	Pnom total	**28.14 kWp**	
Inverter	Model	SE27.6K-EU-APAC/AUS	Pnom	27.60 kW ac	
User's needs	Unlimited load (grid)				

Loss diagram over the whole year

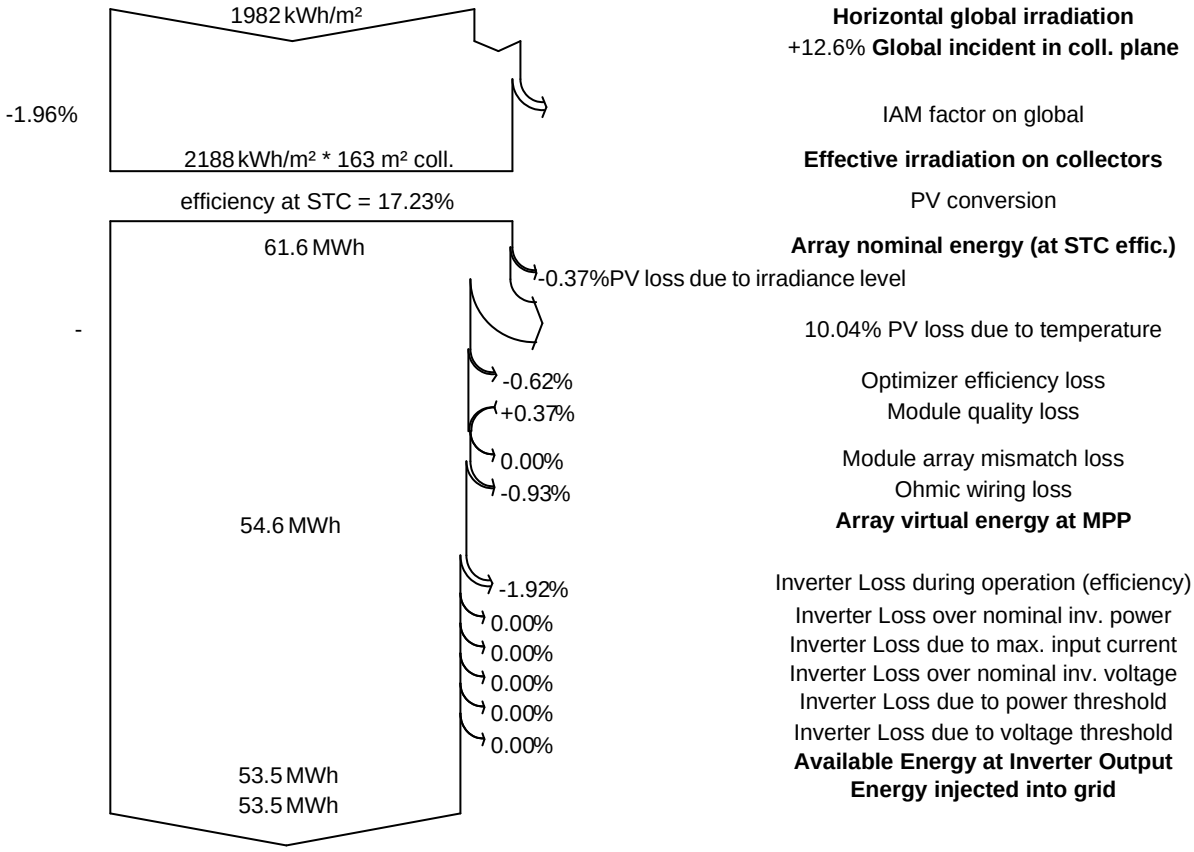

Appendix B – Correlation Graphs

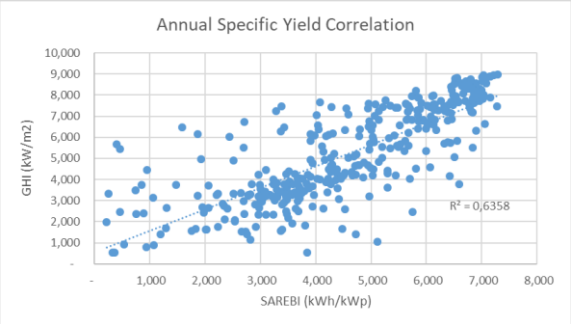

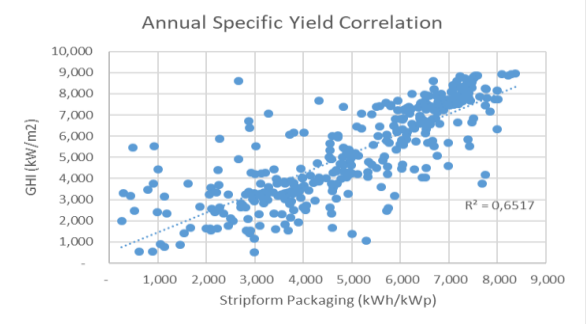

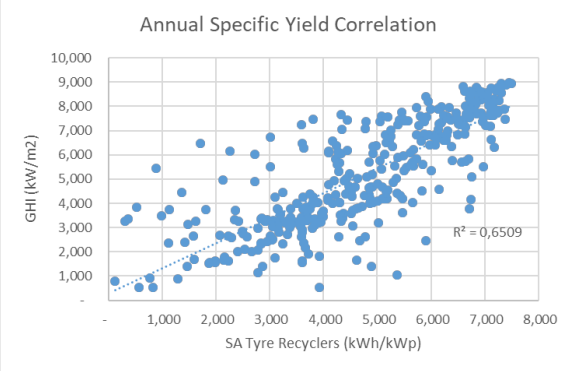

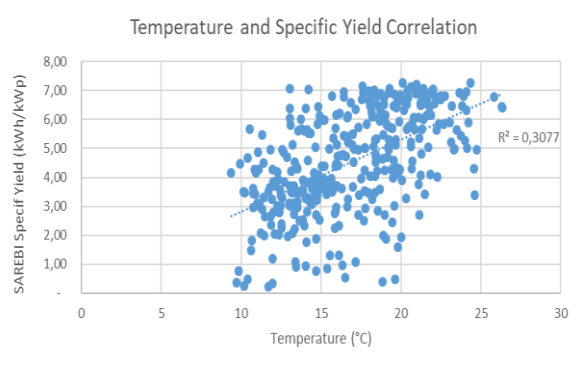

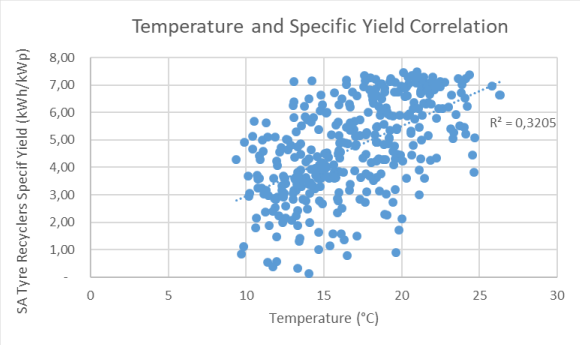

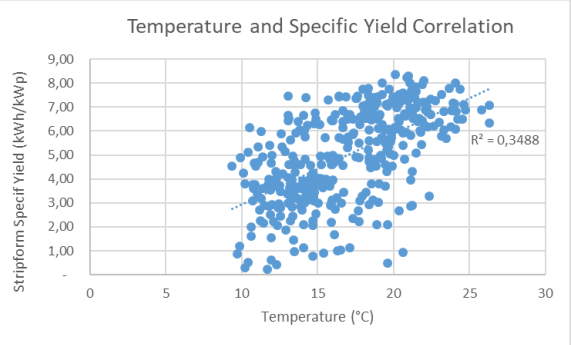

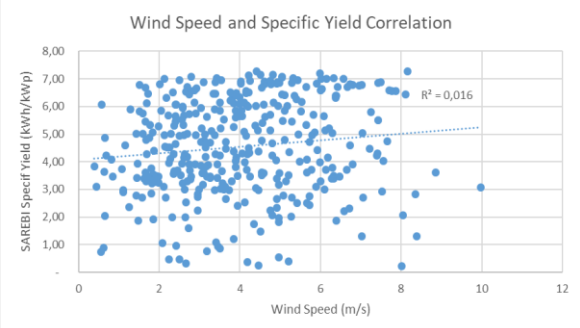

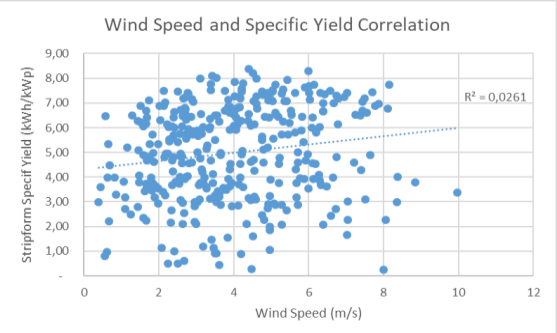

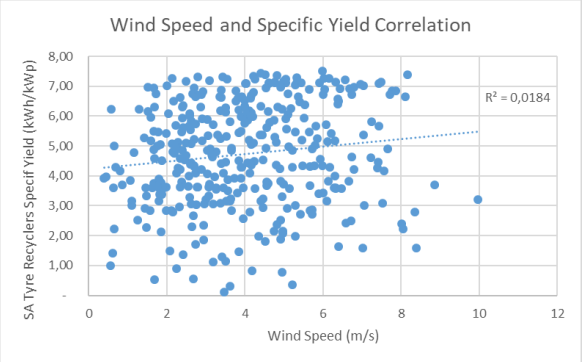
Wind Speed and Specific Yield Correlation
SA Tyre Recyclers Specif Yield (kWh/kWp)
R² = 0,0184
Wind Speed (m/s)

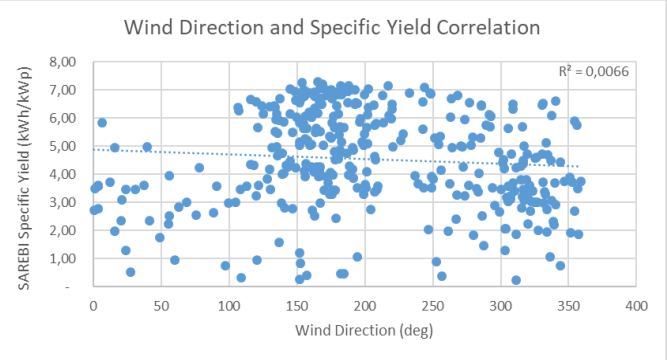
Wind Direction and Specific Yield Correlation
SAREBI Specific Yield (kWh/kWp)
R² = 0,0066
Wind Direction (deg)

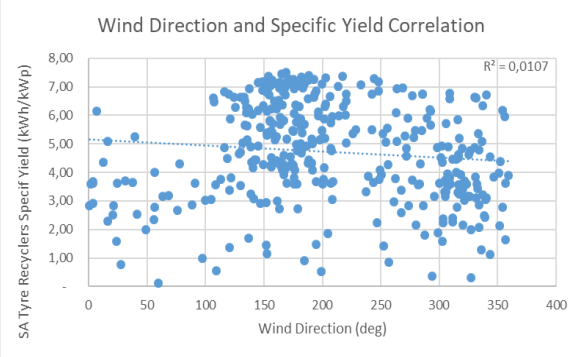
Wind Direction and Specific Yield Correlation
SA Tyre Recyclers Specif Yield (kWh/kWp)
R² = 0,0107
Wind Direction (deg)

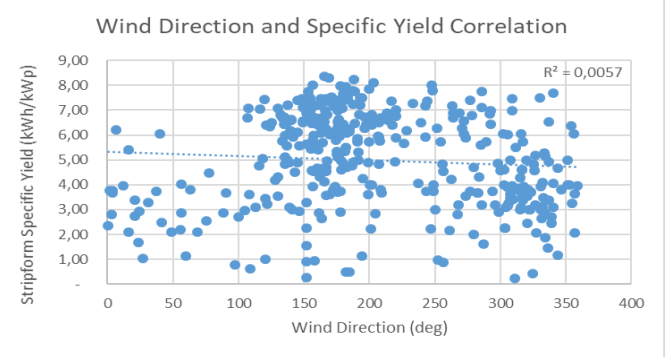
Wind Direction and Specific Yield Correlation
Stripform Specific Yield (kWh/kWp)
R² = 0,0057
Wind Direction (deg)

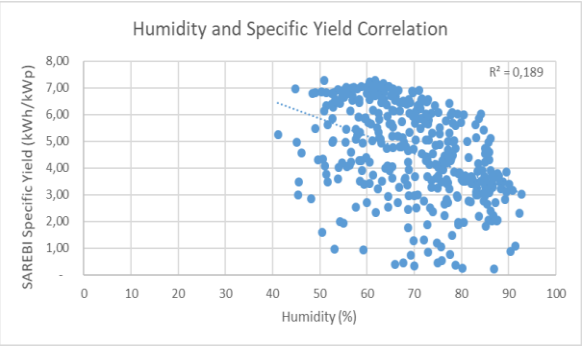
Humidity and Specific Yield Correlation
SAREBI Specific Yield (kWh/kWp)
R² = 0,189
Humidity (%)

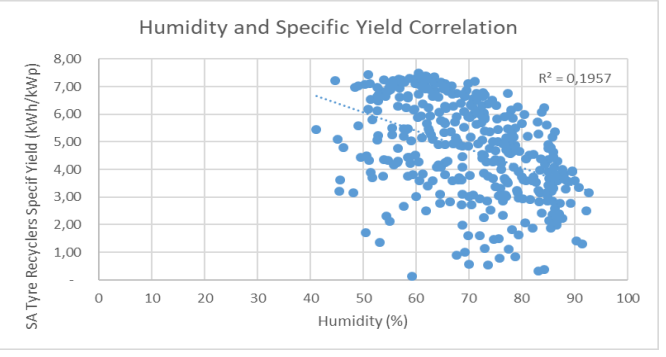
Humidity and Specific Yield Correlation
SA Tyre Recyclers Specif Yield (kWh/kWp)
R² = 0,1957
Humidity (%)

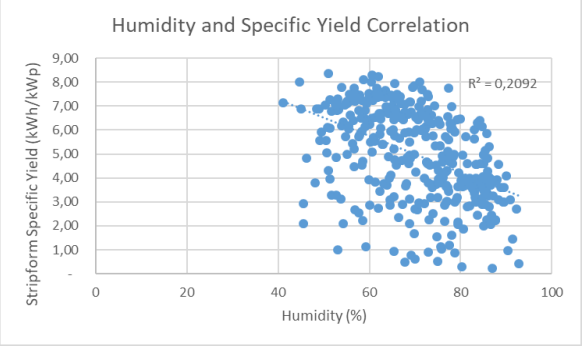
Humidity and Specific Yield Correlation
Stripform Specific Yield (kWh/kWp)
R² = 0,2092
Humidity (%)

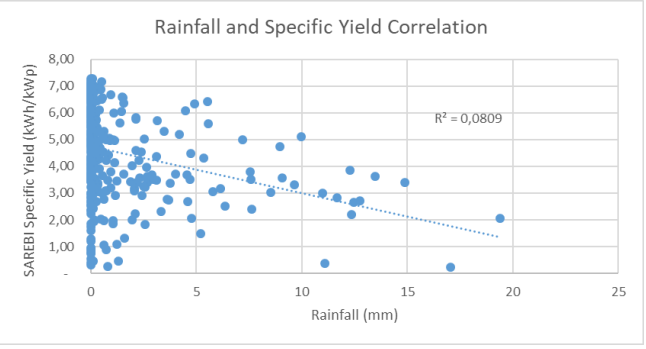
Rainfall and Specific Yield Correlation
SAREBI Specific Yield (kWh/kWp)
R² = 0,0809
Rainfall (mm)

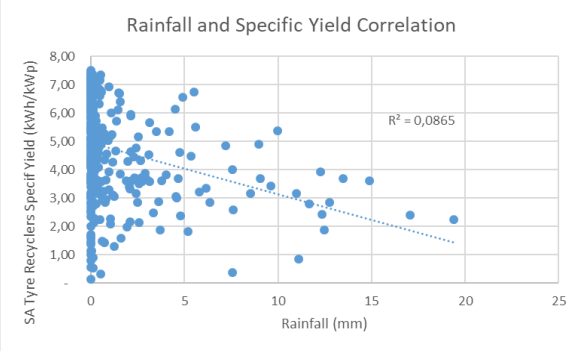
Rainfall and Specific Yield Correlation
SA Tyre Recyclers Specif Yield (kWh/kWp)
R² = 0,0865
Rainfall (mm)

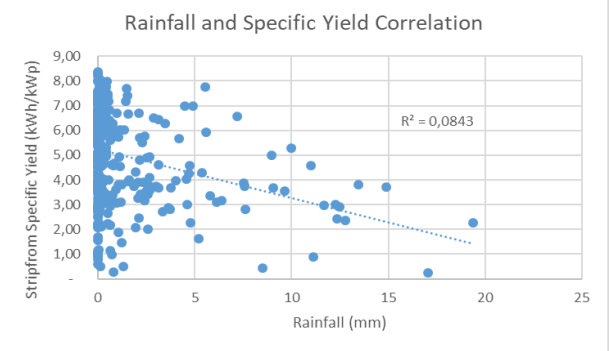
Rainfall and Specific Yield Correlation
Stripfrom Specific Yield (kWh/kWp)
R² = 0,0843
Rainfall (mm)

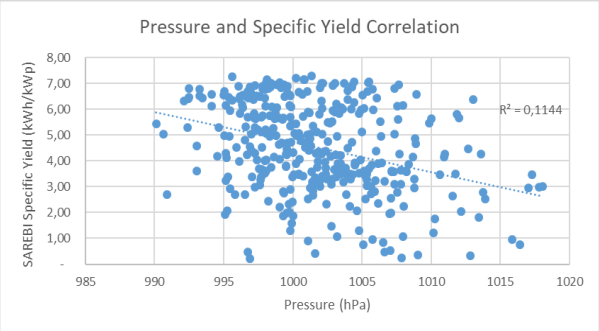
Pressure and Specific Yield Correlation
SAREBI Specific Yield (kWh/kWp)
8,00
7,00
6,00
5,00
4,00
3,00
2,00
1,00
-
985
990
995
1000
1005
1010
1015
1020
Pressure (hPa)
R² = 0,1144

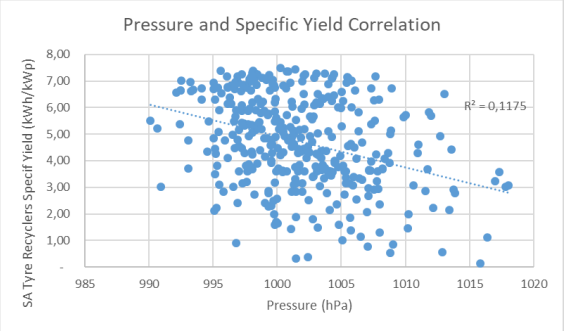
Pressure and Specific Yield Correlation
SA Tyre Recyclers Specif Yield (kWh/kWp)
8,00
7,00
6,00
5,00
4,00
3,00
2,00
1,00
-
985
990
995
1000
1005
1010
1015
1020
Pressure (hPa)
R² = 0,1175

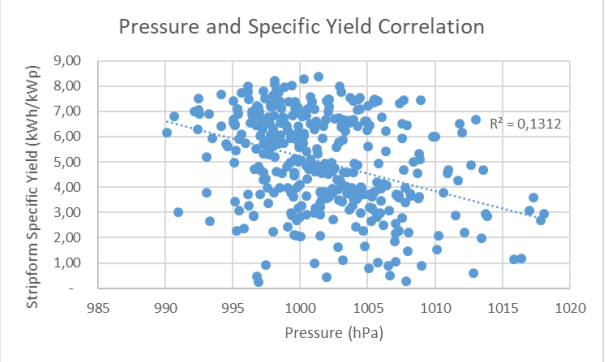
Pressure and Specific Yield Correlation
Stripform Specific Yield (kWh/kWp)
9,00
8,00
7,00
6,00
5,00
4,00
3,00
2,00
1,00
-
985
990
995
1000
1005
1010
1015
1020
Pressure (hPa)
R² = 0,1312

Appendix C – Financial Analysis

SAREBI Solar PV System

Design system installed DC capacity	10,0	kWp
Capital Cost	160 000	R

Basis for Financial Evaluation

Levelised Cost of Energy (LCOE) after-tax (nominal, escalating)	0,85	R/kWh
City of Cape Town Electricity Tariff	1,76	R/kWh
City of Cape Town Electricity Tariff Annual Increase	8%	

SMALL POWER USERS 1 (High consumption >1000 kWh / MONTH)

Assumptions

Lifetime	30	yrs
Duration of O&M	30	yrs
Module Degradation	0,27%	/yr
OPEX per annum as percentage of initial CAPEX	1%	
Replacements in year 11 as percentage of initial CAPEX	9%	
Inflation	6%	
Discount rate (nominal)	10%	
Specific energy yield	1 668	kWh / kWp / yr

LCOE Calculation

	Unit	Year --> 1	2	3	4	5	6	7	8	9	10	11	12	13	14	15	16	17	18	19	20	21	22	23	24	25	26	27	28	29	30
Production on/off	/.	1	1	1	1	1	1	1	1	1	1	1	1	1	1	1	1	1	1	1	1	1	1	1	1	1	1	1	1	1	1
Energy	kWh	16 656	16 656	16 656	16 622	16 610	16 599	16 587	16 576	16 566	16 554	16 543	16 529	16 518	16 506	16 295	16 283	16 272	16 261	16 249	16 197	16 226	16 214	16 203	16 191	16 180	16 168	16 157	16 145	16 134	16 122
Revenue	R	R29 985	R30 299	R30 859	R30 691	R30 358	R62 634	R63 795	R69 425	R54 845	R57 568	R82 140	R67 358	R72 866	R76 500	R84 289	R90 967	R98 175	R105 954	R114 450	R119 453	R169 188	R163 741	R155 193	R167 421	R180 686	R195 060	R203 458	R227 127	R245 122	R264 543
CAPEX	R	-160 000										-14 427																			
OPEX	R	-1 600	-1 696	-1 796	-1 906	-2 020	-2 141	-2 270	-2 406	-2 550	-2 703	-2 865	-3 037	-3 220	-3 413	-3 617	-3 836	-4 065	-4 309	-4 567	-4 841	-5 131	-5 439	-5 766	-6 112	-6 478	-6 867	-7 279	-7 716	-8 179	-8 669
Cash flow	R	-161 600	-1 696	-1 796	-1 906	-2 020	-2 141	-2 270	-2 406	-2 550	-2 703	-17 292	-3 037	-3 220	-3 413	-3 617	-3 836	-4 065	-4 309	-4 567	-4 841	-5 131	-5 439	-5 766	-6 112	-6 478	-6 867	-7 279	-7 716	-8 179	-8 669
Total cash flow discounted (nominal)	**R**	**195 061**																													
Energy stream	kWh	16 656	17 644	18 690	19 558	20 717	21 945	23 245	24 620	26 082	27 627	29 264	30 998	32 835	34 780	36 841	39 026	41 336	43 785	46 380	49 126	52 038	55 122	58 387	61 847	65 511	69 392	73 504	77 858	82 470	87 356
Total energy discounted (nominal)	**kWh**	**801 519**																													
		-161 619	29 828	32 006	34 525	37 298	40 292	43 526	47 018	50 795	54 865	64 908	64 016	69 147	74 668	80 671	87 168	94 111	101 648	109 784	118 569	128 057	138 302	149 364	161 350	174 326	188 145	203 174	219 411	236 963	255 879

Payback Period

Year	CAPEX	OPEX	Income	Cashflow	Discount Factor	Discount Cashflow	Cumulative
1	-R160 000	-R1 600	R28 985	-R132 619	0,909090909	-R120 563	-R120 563
2	R0	-R1 696	R30 299	R28 603	0,826446281	R24 666	-R95 897
3	R0	-R1 796	R30 859	R29 006	0,751314801	R24 046	-R72 051
4	R0	-R1 906	R30 691	R28 525	0,683013455	R23 581	-R48 469
5	R0	-R2 020	R30 358	R28 258	0,620921323	R23 159	-R25 310
6	R0	-R2 141	R62 634	R60 292	0,56447393	R22 744	-R2 566
7	R0	-R2 270	R63 795	R61 526	0,513158116	R22 646	R20 080
8	R0	-R2 406	R69 425	R67 019	0,46650738	R21 935	R41 705
9	R0	-R2 550	R54 845	R52 295	0,424097018	R21 540	R63 245
10	R0	-R2 703	R57 568	R54 865	0,385543199	R21 158	R84 403
11	-R14 427	-R2 865	R82 140	R66 908	0,350494727	R15 750	R100 148
12	R0	-R3 037	R67 358	R64 321	0,318631570	R20 497	R120 646
13	R0	-R3 220	R72 866	R69 647	0,289664636	R20 029	R140 675
14	R0	-R3 413	R76 500	R73 088	0,263331214	R19 248	R160 162
15	R0	-R3 617	R84 289	R80 671	0,239392013	R19 312	R179 555
16	R0	-R3 836	R90 967	R87 130	0,217629196	R18 963	R198 517
17	R0	-R4 065	R98 175	R94 111	0,197844724	R18 619	R217 136
18	R0	-R4 309	R105 954	R101 646	0,179858794	R18 282	R235 418
19	R0	-R4 567	R114 450	R109 884	0,163507995	R17 960	R253 378
20	R0	-R4 841	R119 453	R114 569	0,148644541	R17 025	R270 403
21	R0	-R5 131	R169 188	R164 057	0,135131855	R17 804	R288 208
22	R0	-R5 439	R163 741	R158 302	0,122846504	R19 443	R307 287
23	R0	-R5 766	R155 193	R149 426	0,111678186	R16 685	R323 968
24	R0	-R6 112	R167 421	R161 310	0,101525169	R16 377	R340 345
25	R0	-R6 478	R180 686	R174 208	0,092295608	R16 079	R356 424
26	R0	-R6 867	R195 060	R188 193	0,083905553	R15 786	R372 210
27	R0	-R7 279	R203 458	R196 179	0,076277866	R15 668	R387 707
28	R0	-R7 716	R227 127	R219 411	0,069343514	R15 215	R402 922
29	R0	-R8 179	R245 122	R236 943	0,063039559	R14 937	R417 859
30	R0	-R8 669	R264 543	R255 874	0,057308508	R14 664	R432 522

Payback Period 6,11 years

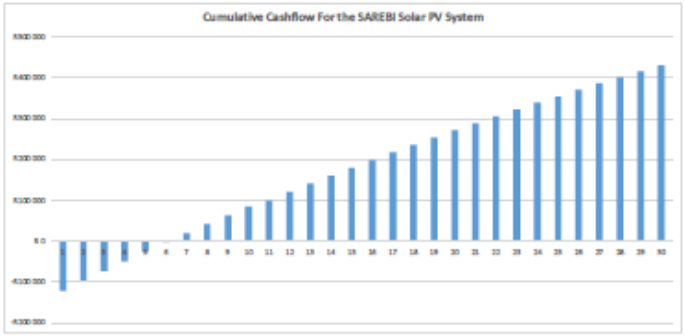

SA Tyre Recyclers Solar PV System

Design system installed DC capacity	291,0	kWp
Capital Cost	2 965 250	R

Basis for Financial Evaluation

Levelised Cost of Energy (LCOE) after-tax (nominal, escalating)	0,00	R / kWh
City of Cape Town Electricity Tariff	1,79	R / kWh
City of Cape Town Electricity Tariff Annual Increase	6%	

SMALL POWER USERS 1 (High consumption >1000 kWh / MONTH)

Assumptions

Lifetime	30	yrs
Duration of O&M	30	yrs
Module Degradation	0,07%	/yr
OPEX per annum as percentage of initial CAPEX	1%	
Replacement in year 11 as percentage of initial CAPEX	5%	
Inflation	6%	
Discount rate (nominal)	10%	
Specific energy yield	1 712	kWh / kWp / yr

LCOE Calculation

	Unit	Year --> 1	2	3	4	5	6	7	8	9	10	11	12	13	14	15	16	17	18	19	20	21	22	23	24	25	26	27	28	29	30
Production on/off	./.	1	1	1	1	1	1	1	1	1	1	1	1	1	1	1	1	1	1	1	1	1	1	1	1	1	1	1	1	1	1
Energy	kWh	395 488	395 488	395 488	394 868	394 381	394 106	393 837	393 592	393 278	392 997	392 720	392 448	392 186	391 889	391 612	391 306	391 098	390 792	390 526	390 228	389 951	389 674	389 398	389 121	388 866	388 567	388 290	388 053	387 797	387 680
Revenue	R	R886 094	R752 214	R812 391	R875 540	R944 959	R1 019 797	R1 100 407	R1 187 830	R1 281 948	R1 383 526	R1 491 158	R1 615 668	R1 759 156	R1 879 965	R2 025 693	R2 188 199	R2 358 436	R2 548 674	R2 748 186	R2 965 883	R3 200 881	R3 454 697	R3 726 227	R4 028 620	R4 342 897	R4 688 453	R5 057 760	R5 458 689	R5 890 998	R6 357 680
CAPEX	R	-2 965 250										-266 726																			
OPEX	R	-29 653	-31 220	-33 093	-35 078	-37 183	-39 414	-41 779	-44 286	-46 943	-49 759	-52 745	-55 910	-59 264	-62 820	-66 589	-70 585	-74 820	-79 309	-84 067	-89 111	-94 458	-100 126	-106 133	-112 501	-119 251	-126 426	-133 991	-142 030	-150 552	-159 585
Cash flow	R	-2 974 726	-31 220	-33 093	-35 078	-37 183	-39 414	-41 779	-44 286	-46 943	-49 759	-319 470	-55 910	-59 264	-62 820	-66 589	-70 585	-74 820	-79 309	-84 067	-89 111	-94 458	-100 126	-106 133	-112 501	-119 251	-126 426	-133 991	-142 030	-150 552	-159 585
Total cash flow discounted (nominal)	**R**	**R 390 277**																													
Energy stream	kWh	395 488	419 257	444 471	470 044	497 997	527 400	558 651	591 756	626 818	663 959	703 301	744 974	789 116	835 872	885 366	937 824	993 437	1 052 287	1 114 666	1 180 874	1 250 827	1 324 729	1 403 209	1 486 944	1 576 406	1 667 680	1 768 681	1 871 186	1 981 964	2 099 427
Total energy discounted (nominal)	**kWh**	**7 234 716**																													
		-2 279 208	720 996	779 298	840 661	907 796	980 883	1 058 828	1 143 514	1 235 000	1 333 746	1 179 680	1 555 559	1 679 896	1 814 145	1 998 105	2 116 616	2 266 626	2 417 065	2 566 069	2 879 771	3 106 429	3 354 972	3 622 079	3 911 299	4 223 168	4 560 061	4 923 768	5 314 656	5 740 427	6 198 126

Payback Period

Year	CAPEX	OPEX	Energy	Cashflow	Discount Factor	Discount Cashflow	Cumulative
1	-R2 965 250	-R29 653	R886 094	-R2 279 208	0,909090909	-R2 071 098	-R2 071 098
2	R0	-R31 220	R752 214	R720 994	0,826446281	R595 868	-R1 475 230
3	R0	-R33 093	R812 391	R779 298	0,751315401	R585 498	-R889 757
4	R0	-R35 078	R875 540	R840 661	0,683013455	R574 068	-R315 691
5	R0	-R37 183	R944 959	R907 796	0,620921323	R563 683	R247 992
6	R0	-R39 414	R1 019 797	R980 883	0,56447393	R553 820	R801 812
7	R0	-R41 779	R1 100 407	R1 058 828	0,513158113	R543 368	R1 344 688
8	R0	-R44 286	R1 187 830	R1 143 514	0,46650738	R533 467	R1 878 155
9	R0	-R46 943	R1 281 948	R1 235 000	0,424097402	R523 761	R2 401 916
10	R0	-R49 759	R1 383 526	R1 333 746	0,385543289	R514 224	R2 916 140
11	-R266 726	-R52 745	R1 491 158	R1 179 680	0,350493899	R413 420	R3 329 560
12	R0	-R55 910	R1 615 668	R1 555 559	0,318630818	R495 949	R3 824 209
13	R0	-R59 264	R1 759 156	R1 679 896	0,289664380	R486 905	R4 310 815
14	R0	-R62 820	R1 879 965	R1 814 145	0,263331256	R477 721	R4 788 536
15	R0	-R66 589	R2 025 693	R1 958 105	0,239392069	R468 991	R5 257 529
16	R0	-R70 585	R2 188 199	R2 116 616	0,217629156	R460 619	R5 717 948
17	R0	-R74 820	R2 358 436	R2 266 626	0,19784644	R451 967	R6 169 915
18	R0	-R79 309	R2 548 674	R2 467 065	0,17986858	R443 723	R6 613 638
19	R0	-R84 067	R2 748 186	R2 666 069	0,163507991	R435 987	R7 049 265
20	R0	-R89 111	R2 965 883	R2 876 771	0,148643629	R427 614	R7 476 879
21	R0	-R94 458	R3 200 881	R3 106 423	0,135130571	R419 779	R7 896 657
22	R0	-R100 126	R3 454 697	R3 354 572	0,122845974	R412 071	R8 308 728
23	R0	-R106 133	R3 726 227	R3 622 079	0,111678158	R404 509	R8 713 238
24	R0	-R112 501	R4 028 620	R3 911 299	0,101525598	R397 277	R9 110 515
25	R0	-R119 251	R4 342 897	R4 223 168	0,092295998	R389 779	R9 500 295
26	R0	-R126 426	R4 688 453	R4 560 061	0,083905453	R382 613	R9 882 908
27	R0	-R133 991	R5 057 760	R4 923 768	0,076277686	R375 574	R10 258 271
28	R0	-R142 030	R5 458 689	R5 316 656	0,069343169	R368 661	R10 626 932
29	R0	-R150 552	R5 890 998	R5 740 627	0,063039245	R361 872	R10 988 804
30	R0	-R159 585	R6 357 680	R6 198 126	0,057308313	R355 209	R11 344 014

Payback Period 4,34 Years

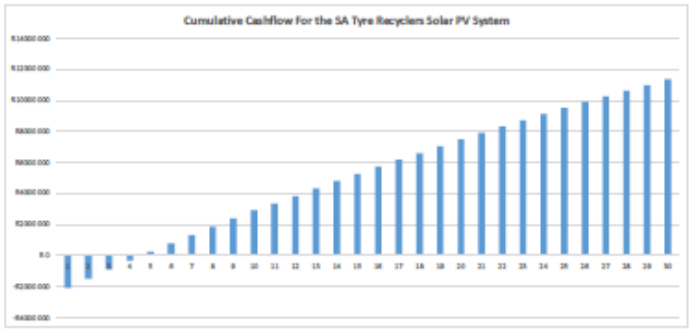

Stripform Packaging Solar PV System

Design system installed DC capacity	20,1	kWp
Capital Cost	820 000	R

Basis for Financial Evaluation

Levelised Cost of Energy (LCOE) after tax (nominal, escalating)	0,60	R / kWh	
City of Cape Town Electricity Tariff	1,75	R / kWh	SMALL POWER USERS 1 (High consumption >=1000 kWh / MONTH)
City of Cape Town Electricity Tariff Annual Increase	8%		

Assumptions

Lifetime	30 yrs
Duration of O&M	30 yrs
Module Degradation	0,07% / yr
OPEX per annum as percentage of Initial CAPEX	1%
Replacements in year 11 as percentage of Initial CAPEX	5%
Inflation	6%
Discount rate (nominal)	10%
Specific energy yield	1 761 kWh / kWp / yr

LCOE Calculation

Year -->

	Unit	1	2	3	4	5	6	7	8	9	10	11	12	13	14	15	16	17	18	19	20	21	22	23	24	25	26	27	28	29	30
Production on/off	/.	1	1	1	1	1	1	1	1	1	1	1	1	1	1	1	1	1	1	1	1	1	1	1	1	1	1	1	1	1	1
Energy	kWh	35 387	35 387	35 387	35 352	35 266	35 268	35 238	35 218	35 168	35 164	35 149	35 114	35 089	35 065	35 040	35 015	34 990	34 966	34 941	34 916	34 891	34 866	34 842	34 817	34 792	34 767	34 743	34 718	34 693	34 668
Revenue	R	R62 019	R62 005	R72 089	R78 843	R86 548	R91 247	R98 478	R106 281	R114 709	R123 792	R133 605	R144 168	R155 618	R167 948	R181 250	R195 612	R211 112	R227 839	R245 892	R265 375	R286 422	R309 096	R333 585	R360 015	R388 540	R419 326	R452 548	R488 424	R527 099	R568 860
CAPEX	R	-820 000										-26 654																			
OPEX	R	-8 200	-8 892	-8 596	-8 815	-8 040	-8 282	-8 534	-8 812	-9 100	-9 406	-9 731	-8 075	-8 699	-8 815	-7 295	-7 609	-8 129	-8 017	-8 184	-8 982	-10 264	-10 879	-11 581	-12 328	-12 957	-13 794	-14 556	-15 492	-16 457	-17 499
Cash flow	R	-828 200	-8 892	-8 596	-8 815	-8 040	-8 282	-8 534	-8 812	-9 100	-9 406	-36 384	-8 075	-8 699	-8 815	-7 295	-7 609	-8 129	-8 017	-8 184	-8 982	-10 264	-10 879	-11 581	-12 328	-12 957	-13 794	-14 556	-15 492	-16 457	-17 499
Total cash flow discounted (nominal)	**R**	**R90 082**																													
Energy stream	kWh	35 387	37 510	39 760	42 058	44 550	47 190	49 988	52 948	56 085	59 408	62 929	66 657	70 607	74 790	79 222	83 916	88 888	94 154	99 733	105 642	111 901	118 581	125 558	132 992	140 871	149 217	158 057	167 425	177 340	187 846
Total energy discounted (nominal)	**kWh**	**847 512**																													
		-260 845	68 918	88 096	74 526	80 526	86 965	93 908	101 470	109 808	118 886	99 217	108 118	169 174	161 118	174 016	187 968	202 982	218 222	236 758	255 868	276 189	298 216	322 058	347 792	375 588	405 560	437 889	472 971	510 761	551 525

Payback Period

Year	CAPEX	OPEX	Income	Cashflow	Discount Factor	Discount Cashflow	Cumulative
1	-R820 000	-R8 200	R62 019	-R290 881	0,909090909	-R207 164	-R207 164
2	R0	-R8 892	R67 005	R58 914	0,826446281	R52 825	-R154 339
3	R0	-R8 596	R72 089	R99 096	0,751314801	R51 911	-R102 428
4	R0	-R8 815	R78 843	R56 528	0,683013455	R50 904	-R51 524
5	R0	-R8 040	R86 548	R80 508	0,620921323	R49 999	-R1 526
6	R0	-R8 282	R91 247	R86 965	0,56447393	R49 089	R47 563
7	R0	-R8 534	R98 478	R93 908	0,513158516	R48 205	R95 755
8	R0	-R8 812	R106 281	R101 470	0,46650738	R47 346	R143 092
9	R0	-R9 100	R114 709	R109 608	0,424097018	R46 482	R189 574
10	R0	-R9 406	R123 792	R118 386	0,385543199	R45 643	R235 217
11	-R26 654	-R5 731	R133 605	R99 217	0,350493809	R34 775	R269 992
12	R0	-R8 075	R144 168	R136 118	0,318631828	R43 357	R313 349
13	R0	-R8 699	R155 618	R147 174	0,28966544	R42 610	R355 959
14	R0	-R8 815	R167 948	R161 118	0,263331254	R42 427	R398 386
15	R0	-R7 295	R181 250	R174 016	0,239392049	R41 658	R440 044
16	R0	-R7 609	R195 612	R187 948	0,217629136	R40 902	R480 946
17	R0	-R8 129	R211 112	R202 982	0,19784469	R40 159	R521 105
18	R0	-R8 017	R227 839	R219 222	0,17986790	R39 429	R560 534
19	R0	-R8 184	R245 892	R236 758	0,163507991	R38 713	R599 246
20	R0	-R8 982	R265 375	R255 044	0,148643628	R38 007	R636 253
21	R0	-R10 264	R286 422	R276 189	0,135130571	R37 315	R673 568
22	R0	-R10 879	R309 096	R298 216	0,122845974	R36 635	R710 203
23	R0	-R11 581	R333 585	R322 058	0,111678158	R35 966	R746 169
24	R0	-R12 328	R360 015	R347 792	0,101525598	R35 310	R781 479
25	R0	-R12 957	R388 540	R375 588	0,092295998	R34 665	R816 144
26	R0	-R13 794	R419 326	R405 560	0,083905453	R34 031	R850 175
27	R0	-R14 556	R452 548	R437 989	0,076277684	R33 409	R883 584
28	R0	-R15 492	R488 424	R472 971	0,069343349	R32 797	R916 381
29	R0	-R16 457	R527 099	R510 741	0,063039408	R32 197	R948 578
30	R0	-R17 499	R568 860	R551 525	0,057308553	R31 607	R980 185

Payback Period **5,84 years**